HOKKAIDO UNIVERSITY

Title	Fast Underwater Adhesion of Hydrogels by Multi-Scale Design
Author(s)	Rao, Ping
Degree Grantor	北海道大学
Degree Name	博士(生命科学)
Dissertation Number	甲第13610号
Issue Date	2019-03-25
DOI	https://doi.org/10.14943/doctoral.k13610
Doc URL	https://hdl.handle.net/2115/91694
Type	doctoral thesis
File Information	RAO_PING.pdf

Hokkaido University Collection of Scholarly and Academic Papers : HUSCAP

Dissertation

Fast Underwater Adhesion of Hydrogels by Multi-Scale Design

(マルチスケール設計によるハイドロゲルの高速水中接着)

By

Ping Rao

Transdisciplinary Life Science Course

Graduate School of Life Science

Hokkaido University

Sapporo, Japan

2019, March

Contents

Chapter 1: General introduction 5

1.1 Overview 5

1.2 Outline of this thesis 6

References 9

Chapter 2: Backgrounds 11

2.1 General concepts on adhesion 11

2.1.1 Adhesion and cohesion 11

2.1.2 Types of adhesion 12

2.1.3 Requirements for a good adhesion 12

2.1.4 Characterization methods of for adhesive joints 17

2.2 A brief review of advancements in developing underwater adhesives 22

2.2.1 Bio-inspired interfacial chemistry adhesion: catechol-based materials used as underwater adhesives 22

2.2.2 Structural design adhesion 27

2.2.3 Mechanical interlock bonding 34

2.3 Hydrogels adhesives 34

2.4 In situ observation of underwater surface contact evolution 36

2.5 Conclusion and objectives of this manuscripts 37

References 39

Chapter 3: Tough hydrogels with fast, strong, and reversible underwater adhesion based on a multi-scale design 43

3.1 Introduction 43

3.2 Experiments 44

3.2.1 Materials choices and preparation 44

3.2.2 In situ observation of the underwater contact formation evolution 46

3.2.3 Measurements of underwater adhesion by probe tack test 46

3.2.4 Rheological test 47

3.2.5 Underwater tensile test and hysteresis test. 48

3.2.6 Preparation of the silicone mold 49

3.3 Results and Discussions 49

3.4 Conclusions 58

References 59

Figures and Tables 63

Supplementary Information 68

Chapter 4: Underwater adhesion behaviors of polyampholyte (PA) hydrogels on soft substrates 80

4.1 Introduction 80

4.2 Experiments 81

4.2.1 Materials and Samples 81

4.2.2 Measurements 83

4.3 Results and discussions 84

4.3.1 Matrix energy dissipation effect on the underwater adhesion between the PA hydrogels. 84

4.3.2 Underwater adhesion behaviors of PA hydrogels with different contact element size. 86

4.3.3 Underwater adhesion behaviors of PA hydrogels polymerized on different templates. 90

4.4 Conclusions 91

References 93

Figures 95

Chapter 5: Porous hydrogels with instant in situ underwater contact and adhesion on diverse nonporous substrates 101

5.1 Introduction 101

5.2 Experiments 103

5.2.1 Materials 103

5.2.2 Measurements 104

5.3 Results and discussions 107

5.4 Conclusions 112

References 113

Schemes and figures 114

Chapter 6: Concluding remarks 119

Accomplishments 122

Acknowledgements 124

Chapter 1: General introduction

1.1 Overview

Adhesion to wet surfaces is of significance in diverse applications including tissue engineering, medical operations, bio-medical devices and underwater soft robotics [1-5]. However, adhesion to wet or underwater surfaces is quite challenging owing to water molecules at the contact interface. Competition between adhesive interactions and interactions with water molecules significantly complicates the problem [6]. Water molecules not only prevent the direct contact at the interfaces, but also can penetrate the gap and reduce the adhesion strength of the materials by hydrating and decomposing [7]. Besides, many of the mechanical properties (such as structure design and Young's modulus) showed significant effects on the adhesion in a dry condition [8-10], are also compromised, especially for the adhesion that involves a soft material.

Scientists have extensively investigated on wet adhesives emulating natural adhesive materials of marine organisms. For instance, wet adhesives mimicking the proteins existing in the biological system such as mussels [11-12], barnacle cements [11, 13], and sandcastle-worm glues [14]. The commonly used 3, 4-dihydroxyphenylalanine (DOPA) and derivatives have demonstrated effective wet adhesion performances. However, several limitations are also accompanied such as adhesion degradation by wet-air oxidation, a long contact forming time and the irreversibility [7].

Hydrogels, consisting of a three dimensional polymer network and a large amount of water, may have immense potential as wet adhesives. Firstly, with the hydrophilic nature,

hydrogels have less effect coming from water penetration and decomposition on adhesion compared with other materials. Secondly, hydrogels with extremely high toughness have been achieved such as double network (DN) hydrogels reported by Gong and co-workers [15]. The high toughness ensure the high cohesion strength of the materials, which is also an important factor to develop a tough underwater adhesives. Moreover, due to the high biocompatibility, there are strong demands in applications including tissue engineering, bio-medical devices, and medical operations.

Recently, prominent progress has been achieved on the irreversible robust bonding of hydrogels to diverse synthetic and biological surfaces, which shows that the importance of the chemical bonding [16] or physical interlocking of the interface [17] and bulk energy dissipation [16, 18]. On the other hand, the research for in situ underwater adhesion of hydrogels is still in its infancy. The state-of-the-art technology suffers from shortcomings including long contact time and very weak adhesion strength. Consequently, a general strategy to develop underwater hydrogels adhesives which can achieve high adhesion strength, form a good contact within an acceptable time as well as a reversibility, are required.

1.2 Outlines of This Thesis

The work described in this dissertation is mainly to study the underwater adhesion behaviors of hydrogels and design strong underwater hydrogels adhesives with fast underwater contact and reversibility.

In **Chapter 2** a review on the foundation of underwater adhesion and advancement of underwater hydrogels adhesives including concepts of adhesion, cohesion, surface

tension, wetting behaviors of liquids; the characterized methods of underwater adhesion; structural design for adhesives with applications mostly in the dry environment; studies on natural adhesive materials of organisms including mussel proteins, sandcastle-worm, geckos, cling-fish, and octopus etc; advances and challenges in bio-inspired adhesives; In situ observation of contact surface evolution. This chapter will help to have a clear understanding on the following chapters.

In **Chapter 3**, tough hydrogels adhesives with fast, strong, and reversible underwater adhesion, are developed based on a multi-scale design. Realizing a tough underwater adhesive with fast and good contact as well as strong and reversible adhesion will cater to many applications such as re-usable sheets for wound dressing and anti-slippery for wall-climbing robotics. However, there are some challenges since many factors which show significant effects on the strength of adhesion, are compromised when it comes to adhesion in these wet environments. Hydrogels usually show poor adhesion to other surfaces in their fully swollen state owing to the strong hydration ability of hydrophilic polymer strands, which prevents the formation of molecular bridges at the interface. It has been illustrated that water at the interface needs a very long time to be drained out, and is also easily got trapped by the soft hydrogels adhesives. To address these challenges, a cling-fish inspired macro-scale surface structure and nano-scale dynamic bonds are combined. The surface structure serves to accelerate water drainage, to prevent water trapping and to delay crack propagation; the dynamic bonds of the gel serves to form reversible bridges at the interface and to dissipate a significant amount of energy in the bulk during detachment. The designed tough adhesives show outstanding adhesion performance on both soft and hard substrates including glass plate, soft gels, and tissue. The strategy of combining macro-scale surface engineering and micro-scale dynamic

bonds is applicable to various recently developed tough hydrogels based on hydrogen, ionic bonds and other dynamic bonds.

In **Chapter 4**, the surface structure size effect and a long contact time effect are further discussed. Polyampholyte (PA) hydrgels with a single hexagonal facet on the surface are prepared. And the underwater adhesion on the flat PA hydrogels is measured by the probe tack test. Meanwhile, crack propagation during the debonding process is record by a camera. The results show that, the underwater adhesion of the hydrogels with smaller facet (decreasing the diameter while keeping the height of the facet), is higher than the bigger one in a short contact time. With the increasing of contact time, the gap between the strength become smaller. Moreover, the recorded video also showed how the crack was initiated and propagated.

Based on the results of **Chapter 3** and **4**, it can be seen that the smaller the facet, the faster the water drainage is. In order to develop adhesives with much smaller facet as well as an efficient water drainage system, in **Chapter 5**, the porous hydrogels consisting of two kind of polymers with opposite charges are prepared for studying the underwater adhesion. The porous structure of the hydrogels results from the phase separation of polyelectrolyte complexation (PEC) triggered by salts exchange. It is found that the porous hydrogels can instantly adhere to diverse nonporous substrates including metal plate, glass plate, silicone rubber, aluminium film and beef heart under water. The surface contact evolution observed clearly shows that the porous hydrogels can drain water much more efficiently than the nonporous PA hydrogels. And there is almost no water drop trapped at the interface, which implies fewer flaws at the bonding interfaces. Moreover, further study on the underwater adhesion of porous hydrogels showed that, there is a suction effect during the debonding process. The suction effect not only increases the

adhesion strength, but also contributes to the bulk energy dissipation. To identify this effect, a series of tack tests including changing the debonding speed, size of the sample, and in viscous polyethylene glycol (PEG) solution, are conducted. All the results illustrates the suction effect during debonding process.

In **Chapter 6** the concluding remarks are included based on the overall work.

References

[1] Bačáková, L., et al., Cell adhesion on artificial materials for tissue engineering. 2004. 53(Suppl 1): p. S35-S45.

[2] Drury, J. L. and D.J.J.B. Mooney, Hydrogels for tissue engineering: scaffold design variables and applications. 2003. 24(24): p. 4337-4351.

[3] Lu, N. and D.-H.J.S.R. Kim, Flexible and stretchable electronics paving the way for soft robotics. 2014. 1(1): p. 53-62.

[4] Mi, F.-L., et al., Fabrication and characterization of a sponge-like asymmetric chitosan membrane as a wound dressing. 2001. 22(2): p. 165-173.

[5] Venkatraman, S. and R.J.B. Gale, Skin adhesives and skin adhesion: 1. Transdermal drug delivery systems. 1998. 19(13): p. 1119-1136.

[6] Sudre, G., et al., Reversible adhesion between a hydrogel and a polymer brush. 2012. 8(31): p. 8184-8193.

[7] Yi, H., et al., Bioinspired Reversible Hydrogel Adhesive for Wet and Underwater Surfaces. 2018.

[8] Pan, T., et al., Experimental and theoretical studies of serpentine interconnects on ultrathin elastomers for stretchable electronics. 2017. 27(37): p. 1702589.

[9] Schneider, A., et al., Polyelectrolyte multilayers with a tunable Young's modulus: influence of film stiffness on cell adhesion. 2006. 22(3): p. 1193-1200.

[10] Matuda, N., S. Baba, and A.J.T.S.F. Kinbara, Internal stress, Young's modulus and adhesion energy of carbon films on glass substrates. 1981. 81(4): p. 301-305.

[11] Waite, J.H.J.I.J.o.A. and Adhesives, Nature's underwater adhesive specialist. 1987. 7(1): p. 9-14.

[12] White, J.D. and J.J.J.M. Wilker, Underwater bonding with charged polymer mimics of marine mussel adhesive proteins. 2011. 44(13): p. 5085-5088.

[13] Yule, A. and G.J.C.i. Walker, Adhesion in barnacles. 1987. 5: p. 389-402.

[14] Hofman, A.H., et al., Bioinspired Underwater Adhesives by Using the Supramolecular Toolbox. 2018. 30(19): p. 1704640.

[15] Gong, J.P., et al., Double‐network hydrogels with extremely high mechanical strength. 2003. 15(14): p. 1155-1158.

[16] Yuk, H., et al., Tough bonding of hydrogels to diverse non-porous surfaces. 2016. 15(2): p. 190.

[17] Nonoyama, T., et al., Double‐network hydrogels strongly bondable to bones by spontaneous osteogenesis penetration. 2016. 28(31): p. 6740-6745.

[18] Li, J., et al., Tough adhesives for diverse wet surfaces. 2017. 357(6349): p. 378-381

Chapter 2: Backgrounds

2.1 General concepts on adhesion

2.1.1 Adhesion and cohesion

Adhesion involves molecular interactions at the interface between materials. Any event described as adhesion is an assembly involving an "adherend" (or substratum) with an applied "adhesive" that creates an intervening "interface". The combination is defined as an "adhesive joint" [1]. Cohesion involves intermolecular attractions between like-molecules/atoms (Figure 2.1). In another word, adhesion are all the forces or mechanisms that keep the adhesive with each substrate, while cohesion forces are all the forces or mechanisms that hold the adhesive itself. The adhesive and cohesive definition refers to the forces that keep together the adhesive with the substrate (adhesion) and the adhesive itself (cohesion), these forces correspond to: the chemical bonds, intermolecular forces.

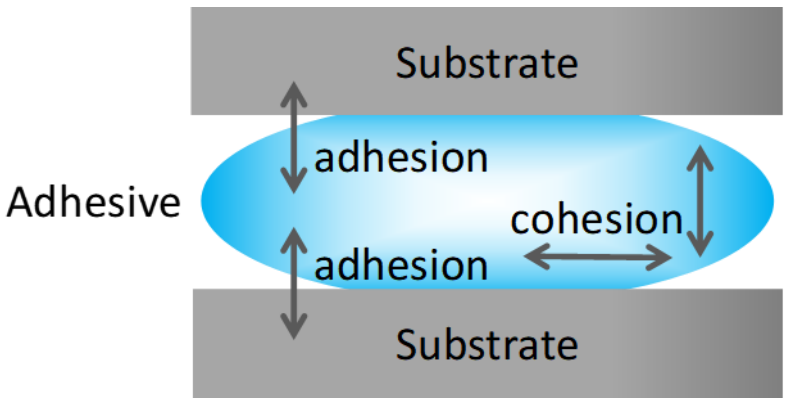

Figure 2.1 Schematic illustration of the definition of adhesion and cohesion

2.1.2 Types of adhesion

Based on the difference of these forces, adhesion can be categorized as physical, chemical and mechanical bonding processes that contribute to the interfacial strength of the assembly. Physical bonding forces are generally quite weak including van der Waals forces, hydrogen bonding and ions attraction [2-3]. Chemical bonding [4] including covalent, ionic, metallic bonding [5], is usually strong but also very difficult to produce in a dense manner across an interface. Because trying to create bonds between unlike surfaces is much more complicated and may result in a very limited chemical bonding and much lower interfacial strengths since contaminants are hard to eliminate completely and interfere with the intimate adaptation needed to form bonds. Mechanical bonding is the most effective means of creating strong joints such as mechanical interlocking which involves the adhesive penetrating into the adherend and become mechanically interlocked at some level [6-8].

2.1.3 Requirements for a good adhesion

(a) Clean surface

To achieve a strong adhesive bonds, one principal requirement is that the surface should be clean and therefore in a high energy state. Films of liquid are always present at interfaces with wetting and spreading, contaminants are remain on the surfaces, which will prevent the surface contact and a tough bonding. Acid etching is one method to remove most of the contaminants, produce surface roughness for micro-mechanical interlocking, and forms facets on the mineral crystals [1].

(b) Good wetting and contact ability

Intimate contact of the materials is required to create a good adhesion. Since the surface of a material is different from the interior, understanding of the surface characteristics of materials is essential to understand and promote adhesion. The surface free energy, represents the difference between an atom on the surface and an atom in the interior. Surface energies are also associated with failure of an adhesive bond. Failure involves forming new surfaces and the appropriate surface energies have to be provided. The surface energy term may be the work of adhesion, W_a; or the work of cohesion, W_c; depending on whether the failure is adhesive or cohesive. They are defined as follows,

$$W_a = \gamma_1 + \gamma_2 - \gamma_{12},\ W_c = 2\gamma_1$$

The practical adhesion, for example fracture energy G; will comprise a surface energy term G_0 (W_a or W_c) to which must be added a term c representing other energy absorbing processes—such as energy dissipation of the materials—which occur during fracture:

$$G = G_0 + G_{dissipation}$$

Usually the $G_{dissipation}$ is very much larger than G_0. This is why practical fracture energies for adhesive joints are almost always orders of magnitude greater than works of adhesion or cohesion. However, a modest increase in G_0 may result in a large increase in adhesion, since stronger bonds (increased G_0) may lead to much larger increases in fracture energy because they allow much more bulk energy dissipation during fracture. The surface energy of the solid can be obtained from equilibrium contact angle measurements of a series of test liquids on the solid surface. The angle of contact θ with the solid is related

to the surface energies by Young's equation (Figure 2.2).

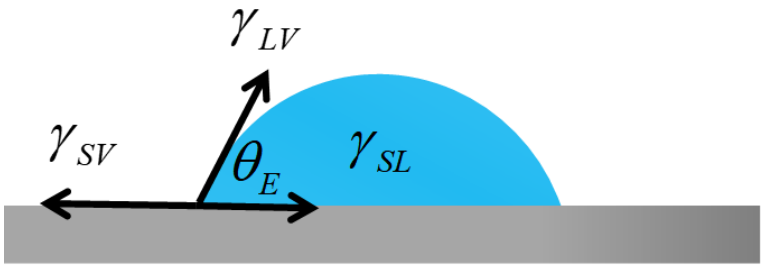

Figure 2.2 The relationship between surface energy and contact angle.

$$\cos\theta_E = \frac{\gamma_{SV} - \gamma_{SL}}{\gamma_{LV}}$$

The spreading coefficient or spreading energy, *S*,

$$S = \gamma_{SV} - \gamma_{LV} - \gamma_{SL}$$

If S is positive, the liquid at equilibrium will be spread completely over the solid.

Therefore, proper contact angle and good wetting ability is quite important for the bonding formation of adhesives.

(c) Surface roughness

Wettability of the adhesive is enhanced by the presence of roughness. Wettability is related to the roughness by the Wenzel equation. We can assume that the local contact angle is given as θ_E, and we seek to determine the apparent angle θ^* on a rough, but chemically homogeneous. Finally, the roughness scale is assumed to be much smaller than the size of our drop. (Figure 2.3)

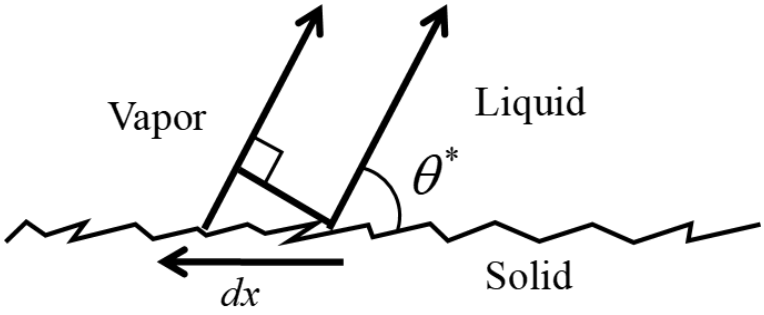

Figure 2.3 Edge of a drop placed on a rough surface.

$$dE = r(\gamma_{SL} - \gamma_{SV})dx + \gamma_{LV}dx\cos\theta^*$$

The minimum of E determines equilibrium, and the contact angle θ_E of a drop is given by the Young relation,

$$\cos\theta_E = \frac{\gamma_{SV} - \gamma_{SL}}{\gamma_{LV}}$$

For r=1 (smooth surface), the Young's relation is recovered. By contrast, when r > 1, the equilibrium condition leads to Wenzel's relation:

$$\cos\theta^* = r\cos\theta_E$$

The relation embodies two types of behavior:

1. If $\theta_E < 90°$ (hydrophilic solid), we will have $\theta^* < \theta_E$ since r > 1.

2. Likewise, if $\theta_E > 90°$, we will have $\theta^* > \theta_E$.

Surface roughness always magnifies the underlying wetting properties. Both hydrophilic and hydrophobic characteristics are reinforced by surface texture [9].

On the other hand, adhesion between fibrillar or patterned surfaces and smooth substrates

can be stronger than between two smooth surfaces [10]. Although fibrillar or patterned surfaces create a less adhesion area with a substrate than a continuous contact, the principle of contact splitting increases adhesion.

The force required to form a circular contact of radius a is given by [11],

$$P = \frac{4E^* a^3}{3R} - \sqrt{8\pi E^* a^3 w}$$

Where, w is the work of adhesion, E^* is the reduced elastic modulus,

$$\frac{1}{E^*} = \frac{1-\nu_1^2}{E_1} + \frac{1-\nu_2^2}{E_2}, \quad \nu_i$$

E_i, ν_i is the Young's modulus and Poisson ratio, and the reduced radius is defined as,

$$\frac{1}{R} = \frac{1}{R_1} + \frac{1}{R_2}$$

Since a << R_i (R_i indicates the two spherical surfaces in contact), in load control, the magnitude of the tensile pull-off forces turn out to be,

$$P_0 = \frac{3}{2}\pi R\omega$$

This shows that the adhesion force is a linear dimension of the contact; therefore, by splitting up the contact into n parts, the total adhesion force is increased to，

$$P_{total} = nP_i = n\frac{3}{2}\pi\frac{R}{\sqrt{n}}\omega = \sqrt{n}\frac{3}{2}\pi R\omega = \sqrt{n}P_0$$

(d) Adhesive solidification

During the contact process, the adhesive generally must be low enough in viscosity and

be capable of sufficient flow within the available application time to spread and adapt to the details of the adherend surface. However, during the debonding process, if the adhesive is too soft or with a very low cohesion strength and fracture energy, the adhesives will be failed easily. Here, the compliance effect on the adhesion is briefly explained.

According to the definition compliance *C*,

$$C = \frac{d\delta_t}{dF},$$

$$U_{stretch} = \int_0^{\delta_{t0}} F d\delta_t = \int_0^{\delta_{t0}} CF dF = \frac{CF_c^2}{2}$$

$$U_{Adhesion} = G_c A,$$

$$F_c \sim \sqrt{G_c}\sqrt{\frac{A}{C}}$$

This is the adhesion scale theory [12]. It can be seen that the adhesion force will increase if the compliance decreases. This indicates that, the good adhesive should be soft and compliant to conform the contact surface, and become stiff to resist debonding failure.

2.1.4 Characterization methods of adhesive joints

The main experimental tests that are generally used to characterize the failure of soft materials as well as their advantages and their limitations are discussed here.

(a) Lap-shear test

Lap-shear is the most common test used in adhesive evaluation. It is simple test to perform, with respect to construction of samples and loading to failure. Test specimens are bonded according to the manufacturer's instructions, as shown in Figure 2.4, and are then tested

to failure. The highest load achieved is recorded and is usually referred to as the lap-shear strength. The method focuses on predicting the adhesive joints strength by using simple linear elastic analysis. Another benefit of this test is the ability to evaluate mechanical properties at high deformation rates [13].

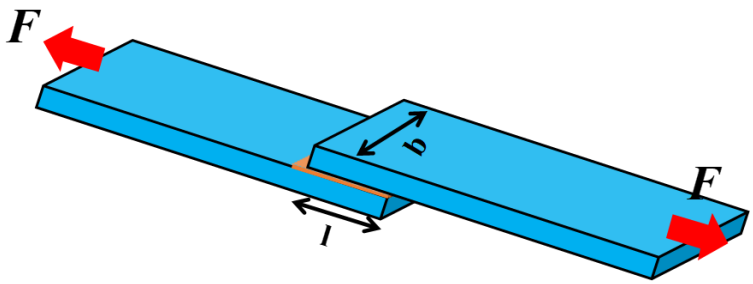

Figure 2.4 Schematic illustration of single lap-shear.

The critical energy release rate, G_c, can be estimated from the method proposed by Kendall for long lap joint.

$$\tau = \frac{F}{bl}$$

$$G_c = (\frac{F}{b})^2 / 4Eh$$

Where F is the measured force, l, is the overlap length, b is the width of the joint, h is the thickness, E is the modulus. It can be seen that for a long joint, the energy is independent of lap length.

One challenge with single lap shear test is that the large amount of joint rotation resulting in a mix-mode loading at the joint. Therefore, especially for the debonding energy evaluation of soft materials, due to deformation of the adherends, peel stresses rather than shear stresses dominate lap joint fracture, the results are quite different from other tests.

(b) Peeling test

The peel test where a thin adhesive strip backed with a stiff layer, is peeled at a constant velocity from the surface of a usually rigid substrate, is typically used to measure the adhesion of tapes and the peel force per unit width of tape is used as a measure of the adherence energy. The experiment is normally carried out at a constant peel angle and by applying either a constant peel velocity or a constant load. Although the effect of the peel angle has been the object of several studies, most materials are tested with at a peel angle of 90 °or 180 °. (Figure 2.5)

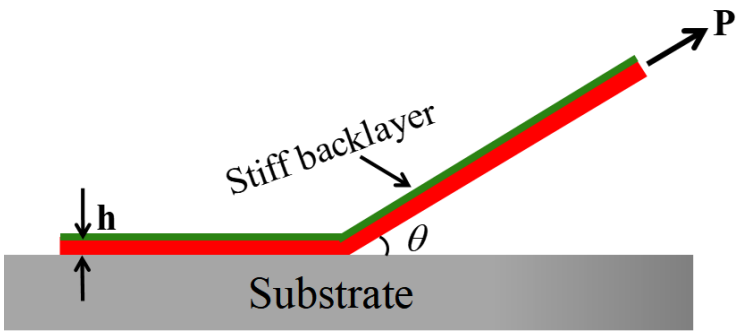

Figure 2.5 Schematic of a peel test.

If the peel angle is not too small, the strain energy release rate is given by,

$$G_C = \frac{F}{b}(1-\cos\theta)$$

Where b is the width of the peeled strip. This reduces to $G=2F/b$ for a T-peel test.

The peel test applies a rather complex strain field in the region of the debonding front, resulting from a coupling between the bending stiffness of the backing and the mechanical properties of the deformable adhesive. However, the advantage is to focus on steady-state

propagation of a crack rather than on its nucleation. And the soft adhesive material is reinforced with a backing that is much stiffer in tension than the adhesive, avoiding to account for the tensile deformation of the arm.

(c) Probe tack test

The probe tack test has been used most extensively to investigate adhesion of soft viscoelastic materials, where a cylindrical, fat or hemispherical-ended probe is pulled at constant speed from an adhesive layer. The method provides very different and complementary information on the adhesive properties of soft materials. In this test an adhesive layer is first compressed between a fat ended cylindrical probe of radius and a hard substrate. After a set contact time, the probe is removed from the surface at a constant velocity V_{deb} and the load F is measured as a function of time or distance, as showed in figure. The results of a probe test are a force versus displacement curve. This curve is usually transformed into a nominal stress *vs.* nominal strain curve, which is obtained by normalizing the force by the maximal area of contact A during the compression stage (related to the probe radius a_0) and the displacement by the initial layer thickness. Several main parameters can be extracted from the curve: the peak stress, the maximum extension, the plateau stress and the work of debonding (Figure 2.6).

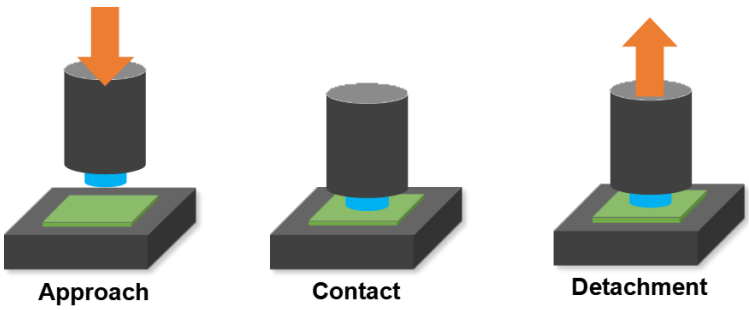

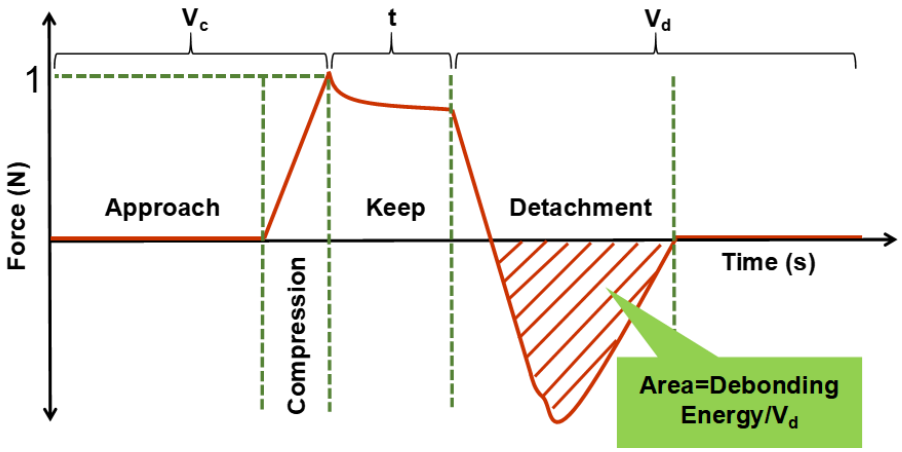

Figure 2.6 Schematic of a probe tack test used to measure adhesion of soft materials.

$$\sigma_{adhesion} = \frac{F_{\max}}{A}$$

$$\varepsilon_{\max} = \frac{d_{\max} - d_0}{d_0}$$

$$W_{deb} = \int_0^{l_0} \sigma dl$$

The advantage of the probe test is the application of a well-defined displacement field to the deformable adhesive. Moreover, a well-defined strain history can be applied to the adhesive before debonding, although the effect of the compression/decompression stage is ignored in most experimental investigations on soft adhesives. The nominal stress-strain curve obtained from the test can be compared for different materials and different test conditions providing significantly more information than the simple value of the peel force. The shape of the stress-strain curve reveals details about the deformation mechanisms. However, the probe test does not provide information on steady-state propagation data from probe tests cannot be easily compared in a quantitative way to a model or to a simulation.

2.2 A brief review of advancements in developing underwater adhesives

It could be found many uses for effective underwater adhesives-attaching sensors, beacons, or ordnance under the waterline, stopping watery leaks, and in medicine, repairing wet tissues. However, Synthetic adhesives developed for dry applications perform poorly on wet surfaces, or underwater. Adhesive scientists have made prominent progress in developing adhesives which perform well to wet or underwater substrates. Herein, they are mainly classified as three categories according to the bonding types.

2.2.1 Bio-inspired interfacial chemistry adhesion: catechol-based materials used as underwater adhesives

Nature has developed protein-based adhesives whose underwater performance has attracted much research attention over last few decades [14-17]. Rich catechols combined with amphiphilic and ionic features are founded in the adhesives. Hydroxylated tyrosine, known as l-3, 4-dihy-droxyphenylalanine (DOPA), has been confirmed to be of importance in natural adhesives and synthetic mimics. This secures the strong adhesion to a variety of underwater surfaces. For instance, barnacles use secretions to glue calcareous base plates to rocks [5, 18], mussels use a network of threads to attach their soft invertebrate [5] body to hard surfaces, and both sandcastle worms and caddisfly larvae assemble a protective tubular shell by gluing together sand grains or stones [19]. The versatile supra-molecular interactions used in such protein-based adhesives mainly include electrostatic interactions, hydrogen bonding, hydrophobic forces, π–π interactions, metal coordination, cation–π complexation, and dynamic covalent linkages

(Figure 2.7).

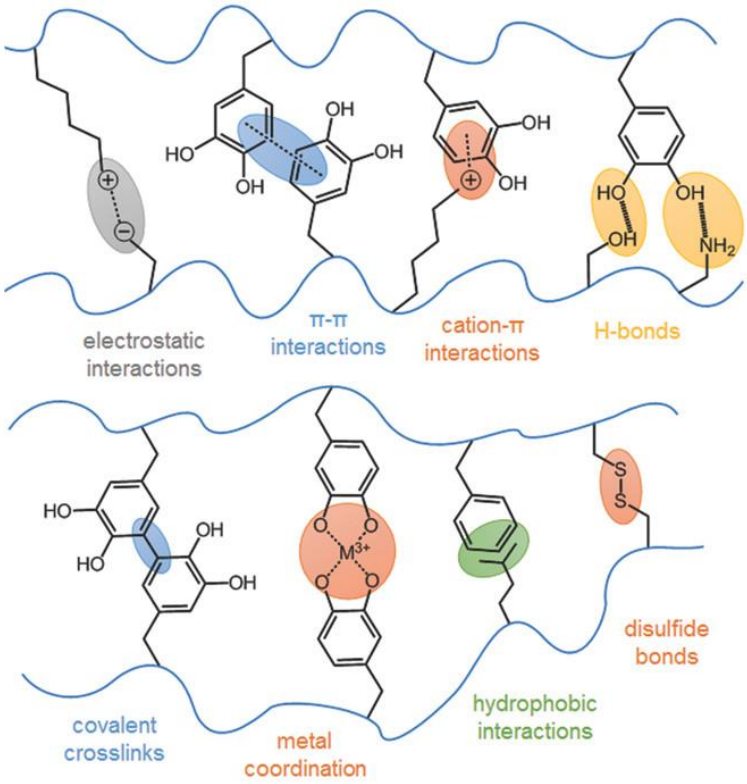

Figure 2.7 Overview of the different adhesive and cohesive interactions as found in or hypothesized for wet adhesion by sandcastle worms and mussels. Color codes used for each interaction correspond to the different sections of this review. Blue section: covalent bonding and π–π interactions; grey section: ionic bonding; yellow section: hydrogen bonding; green section: hydrophobic interactions; and orange section: metal coordination; cation–π interactions and dynamic covalent bonding [5].

(a) Sandcastle worms

Sandcastle worms, are marine organisms who build protective shells which are formed from minerals found in their surroundings. The mineral particles, such as sand grains or pieces of shell, are glued together underwater with a bio-adhesive packaged in granules that are secreted from adhesive glands. After an initial curing period of less than 30 s, the

adhesive is strong enough to hold the particles in place. In the next hours, a second curing step follows which darkens the color caused by the oxidation of DOPA. The resulting cement is a porous solid with the pores being filled with liquid (Figure 2.8). The adhesive proteins in sandcastle worms can roughly be divided into two groups: anionic proteins and cationic proteins. All of the proteins contain at least 10% aromatic amino acids including tyrosine and DOPA.

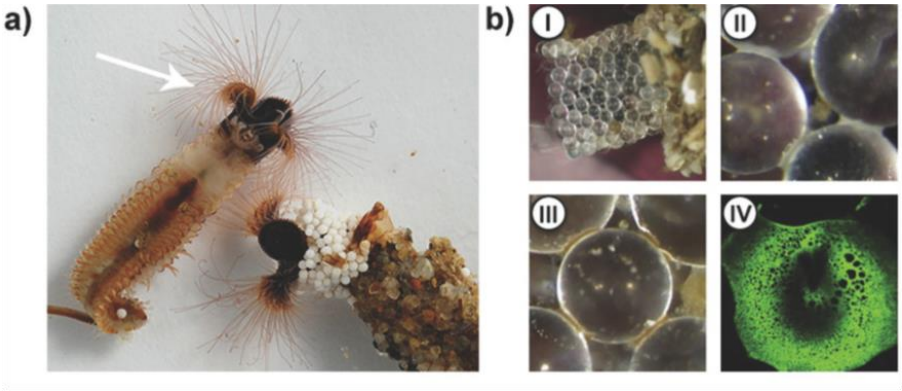

Figure 2.8 Image of sandcastle worms; the worms are depicted inside and outside their protective shells. New particles are placed onto the shell by its ciliated tentacles (white arrow). The shells in the figure were partially built in a laboratory environment, explaining the different colors of the granules [5]. b) Glass beads can also be used by the worms for building shells (I). The adhesive was only applied around the contacts of the beads and spread over the surface, which suggests a low interfacial tension (II). After protein secretion, the initially white glue turned brownish in a few hours as a result of DOPA oxidation (III). The final adhesive has a porous, foam - like structure (IV) [20-21].

(b) Mussels

Mussels are marine organisms that stick to surfaces using their byssal threads. These threads consist of three parts: the adhesive plaque, the rigid distal thread, and the flexible proximal thread, which are all coated by cuticle. The byssal thread is formed by the mussel foot, a flexible organ that is pressed against the surface that the mussel aims to adhere to (Figure 2.9). After all proteins have been secreted, the mussel retracts its foot, and the byssal thread can obtain its final properties through equilibration with the environment. A significant amount of DOPA is found in mussel foot proteins (mfps) which are mainly responsible for the adhesion of plaque to the surface [17].

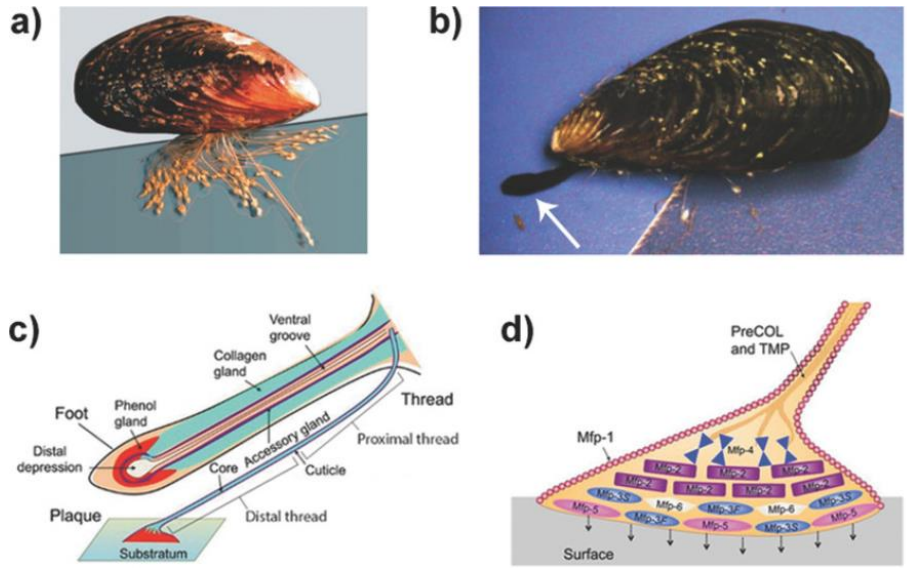

Figure 2.9 Image of an adult mussel, a) that secreted multiple byssal threads b) from the mussel foot (white arrow). The foot is extended from the shell and attaches to the surface before protein secretion. c) Firm attachment to the surface takes place by lifting the ceiling of the distal depression; then, the byssus proteins are secreted into the ventral groove. The phenol gland (red) secretes the proteins that form the plaque (red). The proteins secreted from the collagen gland (green) form the core of the thread (green). The accessory gland (purple) secretes mfp - 1 proteins for the cuticle (purple). d) After protein

secretion, the mussel foot retracts, leaving the byssus behind in which the proteins are highly organized. [17].

DOPA is thought to play a dominant role in both dehydration of and binding to the surface. A submerged hydrophilic surface is generally covered by a layer of ions, water, and several other compounds. For proper adhesion, this layer has to be removed first. Several mimics shown that DOPA efficiently dehydrated surfaces. These experiments also revealed that dehydration was enhanced when DOPA was in the proximity of cationic lysine or incorporated into a coacervate of polyampholytic peptides. After dehydration, DOPA can adhere to a surface by using different mechanisms such as hydrogen bonding, metal oxide coordination, or cation–π interactions. Other amino acids may contribute to adhesion by electrostatic or hydro-phobic interactions.

(c) Catechol-based mimic materials used as underwater adhesives

Based on the studies on sandcastle worms and mussels, the most common method to design biomimetic underwater adhesives is to incorporate DOPA or another catechol functionality into the material such as chitosan, poly (ethylene glycol) (PEG), hyaluronic acid, and alginate [22-23]. A significant amount of studies have successfully developed good underwater water adhesives by incorporating DOPA or another catechol functionality into the material, and the presence of DOPA has been implicated to be the key component that governs adhesion and cohesion of the adhesives. Catechols are able to interact with substrates via hydrogen bonding, metal-catechol coordination or cation-π complexation. However, recent findings have indicated that catechol moieties alone are insufficient to ensure proper underwater adhesion and that the performance is also

determined by other factors. Combinations of noncovalent interactions are highly important to ensure good underwater adhesive performance. Besides, despite the substantial progress, several questions remain. For instance, DOPA is readily oxidized to DOPA-quinone which will reduce the adhesion sharply. Both sandcastle worm and mussel glue are porous solids, but the formation mechanism and the effect on the mechanical properties are not fully understood. Connecting the chemical interactions, the structure and the resulting material properties is essential in developing bio-inspired strategies when developing improved adhesives.

2.2.2 Structural design adhesion

In addition to chemical interactions, the structure design of adhesive is also of great importance to the performance of underwater adhesives. Many organism shows impressive and reversible adhesion performance without special surface chemical secretions such as Geckos [2, 10, 12], tree frogs [24-25], octopus [26-27], echeneid fishes [28-29] and cling fishes [30]. According to the features and mechanism of underwater adhesion, they can be classifies as two categories, the hierarchical surface structures and suction cups.

(a) Hierarchical surface structures

The amazing reversible adhesion of gecko pads to almost any kind of surfaces owes to a fine structure of hierarchically arranged fibrils (Figure 2.10), which enable them to exploit Van der Waals and capillary forces with great efficiency [10]. Similar structures can also be found in tree frog pads and Cling fish's disk. The physical principle of the hierarchical structures on the great improvement of adhesion owes to the contact splitting principle

which we have discussed in **Chapter 2.1.3**. Fibrillar surfaces show smaller effective elastic modulus than planar surfaces, which make resulting in that they can deform easily and form contact effectively, especially for the rough substrates. The elastic-strain energy stored in single fibrils during pull-off is dissipated and then the separation work is higher than for a planar contact of similar material. Moreover, fibrillar structures required frequent re-initiation of the interface crack and the failure of the interface therefore occurs at higher stresses and debonding energy. Researchers have displayed the criteria graphically in the form of adhesion design maps (Figure 2.11) which offer a good starting point for design optimization.

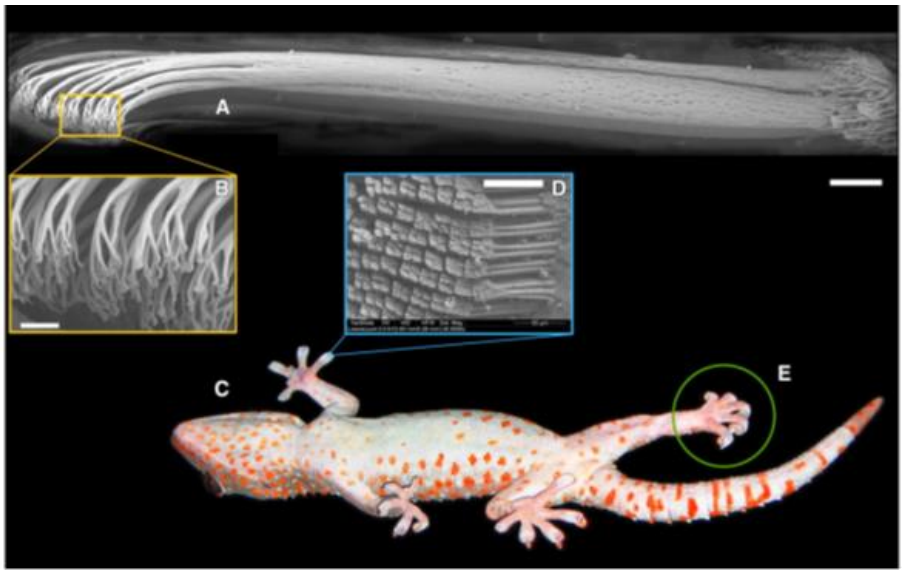

Figure 2.10 Gecko adhesive system. (A) Micrograph of a single gecko seta assembled from a montage of five Cryo-SEM images (image by Stas Gorb and K. Autumn). (B) Nanoscale array of hundreds of spatular tips of a single gecko seta. (C) Ventral view of a tokay gecko (Gekko gecko) climbing a glass surface. (D) Array of setae are arranged in a nearly grid-like pattern on the ventral surface of each scansor. In this scanning electron micrograph, each diamond-shaped structure is the branched end of a group of four setae

clustered together in a tetrad. (E) Toe peeling during detachment. Scale bars, 50 μm (D), 5 μm (A), 1 μm (B) [2].

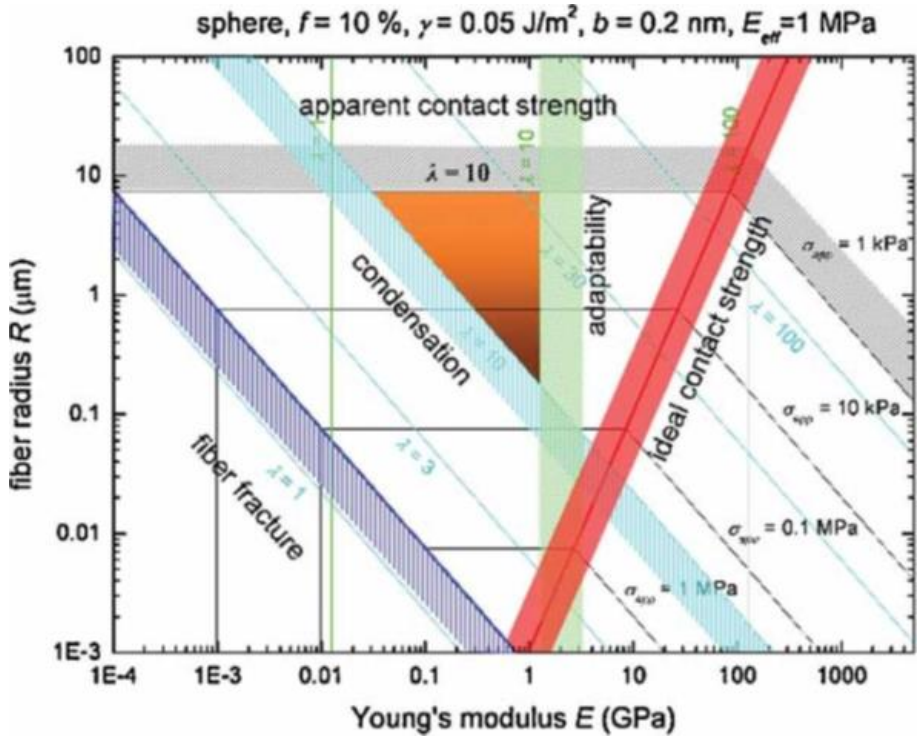

Figure 2.11 Adhesion design map for spherical contact elements. The triangular target area delineates the preferred parameter space for this specific structure Copyright 2005, Elsevier [31].

Moreover, the influence of the fiber geometry on adhesion is also extensively investigated. For flat tips, the pull-off strength increases with $r^{-0.4}$, where r is the fibril radius; Depending on the aspect ratio (AR) of the fibrils, different contributions to the dissipation of elastic energy are present: for AR lower than 0.8, the elastic energy stored in the system is dominated by the deformation of the backing layer, while for higher AR it arises from

bending of the fibrils. The bending contribution increases strongly with fibril AR, leading to increased adhesion up to a limiting value due to buckling and condensation of fibrils; For tip shape, mushroom-shaped tips have so far given the highest adhesion strength values of all polymeric fibers (Figure 2.12) [32]. They also show the highest potential for adhesion enhancement by contact splitting; For tilt angle, there is a large difference in shear stresses when tested parallel to the tilting direction; For hierarchy, theoretical studies have predicted that the hierarchical arrangement of geckos fibrils is essential to provide: mechanical stability of the fibril designs with longer fibers; the ability to conform to roughness at different length scales; to increase the energy needed for crack propagation; For backing layer, an increase in the adhesion force with decreasing thickness of the backing layer was found experimentally on patterned PDMS samples with flat-terminated fibrils and PU patterns with mushroom-terminated fibrils. It can be explained as follows, thin backing layers promote equal load sharing during pull-off and maximize adhesion. Thick backing layers deform during pulling and this leads to stress concentrations at the edge of the substrate, similar to a rigid punch in adhesive contact with a half space [33]. Generally, the backing layer has a more important contribution to the overall adhesion behavior for substrates with low-AR fibrils.

When it comes to the adhesion under wet environments, it was found that the maximum adhesion force was measured at lower fibril density. This result is not compatible with a dominating gecko-like adhesion mechanism. On the other hand, patterned elastic materials coated with a copolymer containing a high amount of catechol show dramatic increase in adhesion forces in wet environment over noncoated control samples. However, such values cannot be extrapolated to macroscopic surfaces. And viscoelastic materials

have not been considered for fibrillar surfaces even though the viscoelastic effect may contribute the adhesion.

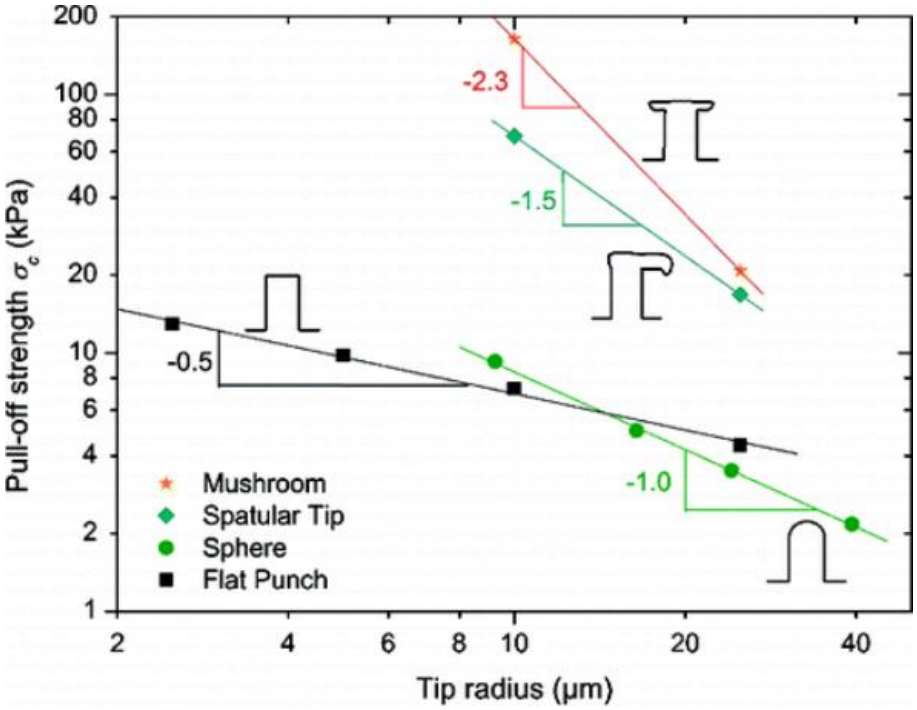

Figure 2.12 The effect of the tip shape, which was varied systematically in fibrillar PDMS surfaces, produced by lithographic and soft-molding methods. For fiber radii between 2.5 and 25 μm, it is found that shape exerts a stronger effect on adhesion than size. The highest adhesion is measured for mushroom-like and spatular terminals, which attain adhesion values 30 times in excess of the flat controls and similar to a gecko toe [32].

(b) Suction cups structures

The octopus sucker represents a fascinating natural system performing adhesion on different substrates. Suckers are muscular-hydrostats [34]; and a single sucker consists of

two general regions connected by a constricted orifice: the infundibulum, the exposed disk-like portion of the sucker, and the acetabulum, the upper hollow portion, which consists of a domed roof (in the upper part) and a wall region (in the remaining parts), as shown in Figure 2.13. In the first stage, a tight seal that prevents water from leaking is formed at the rim. Infundibular radial muscles begin to contract (black arrows) to increase the contact area between (flattened) infundibulum and substrate (Figure 2.14); then the contraction (black arrow) of acetabular radial muscles creates suction and moves water from infundibulum substrate interface toward the acetabulum (blue arrows), as well, enhancing attachment; In the third stage, meridional muscles of acetabulum contract (black arrows), allowing the protuberance makes contact with the upper part of the side walls of the orifice; meanwhile, the acetabular radial muscles are still contracted (gray arrow). Rough surfaces of both orifice and acetabular roof (coming into contact) contribute to adhesion. A torus of water is created in the acetabular cavity around the protuberance itself; finally, acetabular radial and meridional muscles stop to contract. The protuberance is passively kept in contact with the upper part of the side walls of the orifice, due to the cohesive force of water in the infundibular compartment and the friction of the two roughness surfaces that are in contact (acetabular protuberance and upper part of side walls of orifice). These two forces are balanced by the elastic restoring force of acetabular protuberance (Figure 2.14).

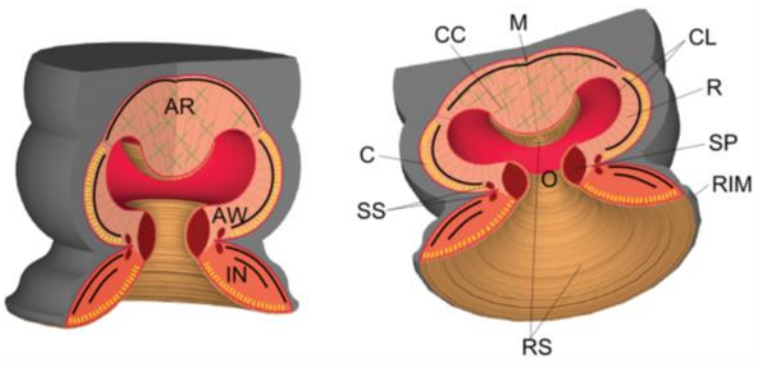

Figure 2.13 Schematic of the octopus suckers. AR, acetabular roof; AW, acetabular wall; C, circular muscle (yellow sections); CC, cross connective tissue fibers (green crosses); CL, connective tissue layer; IN, infundibulum; M, meridional muscle (black lines); O, orifice; R, radial muscle (gray dotted line); RIM, rim around the infundibulum; RS, rough surface located on the surface of the infundibulum, orifice and acetabular protuberance; SP, primary sphincter muscle; SS, secondary sphincter muscle [34].

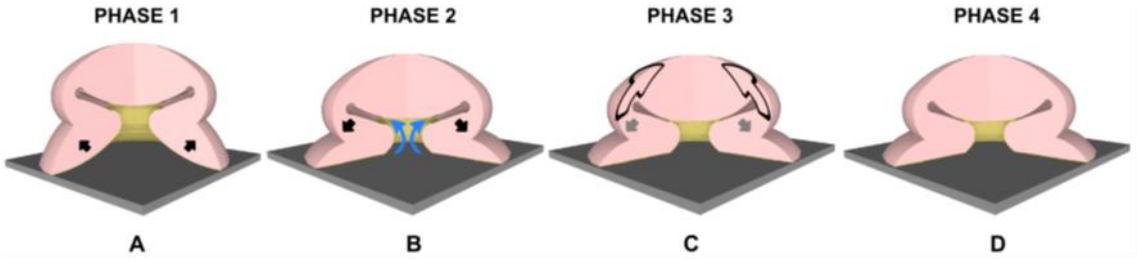

Figure 2.14 Schematic view, in four phases, of the adhesion mechanism proposed for the Octopus sucker. A) Forming of a tight seal that prevents water from leaking at the rim. B) Contraction (black arrow) of acetabular radial muscles creates suction and moves water from infundibulum-substrate interface toward the acetabulum (blue arrows), as well, enhancing attachment; C) Meridional muscles of acetabulum contract (black arrows), D) Acetabular radial and meridional muscles stop to contract. [34].

Inspired from the octopus suction cups, a team of researchers at Sungkyunkwan University in South Korea has developed a type of adhesive patch that works under a variety of conditions including underwater [35]. They mimicked the suction cups by creating polymer sheets with cup-like dimples with soft spheres in the middle of each.

They then tested differently sized dimples and spheres and found that 50 micrometer dimples offered the best grip, which, as it turned out, was the one closest to that used by an octopus in its underwater world. To better understand how the suction cups worked, the researchers studied their own creations under a microscope and discovered the secret to the octopus grip is water getting trapped beneath the sphere near the back edges of the cup-it creates a vacuum chamber when pressure is released. Another work inspired from the remora suckerfish is developed by combining a seal and many divided chambers. The independent chambers inside the big seal make the pads can conform to rough surfaces.

2.2.3 Mechanical interlock bonding

Mechanical interlocking is a common type of adhesion, which involves the adhesive penetrating into the adherend and becoming mechanically interlocked at some level. The mechanical interlocking adhesives are stable and have a high adhesion strength and energy dissipation (usually cohesion failure occurs), and most of the bonding joint is irreversible. Many adhesives developed by mechanical interlocking are applied for tissue engineering. Herein, several typical adhesives developed by researchers are briefly explained.

Inspired by the worm's swelling mechanism, Karp and his team created an adhesive patch that mechanically interlocks with tissue through swellable micro-needle tips [7]. The tips plump up via a water-based mechanism that is both quick and reversible. The adhesion strength of the tips of the micro-needle is more than three times stronger than conventional surgical staples used for skin grafts fixation.

Gong and co-workers, invented the double network (DN) hydrogels which are considered

as attractive candidates for fabrication of artificial cartilages because of their extremely high mechanical strength and low friction. And they attempted to bond DN hydrogels with a porous solid substrates trough a gradient structure. This method results in a DN structure mechanically interlocked with the porous solid substrate. It is found that the strength of the gel-substrate interface depends on the pore size of the solid substrates. Porous solids, with pore sizes in the order of several micrometers, result in the formation of strong gel-substrate interfaces. Under optimal conditions, the bonding strength between the gel and the substrate is comparable to the bonding strength of the bulk DN gel [36].

Recently, Suo and co-workers report a bio-inspired design for adhesives consisting of two layers: an adhesive surface and a dissipative matrix. The former adheres to the substrate by electrostatic interactions, covalent bonds, and physical interpenetration. The latter amplifies energy dissipation through hysteresis. The two layers synergistically lead to higher adhesion energies on wet surfaces as compared with those of existing adhesives. Adhesion occurs within minutes, independent of blood exposure and compatible with in vivo dynamic movements [37].

2.3 Hydrogels adhesives

Recent progress on the development of various hydrogels with high robustness, large deformation capacity, and diverse functions indicates the great promise of the class of materials for various applications. Hydrogels, have immense potential as wet adhesives. Firstly, with the hydrophilic nature, hydrogels have less effect coming from water penetration and decomposition on adhesion compared with other materials. Secondly,

hydrogels with extremely high toughness have been achieved such as double network (DN) hydrogels reported by Gong and co-workers. The high toughness ensure the high cohesion strength of the materials, which is also an important factor to develop a tough underwater adhesives. Moreover, due to the high biocompatibility, there are strong demands in applications including tissue engineering, bio-medical devices, and medical operations.

Prominent progress has been achieved on the irreversible robust bonding of hydrogels to diverse synthetic and biological surfaces, which show that chemical bonding or physical interlocking of the interface and bulk energy dissipation are of great importance for the robust bonding of hydrogels [38]. However, the research for in situ underwater adhesion of hydrogels is still in its infancy, which suffers from shortcomings including short contact forming time and very weak adhesion strength. A general understanding of the underwater contact behaviors and strategy to develop roust hydrogels is required.

2.4 In situ observation of underwater surface contact evolution

Although probe tack test can be used very effectively to gain some information on the mechanisms of debonding of the adhesive [13]. It provides some unique advantages in terms of controlling the experimental parameters. The applied compressive force, contact time and debonding rate can be easily independently controlled and the experiment can be done in a temperature-controlled chamber. However, the detail information on deformation mechanisms of adhesive in a real time during the debonding process is still absent. In situ observation the evolution of contact surface can supplement the information for understanding the details of adhesion behaviors. A side view of the probe

can give a clear indication of the existence of the fibrils in the late stages of debonding. Unfortunately, fibril size and spacing cannot be obtained from such a side view of a cylindrical probe as only the outside surface of the fibrillating structure is visible. A more useful observation viewpoint, from aquantitative analysis standpoint, is underneath the adhesive layer.

Various studies have been done for the growth kinetics of cavities at the interfaces by in situ observations with side view and underneath viewpoint. However, when it comes to the contact information of hydrogels with substrates, the method will compromise due to most of the refractive index of hydrogels is very close to that of water. A novel method to observe the macroscopic contact of hydrogels to solid surface based on the principle of critical refraction was discovered previously [39]. The principle for the observation of gel-glass interface, based on the critical refraction, is shown in Figure 2.15. As the glass have a higher refractive index than the gel, the light from the gel side refracts at angles less than the critical refraction angle θ_{gel}, where $\sin\theta_{gel} = n_{gel}/n_{glass}$. If there is water layer at the interface between the gel and glass, the critical refraction angle θ_{water} is determined by $\sin\theta_{water} = n_{water}/n_{glass}$. Since the refractive index of hydrogel is slightly larger than that of water, the contact can be observed from an angle between these two critical angles. In this case, when the gel is in contact with the substrate, a bright image will occur, while a black image is observed when a water film exists at the interface.

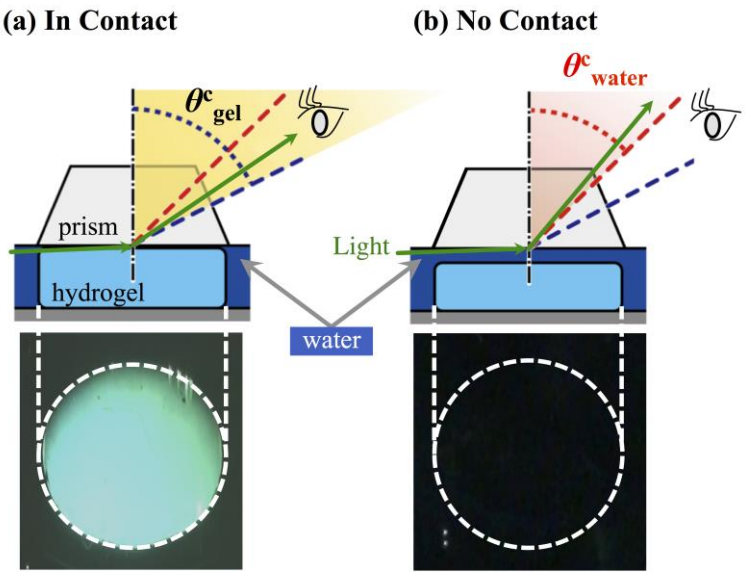

Figure 2.15. Schematic illustration for the observation of gel-glass contact based on the principle of critical refraction using a trapezoidal prism. In (a), where the gel is in contact with the glass prism, the light comes from the gel refracts at the angle less than θ_{gel}.While, in (b), where a water film exists at the gel-glass interface, the light comes from the water film refracts at the angle less than θ_{water}. Here, a bright image of gel is observed in (a), and a black image is observed in (b) [39].

2.5 Conclusion and objectives of this manuscripts

Despite a great progress on irreversible underwater adhesives has been made, several challenges still exist to develop the underwater hydrogels adhesives. Firstly, the thin hydration layer on the substrate prohibits the intimate contact, and thereby create an obstacle for achieving satisfying wet adhesion. Water drainage between two approaching surfaces should be considered. Depending the contact area and normal pressure, it may take a very long time to squeeze out the interface water during the contact process. Another challenge is that, hydrogels usually are soft and hydrophilic in their fully swallow

state, with the decreasing of the stiffness and increasing of the surface bonding, water drop can be easily trapped at the interfaces, which not only create an obstacle for achieving good contact, but also acts as defect to initiate the bonding joint. Thirdly, hydrogels usually favor, themodynamically, the formation of a water film at the interface owing to the strong hydration ability of hydrophilic polymer strands, which prevents the formation of molecular bridges at the interface. Moreover, to decrease the production cost, reversible or reusable underwater adhesives are required, to achieve a high debonding energy, viscoelastic effect of the adhesive matrix should be also taken into considered.

In this thesis, in situ underwater adhesion behaviors of hydrogels crosslinked with dynamic bonds are explored by using a homemade system to observe the contact evolution in situ. Strategies to develop hydrogels adhesives with fast contact formation underwater are proposed and energy dissipation of the matrix contributing to the adhesion are discussed.

References

[1] Marshall, S. J., Bayne, S. C., Baier, R., Tomsia, A. P. & Marshall, G. W. J. d. m. A review of adhesion science. 26, e11-e16 (2010).

[2] Autumn, K. et al. Evidence for van der Waals adhesion in gecko setae. 99, 12252-12256 (2002).

[3] Fowkes, F. M. J. J. o. A. S. & Technology. Role of acid-base interfacial bonding in adhesion. 1, 7-27 (1987).

[4] Yoshida, Y. et al. Evidence of chemical bonding at biomaterial-hard tissue interfaces. 79, 709-714 (2000).

[5] Hofman, A. H., van Hees, I. A., Yang, J. & Kamperman, M. J. A. M. Bioinspired Underwater Adhesives by Using the Supramolecular Toolbox. 30, 1704640 (2018).

[6] Liu, Z. et al. High‐Adhesion Stretchable Electrodes Based on Nanopile Interlocking. 29, 1603382 (2017).

[7] Yang, S. Y. et al. A bio-inspired swellable microneedle adhesive for mechanical interlocking with tissue. 4, 1702 (2013).

[8] Chen, C. M., Chiang, C. L., Lai, C. L., Xie, T. & Yang, S. J. A. F. M. Buckling‐based strong dry adhesives via interlocking. 23, 3813-3823 (2013).

[9] de Gennes, P.-G., Brochard-Wyart, F. & Quere, D. J. B., Pearls, Waves. Capillarity and Wetting Phenomena: Drops. 291 (2004).

[10] Boesel, L. F., Greiner, C., Arzt, E. & Del Campo, A. J. A. M. Gecko‐inspired surfaces: a path to strong and reversible dry adhesives. 22, 2125-2137 (2010).

[11] Kendall, K. J. J. o. P. D. A. P. The adhesion and surface energy of elastic solids. 4, 1186 (1971).

[12] Bartlett, M. D. et al. Looking beyond fibrillar features to scale gecko‐like adhesion. 24, 1078-1083 (2012).

[13] Creton, C. & Ciccotti, M. J. R. o. P. i. P. Fracture and adhesion of soft materials: a review. 79, 046601 (2016).

[14] Lee, H., Lee, B. P. & Messersmith, P. B. J. N. A reversible wet/dry adhesive inspired by mussels and geckos. 448, 338 (2007).

[15] Zhao, Y. et al. Bio-inspired reversible underwater adhesive. 8, 2218 (2017).

[16] Zhao, Q. et al. Underwater contact adhesion and microarchitecture in polyelectrolyte complexes actuated by solvent exchange. 15, 407 (2016).

[17] Lee, B. P., Messersmith, P. B., Israelachvili, J. N. & Waite, J. H. J. A. r. o. m. r. Mussel-inspired adhesives and coatings. 41, 99-132 (2011).

[18] Kamino, K. in Biological adhesives 153-176 (Springer, 2016).

[19] Stewart, R. J., Ransom, T. C. & Hlady, V. J. J. o. P. S. P. B. P. P. Natural underwater adhesives. 49, 757-771 (2011).

[20] Stewart, R. J., Wang, C. S., Song, I. T., Jones, J. P. J. A. i. c. & science, i. The role of coacervation and phase transitions in the sandcastle worm adhesive system. 239, 88-96 (2017).

[21] Endrizzi, B. J. & Stewart, R. J. J. T. J. o. A. Glueomics: an expression survey of the adhesive gland of the sandcastle worm. 85, 546-559 (2009).

[22] Lee, H., Scherer, N. F. & Messersmith, P. B. J. P. o. t. N. A. o. S. Single-molecule mechanics of mussel adhesion. 103, 12999-13003 (2006).

[23] Faure, E. et al. Catechols as versatile platforms in polymer chemistry. 38, 236-270 (2013).

[24] HANNA, G., Jon, W. & BARNES, W. J. J. J. o. E. B. Adhesion and detachment of the toe pads of tree frogs. 155, 103-125 (1991).

[25] Green, D. M. J. C. Adhesion and the toe-pads of treefrogs. 790-796 (1981).

[26] Tramacere, F., Beccai, L., Sinibaldi, E., Laschi, C. & Mazzolai, B. J. P. C. S. Adhesion mechanisms inspired by octopus suckers. 7, 192-193 (2011).

[27] Tramacere, F., Beccai, L., Mattioli, F., Sinibaldi, E. & Mazzolai, B. in Robotics and Automation (ICRA), 2012 IEEE International Conference on. 3846-3851 (IEEE).

[28] Fulcher, B. & Motta, P. J. C. j. o. z. Suction disk performance of echeneid fishes. 84, 42-50 (2006).

[29] Nadler, J. H. et al. Structures and function of remora adhesion. 1498, 159-168 (2013).

[30] Wainwright, D. K., Kleinteich, T., Kleinteich, A., Gorb, S. N. & Summers, A. P. J. B. l. Stick tight: suction adhesion on irregular surfaces in the northern clingfish. 9, 20130234 (2013).

[31] Spolenak, R., Gorb, S. & Arzt, E. J. A. b. Adhesion design maps for bio-inspired attachment systems. 1, 5-13 (2005).

[32] Del Campo, A., Greiner, C. & Arzt, E. J. L. Contact shape controls adhesion of bioinspired fibrillar surfaces. 23, 10235-10243 (2007).

[33] Kim, S., Sitti, M., Hui, C.-Y., Long, R. & Jagota, A. J. A. P. L. Effect of backing layer thickness on adhesion of single-level elastomer fiber arrays. 91, 161905 (2007).

[34] Tramacere, F. et al. The morphology and adhesion mechanism of Octopus vulgaris suckers. 8, e65074 (2013).

[35] Baik, S., Park, Y., Lee, T.-J., Bhang, S. H. & Pang, C. J. N. A wet-tolerant adhesive patch inspired by protuberances in suction cups of octopi. 546, 396 (2017).

[36] Nonoyama, T. et al. Double‐network hydrogels strongly bondable to bones by spontaneous osteogenesis penetration. 28, 6740-6745 (2016).

[37] Li, J. et al. Tough adhesives for diverse wet surfaces. 357, 378-381 (2017).

[38] Yuk, H., Zhang, T., Lin, S., Parada, G. A. & Zhao, X. J. N. m. Tough bonding of hydrogels to diverse non-porous surfaces. 15, 190 (2016).

[39] Yamamoto, T. et al. In situ observation of a hydrogel–glass interface during sliding friction. 10, 5589-5596 (2014).

Chapter 3 Tough hydrogels with fast, strong, and reversible underwater adhesion based on a multi-scale design

3.1 Introduction

Recent progress on the development of various hydrogels with high robustness, large deformation capacity, and diverse functions indicates the great promise of this class of materials for various applications [1-11]. Due to their water-containing nature, the major potential applications of hydrogels are in wet environments, such as artificial organs, tissue engineering, bio-medical devices in the human body, and underwater soft robotics. In many such applications, permanent bonding or reversible attachment of hydrogels to other surfaces, synthetic or natural, hard or soft, is required. However, hydrogels usually show poor adhesion to other surfaces in their fully swollen state. Recently, prominent progress has been achieved on the irreversible robust bonding of hydrogels to diverse synthetic and biological surfaces, which shows that chemical bonding or physical interlocking of the interface and bulk energy dissipation are critical for the robust bonding of the hydrogels [12-19]. On the other hand, the research for in situ underwater adhesion of hydrogels is still at its born [20-22]. The state-of-the-art technology suffers from shortcomings including long contact forming time and very weak adhesion strength. A general strategy to develop hydrogels with fast, strong, and reversible adhesion underwater, is still lacking.

Realization of fast, strong and reversible underwater adhesion of soft materials needs to solve multi-scale and multi-factor problems, involving fluid mechanics, soft matter mechanics, material science, and surface chemistry [23-25]. At the macro-scale, the water drainage between two approaching surfaces should be considered. Depending on the

contact area and normal pressure, it may take a very long time to squeeze out the interface water during the contact process [26, 27]. At the inter-mediate scale, the permanent water entrapment usually occurs at the soft interface. The stronger the adhesion and the softer the gel, the easier it is for water to become trapped. This not only reduces the true contact area, but also acts as a flaw for initiating the debonding at the interface [28,29] At the nanoscale, the hydrogels usually favour, thermodynamically, the formation of a water film at the interface owing to the strong hydrating ability of hydrophilic polymer strands, which prevents the formation of molecular bridges at the interface [30].

In this chapter, we present a design strategy to obtain hydrogels with fast, strong, and reversible adhesion underwater by combining energy dissipative hydrogels with dynamic bonds and bio-inspired surface drainage architecture.

3.2 Experiments

3.2.1 Materials choices and preparation

1) Synthesis of PA patterned hydrogels. The tough polyampholyte (PA) hydrogels were prepared by the random copolymerization of NaSS and DMAEA-Q at a NaSS : DMAEA-Q monomer ratio of 0.52 : 0.48, as described in previous studies [1] . An aqueous solution containing 2.5 M total monomer concentration, 2.5 mM, 2-oxoglutaric acid as UV initiator, and 2.5 mM N,N-methylenebisacrylamide crosslinker was poured into a reaction cell consisting of a piece of fresh glass plate and a piece of silicone mold separated by a silicone spacer of prescribed thickness. Then the reaction cell was irradiated with 365 nm UV light for 10 h. To remove the oxygen, the silicone mold and spacer were placed in an Ar atmosphere before use for more than 36 h. After polymerization, the gel was immersed

in excess amount of water for 1 week to dialyze the mobile counter-ions, and allow the oppositely charged polyions on the copolymers to form stable ionic complexes through intra- or inter-chain interactions. The PA gel deswelled to 87.5% of its as-prepared size in each direction after dialysis, and became very tough.

To induce surface groove features, the gelation of the PA gels was performed in a rectangular reaction cell with a t'=2.0 mm thick spacer where one cell wall was made from a silicone mold with honeycomb-like grid structure. The width (w') and height (h') of the grid molds were kept constant at 0.75, and 0.5 mm, respectively, while the hexagon side length (a') of the ridge varied from 1 to 2 mm. By using this method, we obtained PA gels with flat hexagonal facets separated by interconnecting grooves. The size of the grooves on the PA gel surface was tailored using the grid of the mold and the total thickness of the gel using the silicone spacer, but all these sizes were reduced to 87.5% due to the deswelling of the gel by dialysis.

2) Synthesizing hydrogels with hydrogen bonds. The tough P($(PEG)_{200}$OMe-co-AAc) hydrogels (denoted as POA gels) with hydrogen bonds were prepared using the random copolymerization of the poly(ethylene glycol)$_{200}$ monomethyl ether monomethacrylate ($(PEG)_{200}$OMe) macromer, and acrylic acid (AAc) monomer with a 1.5 molar ratio of PEG segments in $(PEG)_{200}$OMe to pendant carboxylic acids in AAc. The POA hydrogels were prepared using the same procedure as the polyampholyte (PA) hydrogels from a dimethyl sulfoxide (DMSO) solution containing 2 M in total macromer and monomer, and 2 mM 2-oxoglutaric acid as UV initiator. After the gelation, the POA hydrogels were immersed in water to remove the DMSO and allow the forming of hydrogen bonds. The POA hydrogels deswelled to 81% of their as-prepared size in each direction in water.

3.2.2 *In situ* observation of the underwater contact formation evolution

Underwater contact formation evolution was observed using a homemade system as shown in. The observation was based on the critical refraction principle [2-4]. Since the hydrogel has a smaller refractive index than glass, but a slightly larger one than water, the light from the gel side reflects at angles between the critical angles of glass and water. A light image is observed when the gel is in contact with the substrate, and a black image when water drops exist at the interface. A 35 mm diameter disc shaped gel (flat or patterned) was placed on a plastic substrate in the stage box filled with water. An isosceles trapezoidal prism (angle 70 °, length 66 mm, height 22.08 mm, and width 50 mm), attached to the load cell using a rigid holder, approached the gel from the top at a steady 10 μm/s rate until the force reached the designed 15 N value. At the same time, the contact image of the gel on the prism surface was observed from an angle between the critical angles of water and gel using a zoom camera. The evolution of the contact image in time was subsequently recorded at the fixed displacement for different samples. The contact areas for these snapshots at different times were calculated using the Image-J software, and the contact area ratios were calculated respective to the nominal area of the flat sample or the hexagonal pads area of the patterned gels.

3.2.3 Measurements of underwater adhesion by probe tack test.

The probe tack tests, for measuring the adhesion strength and energy dissipation of the hydrogels, were performed on a Shimadzu Autograph AG-X 20KN tensile machine in water at 25 ℃. The set-up consisted of mainly two parts: the bottom part, a cell with a rigid stage providing the deionized water environment for the tack test, and the upper one,

a copper shaft connected with the load cell. The gel was cut into disc shapes of prescribed diameter, and bonded to the copper shaft using a very thin super glue (Konishi Co., Ltd.). We used copper plate, glass plate, polystyrene, flat gel, and pork heart tissue glued to the glass plate as counter substrates. The copper and glass plate we used were first washed by acetone and then washed by deionized water. The glass used was micro slide glass made by the MATSUNAMI Company of Japan (product number S2112). The glass carried negative surface charges, and the Zeta potential measured in 10 mM sodium chloride (NaCl) aqueous solution was -32.44 mV, measured by the Zeta potential and Particle size analyzer (ELSZ-2000, Otsuka Electronics Co., Ltd (Osaka, Japan)). The contact angle to water was 19.6±2.2 ℃ at 25 ℃. Polystyrene used for Petri dish is made by the IWAKI Company of Japan. Fresh pork heart, beef heart were purchased from Nippon Food Packer Inc. (Japan) and used as received without any surface pretreatment. Then the substrate was directly secured to the stage using a hard cover with screws. Before starting to measure, both parts were immersed in water and we waited for 30 min for the equilibrium state to be reached.

For the test, the upper gel was first compressed to the lower substrate at a constant compressing rate until it reached the set force (F). Afterward, the sample was held in this position for the described contact time (t). Subsequently, the probe was retracted at a constant rate until the debonding finished. The force, displacement, and time were recorded during the process.

3.2.4 Rheological test.

The rheological test was performed using an advanced rheometric expansion system (ARES) (Rheometric Science Inc.). A disc sample with a 15 mm diameter and a 2.5× 87.5% mm thickness, was glued between the metal plates and surrounded by water. A rheological frequency sweep from 0.01 to 100 rad/s was performed at a constant strain of 0.1% and at temperature of 25 ℃.

3.2.5 Underwater tensile test and hysteresis test.

The tensile test was performed using a tensile-compressive tester (TENSILON ORIENTEC RTC-1150A) underwater at 25 ℃. The sample was cut into a Dumbbell-shape with the JIS-K6251-7 standard size: 6×2×2 mm^3. The tensile velocity was 100 mm/min, corresponding to a 0.28 s^{-1} strain rate. The nominal stress was obtained by dividing the tensile force by the initial cross-sectional area of the sample.

The hysteresis test was performed using the same set-up and sample size as the underwater tensile test. The sample was first stretched to the designed critical strains ε= 3, 6, and 8, respectively with a 0.28 s^{-1} strain rate, followed by immediately unloading the sample to the original clamp position at the same loading-unloading velocity without waiting at the prescribed stretch peak. After the sample was held in this position for a waiting period, t, it was stretched to the same extension ratio, λ, and returned to the original position again, completing the second cycle. Subsequent tensile cycles were performed for various waiting times between two adjacent cycles. Hysteresis or energy dissipation was calculated from the area enclosed by the loading-unloading curve. The hysteresis ratio is calculated by hysteresis after the first loop divided by the hysteresis of the virgin samples.

3.2.6 Preparation of the silicone mold

A plastic mold (10 × 10 cm) with a concave honeycomb pattern was prepared using a 3D Keyence printer. The hexagonal honeycomb concave areas with a side length of 1 or 2 mm were separated by 0.5 mm high and 0.75 mm wide grooves. The mixed two-part polymers with 0.5 wt.% silicone solution curing agent for silicone rubbers was cased into the plastic mold, and the sample was placed in a vacuum chamber for 30 min to remove the bubbles. Subsequently, the sample was exposed to the moisture in the air at 25 ℃ for 24 h for curing the silicone rubber. After removing the plastic mold, we obtained a 5 mm thick silicone mold with honeycomb-like surface ridges, and the dimension of the ridge are 0.5 mm height (h'), 0.75 mm width (w') and 1 or 2 mm hexagonal side length (a').

3.3 Results and Discussion

We choose hydrogels with dynamic bonds for their high capacity of energy dissipation that favours toughness and strong adhesion. Most importantly, they are intrinsically adhesive in water. Since dynamic bonds are reversible in swollen hydrogels and contribute to the toughness and self-recovery of the hydrogels, they also have the potential to form reversible bridges with other surfaces in wet environments when properly choosing the surface chemistry of the substrates. In this study, we first select a charge-balanced polyampholyte (PA) hydrogel [31-33] with dynamic ionic bonds and then a tough and self-recovery hydrogel with dynamic hydrogen bonds. The PA hydrogels are generated by using the random copolymerization of the sodium p-styrenesulfonate (NaSS) anionic monomer, and the methyl chloride quarternized N,N-dimethylamino ethylacrylate (DMAEA-Q) cationic monomer, with a very small amount of chemical

cross-linker (Figure S1, Supplementary Information). Given the dynamic nature of the ionic bonds, the PA gel is strongly viscoelastic (Figure S2, Supplementary Information), and it exhibits superior strength and toughness (Figure S3a, Supplementary Information). Moreover, as revealed by the Mooney-Rivlin plot [34], it shows strain softening and then strain-hardening (Figure S3b, Supplementary Information). The gel also shows excellent self-recovery and the time for the full self-recovery increases with the applied strain (Figure S4, Supplementary Information). The ionic bonds exchanging time is in the ms range [32]. These results suggest that this PA gel is a suitable candidate as an underwater adhesive.

Then, in order to obtain fast water drainage at the gel-substrate interface, we analyzed the clingfish that shows fast and reversible adhesion to various surfaces underwater. The adhesive disc of the clingfish has many hexagonal features separated by interconnecting grooves (Figure 1a) that are considered to enhance the water drainage rate [35-36]. Inspired by the clingfish, we engineered the gel surface with hexagonal facets separated by interconnecting grooves (Figure 1b). Such interconnecting surface grooves serve as channels for fast water drainage during contact underwater (Figure 1c). Once the hexagonal facets are in contact with the substrate, the dynamic bonds of the hydrogel form bridges with the substrate (Figure 1d). In addition to the good contact formation, the discontinuous hexagonal facets also have effects on increasing the compliance of the gel and on preventing continuous crack propagation throughout the interface, similar to the contact splitting effect observed for micro-fibrillar surfaces [37-40]. These two effects significantly enhance the bulk gel energy dissipation [12,19,23] and delay the interfacial debonding (Figure 1e), leading to strong yet reversible adhesion.

To avoid water-drop trapping at the interface, we need to design hexagonal facets with proper sizes (Figure 1f). Since the water-drop trapping is governed by the competition between the elastic energy to deform the gel and the adhesive energy of the gel to the substrate, the size of the hexagonal facets should not be much larger than the elastic length, l0, that is determined by equation: l0=W/G', where W and G' are the adhesion energy per unit area of the gel to the substrate and the storage shear modulus of the gel, respectively [41]. The adhesion energy for the adhesion of a PA gel onto a glass substrate in air is ~50 J/m^2 [42]. Using the storage shear modulus G' of the PA gel as ~30 kPa at the low frequency limit (Figure S2, Supplementary Information), the elastic length of the PA-glass system is approximately 1 mm. Using silicone molds (Figure S5, Supplementary Information), we subsequently prepared two sets of gels having hexagonal facets of 0.875 mm (sample P1) and 1.75 mm (sample P2) in length (a). The height of hexagonal facets (h), groove width (w), and total thickness (h+t) were kept the same as 0.483, 0.656, and 2.19 mm, respectively, for the two samples. A control sample that does not contain hexagonal facets with the same total thickness was also prepared, labelled as sample P0 (see "Experimental Section" and Table S1, Supplementary Information). Figure 2a shows the typical optical and microscopic images of the surface engineered PA gel (P1). Well-defined hexagonal facets separated by grooves are formed on the gel surface.

To test the idea, we first observed the evolution of the contact formation underwater for flat and surface engineered PA gels using a home-made set-up using critical refraction [29] as shown in Figure 2b. In brief, a gel disc with diameter of 35 mm and total thickness of 2.19 mm was placed on the upper side of the substrate with the engineered surface. A trapezoidal prism, attached to the load cell, approached the gel in water from above, at a

steady rate of 10 μm/s until the normal force reached the 15 N designed value, and then was held in that position (Figure 2c-i, and c-ii). The corresponding nominal pressure estimated from the projected area of the sample surface was 15.6 kPa. During this process, the contact image of the gel to the prism surface was observed from an angle between the critical refraction angles of water θ_w and the gel θ_g (Figure 2b).

Figure 2d shows snapshots of the contact images, where the bright region is in contact with the glass and the dark region is trapped with water, for the three samples: P0, P1, and P2. For the flat PA gel (P0), the contact started from the periphery then gradually and irregularly developed into the whole region as time elapsed. The normal force rapidly reached the pre-set value after 22 s (Figure 2c-ii), although the gel was hardly in contact with the substrate yet, indicating that the interface is intermediated by water. Even after more than 1000 s, some regions still remained dark, with lots of dark points distributed heterogeneously, indicating the permanent entrapment of water (see Movie S1, Supplementary Information). It should be mentioned that the compressive strain rate applied to the sample, estimated from the contact rate and sample thickness, was about 4 $\times 10^{-3}$ s^{-1} (~2.5×10^{-2} rad/s). At this strain rate, the PA sample was very soft (storage shear modulus of ~30 kPa, as shown in Figure S2, Supplementary Information), and the 15.6 kPa nominal pressure gave a compressive deformation of ~50% average to the flat gel, which is large enough to cause full contact if there is no water entrapment.

On the other hand, the contacting process finished within 30–40 s for both the P1 and P2 samples, much faster than the flat sample that took more than 1000 s. For the P2 sample, the center of each hexagonal facet remained dark even after more than 1000 s, suggesting that the water trapping occurred for this hexagonal facet size, while, for the P1 sample,

each hexagonal facet became brighter, indicating that the water drop trapping is completely suppressed for this facet size. These results imply that the critical length for the water trapping to occur is between 0.875 and 1.75 mm for this PA gel-glass system at the relevant strain rate, which is consistent with the estimated scale for the elastic length.

From the time profile of the contact area formation, we observed that the surface engineered samples form contacts with the substrate much quicker than the flat sample. The P1 sample forms full contact while the P2 sample forms 85.8% contact relative to the hexagonal facet area at equilibrium due to water entrapment (Figure 2c-iii), however the time to reach the equilibrium contact area is almost identical for these two samples within the time resolution of the experiment. The above results indicate that engineering the hydrogel surfaces with millimeter-scale facets leads to quick underwater contact.

Further, we observed that the quick contact of the surface engineered gels induced quick and strong adhesion to the rigid glass using only light compression, while the flat PA gel did not (Movie S2, Supplementary Information). The surface engineered PA gels also showed good adhesion to soft surfaces including the flat PA gel (Movie S3, Supplementary Information) and tissue (Movie S4, Supplementary Information). For the first case, we cut one piece of P1 sample into two pieces and tested the self-adhesion between different surfaces underwater. The engineered surface strongly adhered to the flat surface, while the self-adhesion of flat-on-flat and engineered-on-engineered surfaces was very weak. The poor adhesion between flat surfaces is apparently due to the long water drainage time at the interface while the poor adhesion between the engineered surfaces should be attributed to the decreased contact area even though water drainage was fast.

To measure the adhesion strength, we used the standard probe tack test [41] with a set-up as illustrated in Figure S6, Supplementary Information. In brief, the PA gel (15 mm diameter) was compressed onto the glass substrate underwater at a steady contact rate of 10 μm/s until the contact force increased to 1 N, corresponding to a 5.7 kPa nominal pressure. Then, the gel was held in that position for 10 s, and finally, it was retracted from the substrate at a steady debonding rate of 10 μm/s (see the Experimental Section for details).

The displacement-time and force-time profiles of the three samples on glass are shown in Figure 3a. The glass we used was first washed by acetone and then washed by deionized water. It carried negative surface charges, and the Zeta potential measured in 10 mM sodium chloride (NaCl) aqueous solution was -32.44 mV and the contact angle to water was 19.6±2.2° at the temperature of 25 ℃. The surface engineered PA gels showed much stronger debonding forces and larger deformation than the flat PA gel. Furthermore, the P1 sample showed stronger adhesion than the P2 sample, as seen from both the maximum force and the deformation at the maximum debonding force. It should be mentioned that even considering partial contact of P2 due to the entrapment of water drops, the true contact area of P2 was larger than that of P1.

From these results, we concluded that the poor contact of the P0 sample is due to the slow water drainage, while the entrapment of water drops leads to the poor contact of P2 relative to P1. In addition to such effect of the contact area, crack initiation and propagation at the interface also play important roles in underwater adhesion. The energy needed to initiate the crack is generally much higher than that of crack propagation. For the flat gel, there are more trapped water areas acting as flaws, making it much easier to initiate and propagate the crack. However, for the surface engineered hydrogel, less flaws

exist and the pillars are independent from one other. To overcome all the bonded pillars, frequently crack re-initiation is needed, which largely delayed the debonding of the adhesive. This is confirmed by observing the interface during debonding (Figure 3b and Movie S5, Supplementary Information). Furthermore, the difference in the deformability of the samples during detachment should also play an important role in the adhesion, strength, and debonding energy per unit area, as suggested by the change in the deformation of these samples. As shown in Figure 3a, the debonding of the P1 sample was largely delayed compared to P2 and P0. This indicates that the P1 sample was substantially stretched during the debonding process, and clearly illustrates the effect of bulk energy dissipation on adhesion strength and debonding energy per unit area during the detachment process.

Since the rigid glass substrate does not contribute to the debonding energy dissipation, we proceeded to study the adhesion of the patterned gels on soft and energy dissipative substrates using the flat PA gel as a counter substrate. The results are shown in Figure 3c. The trend of adhesion strength is identical to that of the glass substrate, that is, the P1 sample showed higher adhesion strength than the P2 sample, and the flat sample showed the weakest adhesion of all three samples. However, comparing these results with those for the flat glass substrate, both the maximum debonding force and the deformation on the soft PA gel are systematically higher. These results suggest that the contact formation process on the flat PA gel is similar to that on glass, while the interfacial bridging strength and bulk deformability of the soft substrate are much larger than the rigid glass substrate, which substantially delays the debonding. Observation of the interface during the tack test (Figure 3d and Movie S6, Supplementary Information) showed that for the flat gel, only a small part of the interface was in contact with the soft substrate while for the P1

sample, most of the hexagonal facets were in good contact with the substrate. We also confirmed that the soft substrate was substantially deformed during the debonding process. Furthermore, the delayed fracture due to the independent crack propagation and the increased compliance of the system was also confirmed in the debonding process of the engineered surface. The P1 gel in particular, was significantly stretched during detachment.

Given the reversible nature of the ionic bonds, the adhesion of the PA hydrogels is, in principal, reversible. Furthermore, we quantitatively investigated the adhesion reversibility for the surface engineered PA gels on flat PA gels by conducting cyclic tack tests at different waiting times while maintaining the other conditions as described above. As shown in Figure 3e and f, for the P2 sample, the probe tack test curves with different waiting times from 1 to 30 min almost overlapped, and ~ 90% of the adhesion strength and debonding work were recovered within 1 min. These results indicate excellent reversibility. On the other hand, the P1 sample, with higher maximum debonding force and larger debonding deformation than the P2 sample, only showed partial recovery even after 30 min waiting, and the adhesion force and energy decreased with the cyclic test. This result suggests that it took longer for the P1 sample to recover, due to the significant stretching during debonding. During this process, significant number of primary bonds in the bulk gel are broken. These broken bonds form temporary bonds with other ionic groups during the recovery process, resulting in much longer recovery times. This is confirmed by the underwater cyclic tensile behaviors of the PA gel at different maximum strains (Figure S4, Supplementary Information). The hysteresis area between the loading and unloading curves, corresponding to the amount of broken bonds during loading, increases with the maximum strain. The recovery ratio of the hysteresis at different

waiting times, corresponding to the reforming of the ionic bonds between the original ion pairs, increases with the waiting time between subsequent cycles [31]. At a relatively small strain, ε=3, the sample fully recovered within 1 min, while it took 15 min for the full recovery when ε=6. At a larger strain, ε=8, the sample did not show full recovery even after 45 min. From the debonding deformation, the maximum tensile strain at the debonding point was determined as 3.5 for the P2 sample and 10.0 for the P1 sample. The large difference in the maximum tensile strain values accounts for the reversibility differences between the P2 and P1 samples, therefore, it is a compromise between high adhesion strength and fast reversibility. For a hydrogel with given mechanical properties and self-recovery kinetics, we need to design proper size hexagonal facets to balance the strong underwater adhesion and reversibility for a given waiting time.

We also conducted underwater probe tack tests (maintaining the conditions mentioned above) on diverse substrates varying from hard to soft, including copper plate, polystyrene (PS), and pork heart tissue. The adhesion strength, calculated from the ratio of the debonding peak force to the surface area of the PA gel, and the debonding energy per unit area, calculated from the area under the force-displacement curve and the surface area of the PA gel, are summarized in Figure 4a and b, respectively. It should be emphasized that the adhesion strength and debonding work are as high as ~25 kPa and ~50 J/m^2, respectively, for the P1 sample on the flat PA gel. This adhesion strength is as high as 1/3 of the gecko that shows strong adhesion in air [41]. Considering that the adhesion tests were performed under a very weak compressive pressure (5.7 kPa, or 60 g/cm2) for a very short contact time (10 s), the results in Figure 4 indicate a significant progress in comparing with previously reported underwater adhesion of bulk hydrogels that lack water-drainage mechanism and energy dissipation mechanism [21, 22].

The strategy of combining macroscale surface engineering and micro-scale dynamic bonds is applicable to various recently developed tough hydrogels based on hydrogen and ionic bonds, hydrophobic interaction, coordinate bonds, etc [16,31,32,44,45,46]. For example, a surface engineered tough hydrogel based on hydrogen bonding, synthesized from copolymerization of poly(ethylene glycol)$_{200}$ monomethyl ether monomethacrylate ((PEG)$_{200}$OMe) macromer and acrylic acid monomer (denoted as POA hydrogel), shows similar trends of underwater adhesion behavior on glass and tissue as PA gels, as shown in Figure 4 (for more details see Figure S7, Supplementary Information).

3.4 Conclusions

In summary, the above success in developing hydrogels showing fast, strong, and reversible underwater adhesion is due to the synergetic effect brought about by integrating macroscopic surface engineering and the tough hydrogels with dynamic bonds. The surface grooves not only accelerate water drainage and prevent water trapping, but also delay crack propagation during detachment. Specifically, the discontinuous contact pattern leads to independent detachment of contacts, which requires re-initiation of the crack for each contact. The splitting of contact also leads to an increase in the compliance of the contact point, which significantly enhances the bulk deformation of the gel. The dynamic bonds of the gel not only form reversible bridges at the interface to show reversible adhesion, but also dissipate a significant amount of energy in bulk during deformation. Smaller feature sizes lead to stronger underwater adhesion but poorer reversibility as the self-recovery time increases with the deformation at debonding. Such trade-off relations, determined by the adhesion strength, the modulus, and the self-recovery kinetics of the hydrogel, should be considered when designing the size of the

surface features. This research could be used in some hydrogels applications requiring fast and reversible adhesion in wet environments or underwater, such as re-usable sheets for wound dressing, temporary adhesives for tissue healing, and anti-slippery gloves for wall-climbing robotics. The proposed method is simple but effective, and suitable for large-scale manufacturing with feature size dimensions of several millimeters.

References

[1] J. P. Gong, Y. Katsuyama, T. Kurokawa, Y. Osada, Adv. Mater. 2003, 15, 1155.

[2] J. -Y. Sun, X. Zhao, W. R. K. Illeperuma, O. Chaudhuri, K. H. Oh, D. J. Mooney, J. J. Vlassak, Z. Suo, Nature 2012, 489, 133.

[3] H. J. Zhang, T. L. Sun, A. K. Zhang, Y. Ikura, T. Nakajima, T. Nonoyama, T. Kurokawa, Y. Katsuyama, T. Kurokawa, O. Ito, H. Ishitobi, J. P. Gong, Adv. Mater. 2016, 28, 4884.

[4] D. R. King, T. L. Sun, Y. Huang, T. Kurokawa, T. Nonoyama, A. J. Crosby, J. P. Gong, Mater. Horiz. 2015, 2, 584.

[5] S. Naficy, H. R. Brown, J. M. Razal, G. M. Spinks, P. G. Whitten, Aust. J. Chem. 2011, 64, 1007.

[6] D. J. Beebe, J. S. Moore, J. M. Bauer, Q. Yu, R. H. Liu, C. Devadoss, B. ‐H. Jo, Nature 2000, 404, 588.

[7] A. Richter, G. Paschew, S. Klatt, J. Lienig, K. ‐F. Arndt, H. -J. P. Adler, Sensors 2008, 8, 561.

[8] M. A. Haque, G. Kamita, T. Kurokawa, K. Tsujii, J. P. Gong, Adv. Mater. 2010, 22, 5110.

[9] T. Miyata, N. Asami, T. Uragami, Nature 1999, 399, 766.

[10] E. Ruel-Gariepy, J. C. Leroux, Eur. J. Pharm. Biopharm. 2004, 58, 409.

[11] G. W. Ashley, J. Henise, R. Reid, D. V. Santi, Proc. Natl. Acad. Sci. U.S.A. 2013, 110, 2318.

[12] T. Kurokawa, H. Furukawa, W. Wang, Y. Tanaka, J. P. Gong, Acta Biomater. 2010, 6, 1353.

[13] D. L. Hern, J. A. Hubbell, J. Biomed. Mater. Res. 1998, 32, 266.

[14] S. Y. Yang, E. D. O'Cearbhaill, K. M. Park, W. K. Cho, M. Villiger, B. E. Bouma, B. Pomahac, J. M. Karp, Nat. Commun. 2013, 4, 1702.

[15] C. J. Wu, J. J. Wilker, G. Schmidt, Macromol. Biosci. 2013, 13, 59.

[16] M. Nakahata, Y. Takashima, H. Yamaguchi, A. Harada, Nat. Commun. 2011, 2, 511.

[17] M. T. I. Mredha, N. Kitamura, T. Nonoyama, S. Wada, K. Goto, X. Zhang, T. Nakajima, T. Kurokawa, Y. Takagi, K. Yasuda, J. P. Gong. Biomaterials 2017, 132, 85.

[18] T. Nonoyama, S. Wada, R. Kiyama, N. Kitamura, M. T. I. Mredha, X. Zhang, T. Kurokawa, T. Nakajima, Y. Takagi, K. Yasusa, J. P. Gong, Adv. Mater. 2016, 28, 6740.

[19] H. Yuk, T. Zhang, S. Lin, G. A. Parada, X. Zhao, Nat. Mater. 2016, 15, 190.

[20] S. Rose, A. Prevoteau, P. Elzière, D. Hourdet, A. Marcellan, L. Leibler, Nature 2014, 505, 382.

[21] L. C. Bradley, N. D. Bade, L. M. Mariani, K. T. Turner. ACS Appl. Mater. Interfaces 2017, 9, 27409.

[22] G. Sudre, L. Olanier, Y. Tran, D. Hourdet, C. Creton, Soft Matter 2012, 8, 8184.

[23] J. Li, A. D. Celiz, J. Yang, Q. Yang, I. Wamala, W. Whyte, B. R. Seo, N. V. Vasilyev, J. J. Vlassak, Z. Suo, D. J. Mooney, Science 2017, 357, 378.

[24] L. Khandeparker, A. C. Anil, Int. J. Adhes. Adhes. 2007, 27, 165.

[25] Z. Qin, M. J. Buehler, J. Mech. Phys. S. 2014, 62, 19.

[26] R. Gupta, J. Frechette, Langmuir 2012, 28, 14703.

[27] J. H. Waite, Chemtech 1987, 17, 692.

[28] J. Ahmed, H. Guo, T. Yamamoto, T. Kurokawa, M. Takahata, T. Nakajima, J. P. Gong, Macromolecules 2014, 47, 3101.

[29] T. Yamamoto, T. Kurokawa, J. Ahmed, G. Kamita, S. Yashima, Y. Furukawa, Y. Ota, H. Furukawa, J. P. Gong, Soft Matter 2014, 10, 5589-5596.

[30] D. J. Broesch, J. Frechette, Langmuir 2012, 28, 15548.

[31] T. L. Sun, T. Kurokawa, S. Kuroda, A. B. Ihsan, T. Akasaki, K. Sato, M. A. Haque, T. Nakajima, J. P. Gong, Nat. Mater. 2013, 12, 932.

[32] A. B. Ihsan, T. L. Sun, T. Kurokawa, S. N. Karobi, T. Nakajima, T. Nonoyama, C. K. Roy, F. Luo, J. P. Gong, Macromolecules 2016, 49, 4245.

[33] T. L. Sun, F. Luo, T. Kurokawa, S. N. Karobi, T. Nakajima, J. P. Gong, Soft Matter 2015, 11, 9355.

[34] R. E. Webber, C. Creton, H. R. Brown, J. P. Gong, Macromolecules 2007, 40, 2919.

[35] D. K. Wainwright, T. Kleinteich, A. Kleinteich, S. N. Gorb, A. P. Summers, Biol. Lett. 2013, 9, 20130234.

[36] P. Ditsche, D. K. Wainwright, A. P. Summers, J. Exp. Biol. 2014, 217, 2548.

[37] E. Arzt, S. Gorb, R. Spolenak, Proc. Natl. Acad. Sci. U.S.A. 2003, 100, 10603.

[38] R. Spolenak, S. Gorb, E. Arzt, Acta Biomater. 2005, 1, 5.

[39] M. Kamperman, E. Kroner, A. del Campo, R. M. McMeeking, E. Arzt, Adv. Eng. Mater. 2010, 12, 335.

[40] A. del Campo, C. Greiner, E. Arzt, Langmuir 2007, 23, 10235.

[41] C. Creton, M. Ciccotti, Rep. Prog. Phys. 2016, 79, 046601.

[42] C. K. Roy, H. L. Guo, T. L. Sun, A. B. Ihsan, T. Kurokawa, M. Takahata, T. Nonoyama, T. Nakajima, J. P. Gong, Adv. Mater. 2015, 27, 7344.

[43] H. Lee, B. P. Lee, P. B. Messersmith, Nature 2007, 448, 338.

[44] D. C. Tuncaboylu, M. Sari, W. Oppermann, O. Okay, Macromolecules 2011, 44, 4997.

[45] F. Luo, T. L. Sun, T. Nakajima, T. Kurokawa, Y. Zhao, K. Sato, A. B. Ihsan, X. Li, H. Guo, J. P. Gong, Adv. Mater. 2015, 27, 2722.

[46] T. Kakuta, Y. Takashima, M. Nakahata, M. Otsubo, H. Yamaguchi, A. Harada. Adv. Mater. 2013, 25, 2849.

Figures and Tables

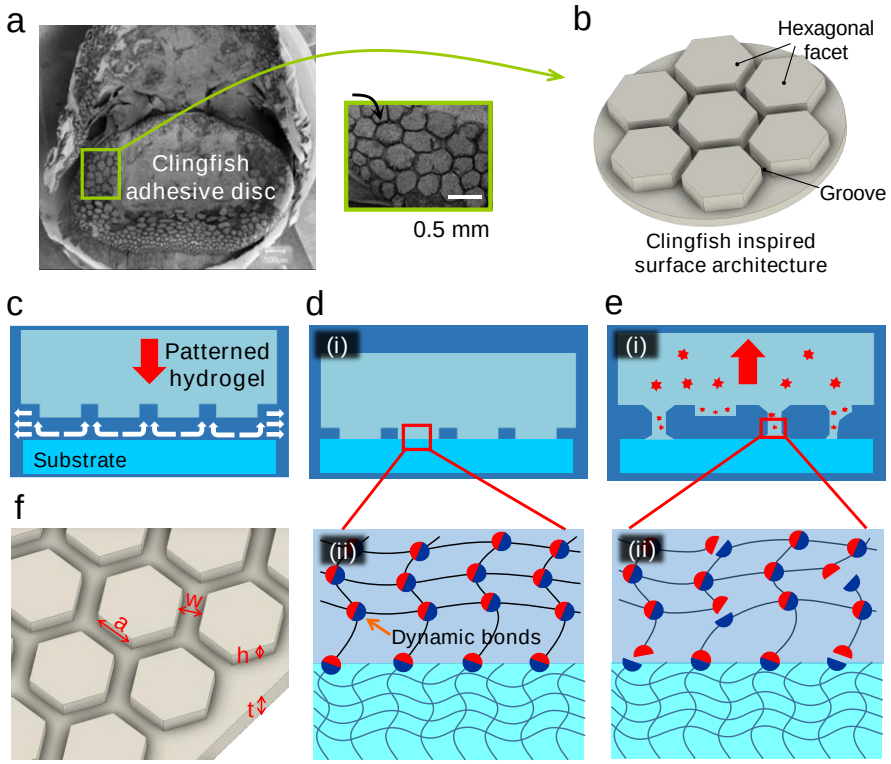

Figure 1. Schematic illustration of the multi-scale design of tough hydrogels with fast, strong, and reversible underwater adhesion. Inspired from the geometry of the adhesive discs of clingfish a). A tough hydrogel with hexagonal facets separated by grooves and dynamic bonds was surface engineered b). The grooves work as water drainage channels to facilitate the fast contact of the hexagonal facets with the substrate underwater c). The dynamic bonds on the hexagonal facets of the gel form bonds with the substrates to bridge the interface d). During stretching, the rupture of bulk dynamic bonds dissipates energy, which delays the debonding at the interface e). Moreover, the independent hexagonal facets prevent continuous crack propagation throughout the interface thus also enhancing the adhesion strength and debonding energy f). The adhesion of the hydrogel is reversible due to reversible dynamic bonding. The dimensions of the surface geometry strongly influence the adhesion behaviour.

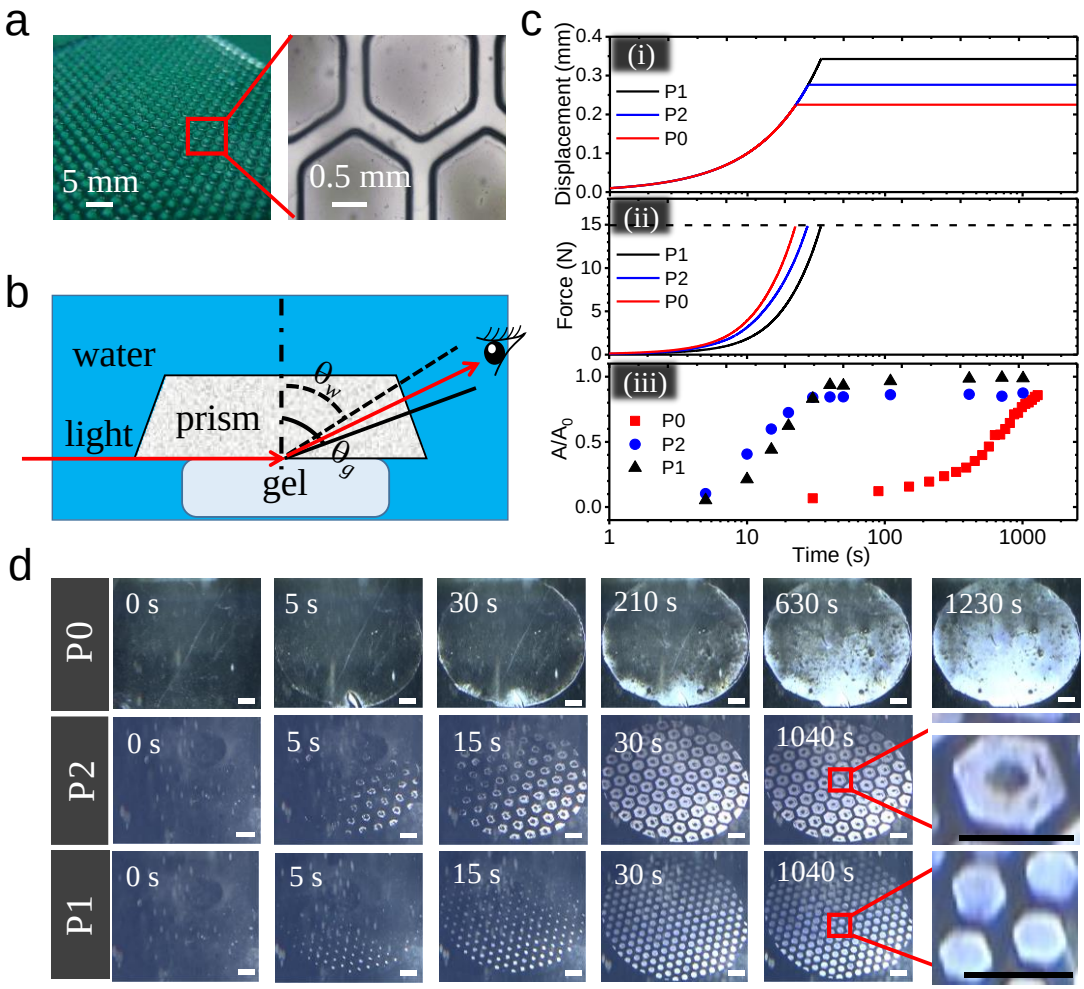

Figure 2. **In situ observation of the underwater contact evolution for surface engineered hydrogels on glass substrates.** a) Optical and microscopic images of the surface structure of a polyampholyte (PA) hydrogel (sample P2). b) Illustration of the set-up to observe the contact evolution in water. The prism was pushed toward the sample gel at a 10 μm/s rate until the load reached 15 N and then it was held in that position. c) Time profiles of prism displacement (i), normal force (ii), and contact area ratio (A/A0) (iii) during the contact test. d) Snapshots of the contact images for the P0, P1, and P2 samples. The bright region is in contact with the glass and the dark region is trapped by water. The contact area ratio A was estimated from d) while A0 is the nominal area of the hexagonal facets. Scale bars: 4 m

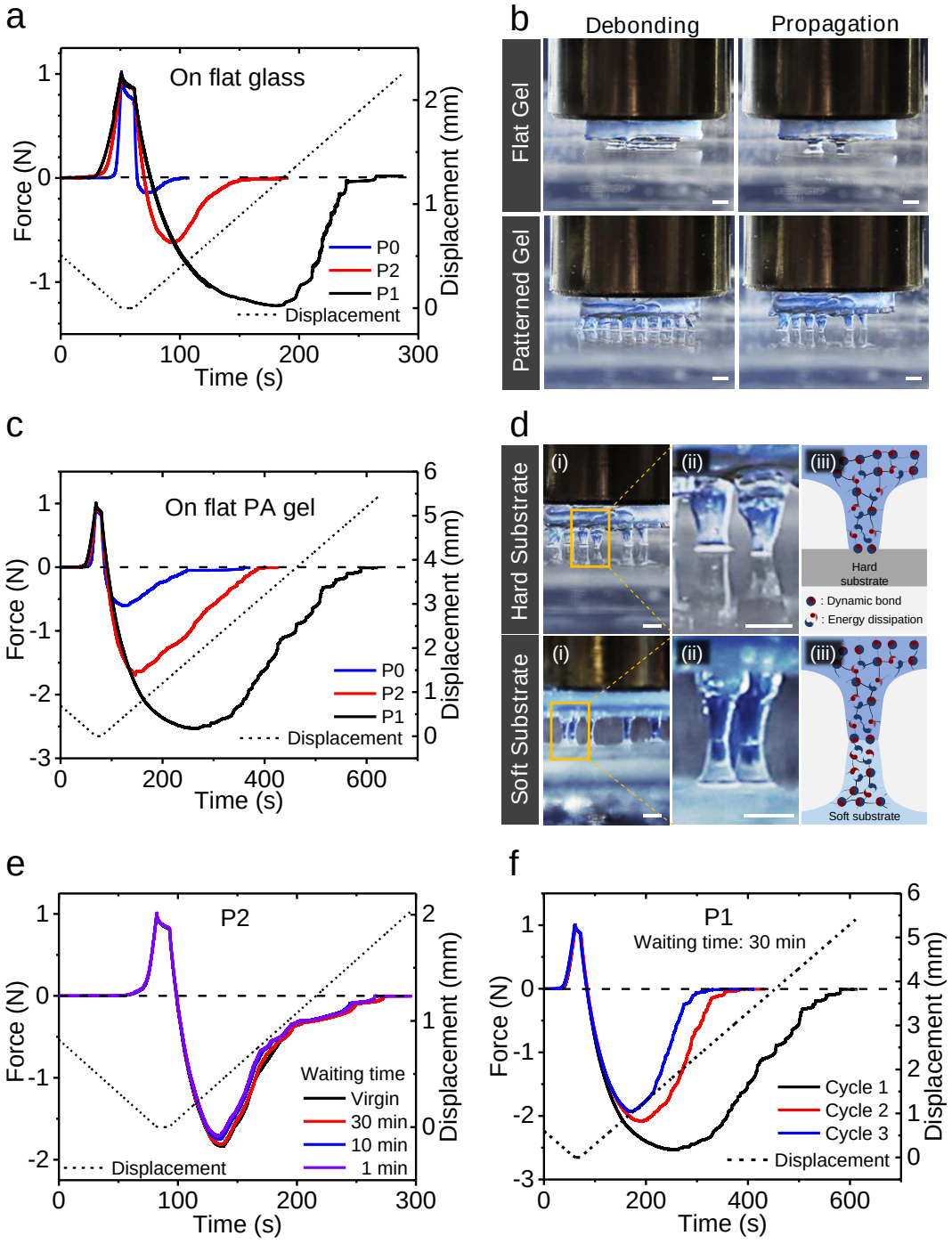

Figure 3. **Strong and reversible underwater adhesion of surface engineered PA hydrogels.** a) Displacement and force-time profiles of underwater tack tests on a flat glass plate for PA gels with different surface patterns. b) Optical images of the deformation evolution of flat and patterned gels during debonding from the glass plate. c)

Displacement and force-time profiles of underwater tack tests on the flat PA gel for PA gels with different surface patterns. d) Optical images of the deformation of the P1 sample on hard glass and soft PA gel. e) Displacement and force - time profiles for cyclic probe tack tests at varied waiting times between successive measurements for a P2 sample on flat PA gel. f) Displacement and force - time profiles for cyclic probe tack tests at 30 min waiting time for a P1 sample on flat PA gel. P0, P1, and P2 represent the PA gels with flat surface, hexagon facets length (a) of 0.875 and 1.75 mm, respectively. Scale bars: 2 mm.

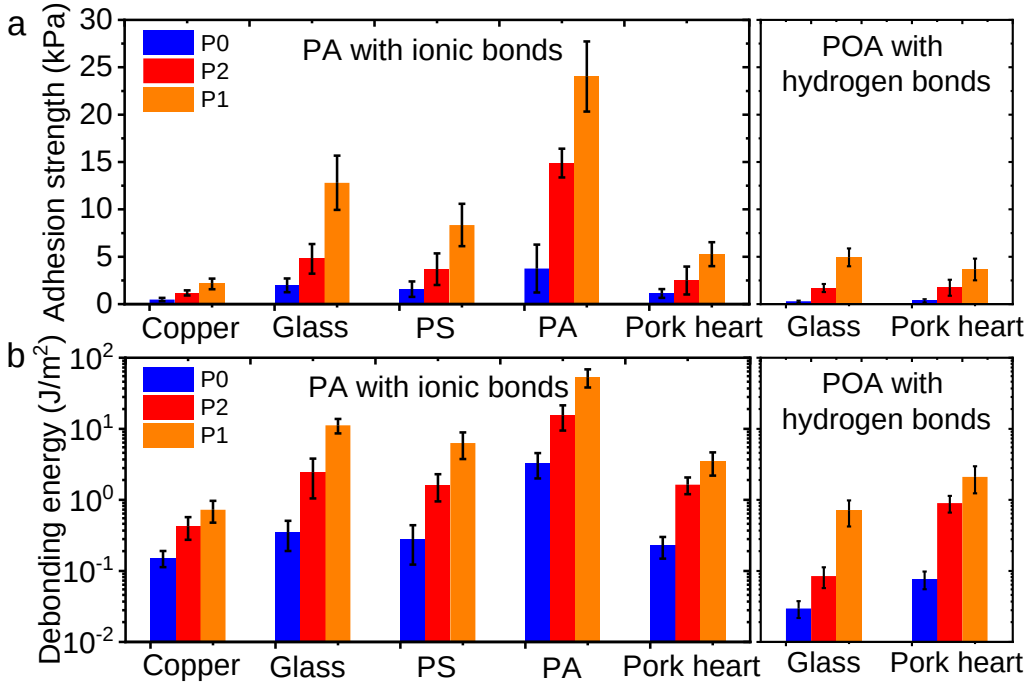

Figure 4. **Underwater adhesion strength of surface engineered tough hydrogels with dynamic bonds on diverse substrates.** Results for PA hydrogels based on ionic bonds and for POA hydrogels based on hydrogen bonds. a) Adhesion strength, calculated from the ratio of the debonding peak force to the nominal surface area of the samples and b) Debonding energy per unit area, calculated from the ratio of the area under the force-displacement curves to the nominal surface area of the sample. For patterned gels, the facet area was used. Error bars are standard deviation for n=3-5 measurements. Sample diameter 15 mm; contact and debonding rate: 10 µm/s; contact force: 1 N (nominal pressure: 5.7 kPa), holding time: 10 s. PS: polystyrene used for Petri dishes; PA: flat PA gels.

Supplementary Figures

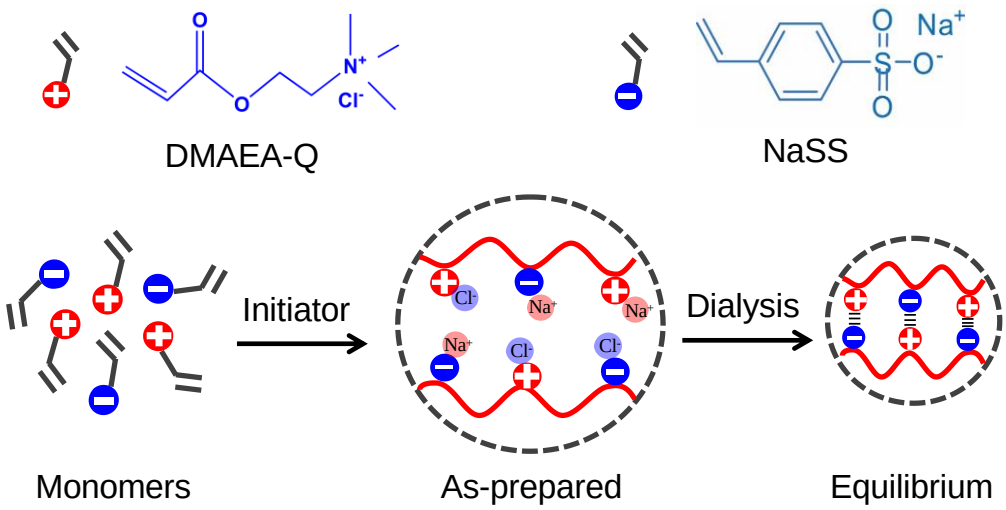

Figure S1. Schematic illustration of the polyampholyte (PA) hydrogels synthesis.

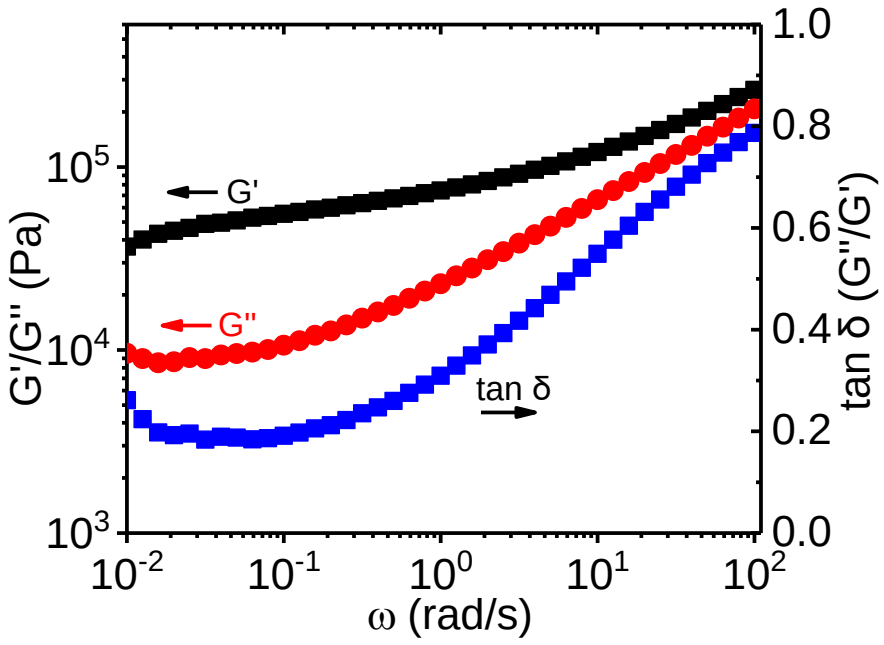

Figure S2. Rheological characterization of the PA hydrogel at 25 ° C. G', G", and tanδ represent the storage and loss modulus, angular frequency and loss factor, respectively.

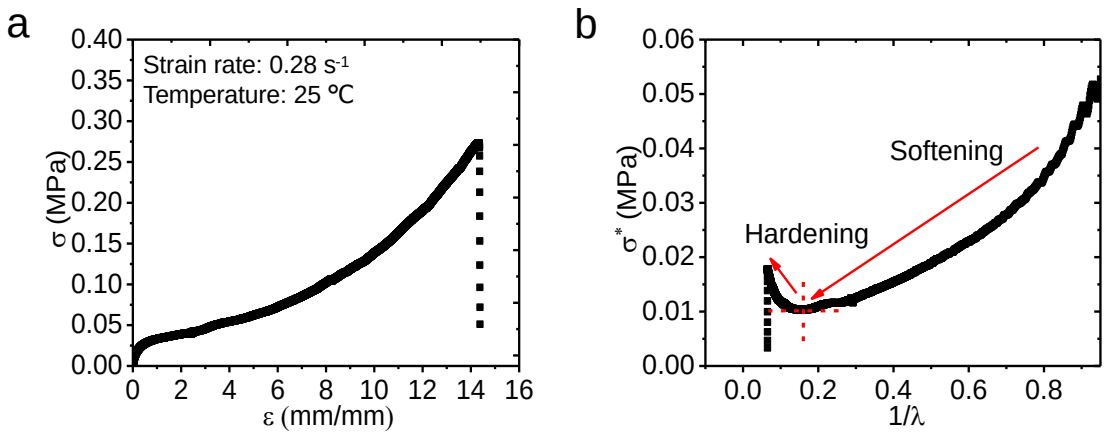

Figure S3. Tensile behavior of the PA hydrogel. a) Nominal stress (σ) vs. strain (ε) curve. b) Mooney representation of the same data as a function of 1/λ, where $\lambda = \varepsilon + 1$ is the deformation ratio. The reduced stress also called Mooney stress is defined as $\sigma^* = \sigma/(\lambda-\lambda^{-2})$. The mechanical properties of the hydrogel are characterized using the underwater tensile test at a steady 0.28 s^{-1} loading strain rate at 25 ℃.

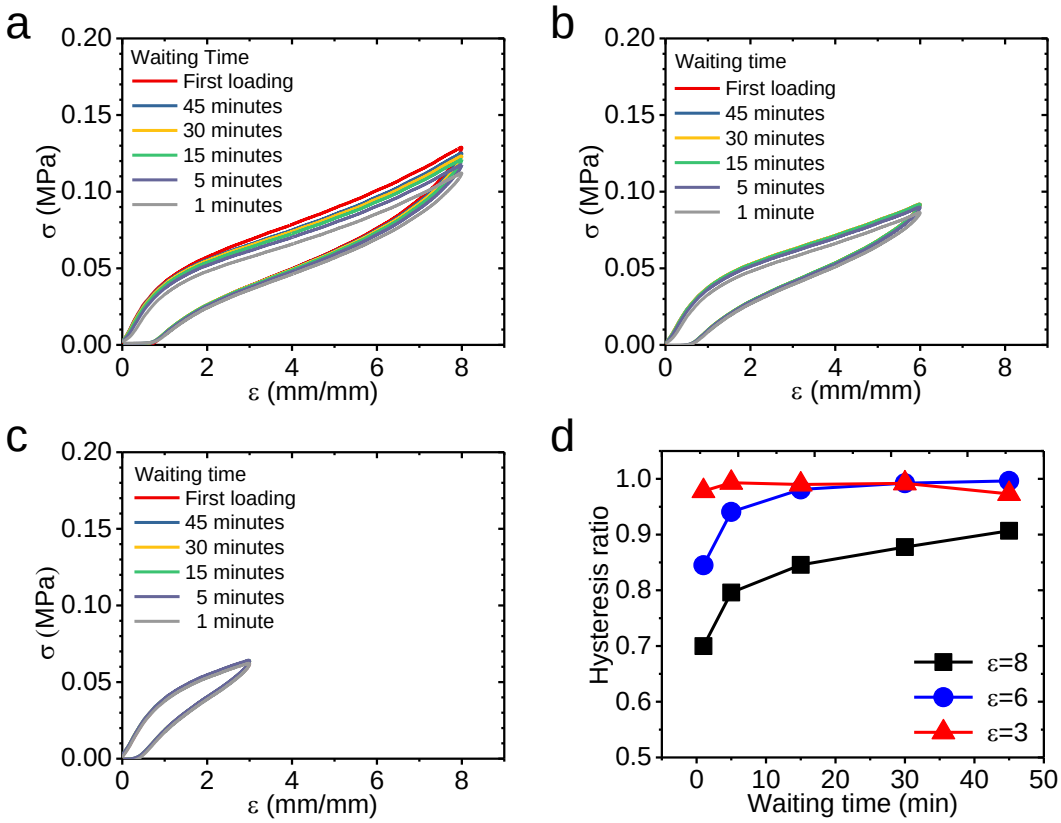

Figure S4. Mechanical hysteresis tests of the PA hydrogel. a–c) Nominal stress (σ) vs. strain (ε) cyclic tensile curves for different waiting times (t) at different maximum stretch strains (ε). d) Hysteresis ratio vs. waiting time curves for different maximum stretch strains. The tests were performed underwater at a 0.28 s^{-1} strain rate.

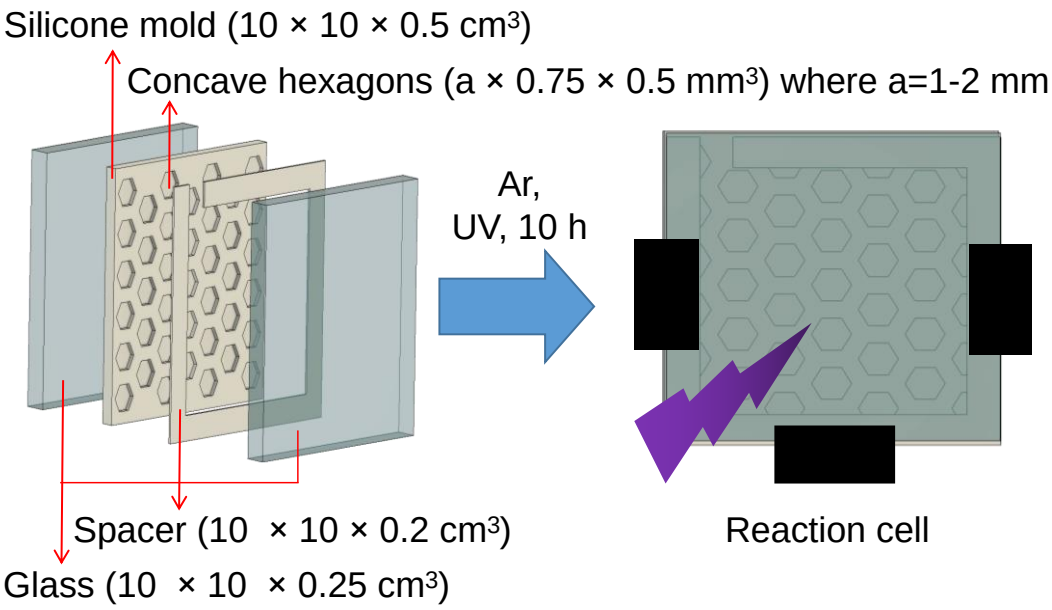

Figure S5. Schematics for the synthesis of the surface patterned hydrogel. A reaction cell was prepared by assembling two glass plates, a silicone mold with honeycomb ridges and a silicone spacer. The precursor solution was added to the reaction cell, and after removing the bubbles in an argon atmosphere, the reaction cell was irradiated with UV light (365 nm wavelength) for 10 h to obtain the solidified hydrogel. The side length of each hexagonal concave area of the silicone mold varied from 1 to 2 mm, while the depth was 0.5 mm.

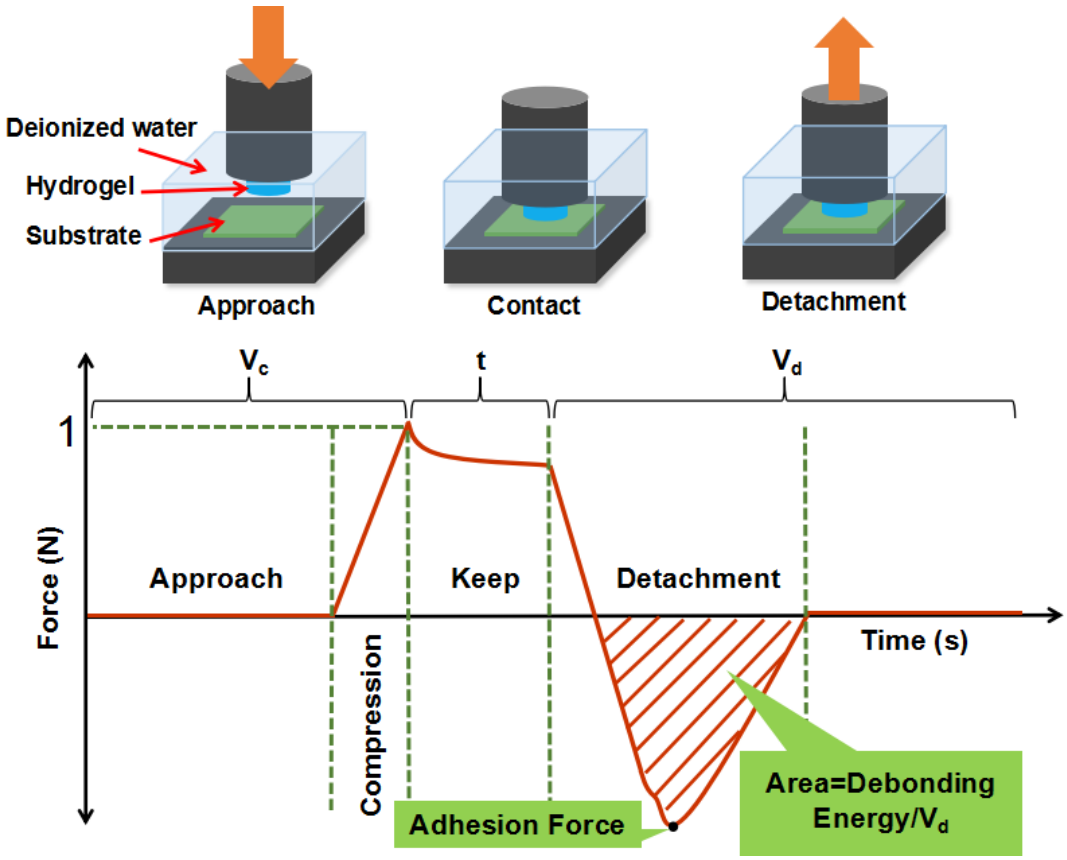

Figure S6. Schematics for the set-up and procedures of the underwater probe tack test. The hydrogel sample was fastened to the jigs and the system immersed in deionized water. The jig approached the substrate at a steady Vc=10 μm/s rate until the applied force reached 1 N and subsequently held the position for 10 s. Afterward, the jig retracted at a steady V_d=10 μm/s rate. The adhesion strength was calculated from the ratio of the debonding peak force to the projected area of the sample surface. The debonding energy per unit area was calculated from the ratio of the area under the force-displacement curve to the projected area of the sample surface.

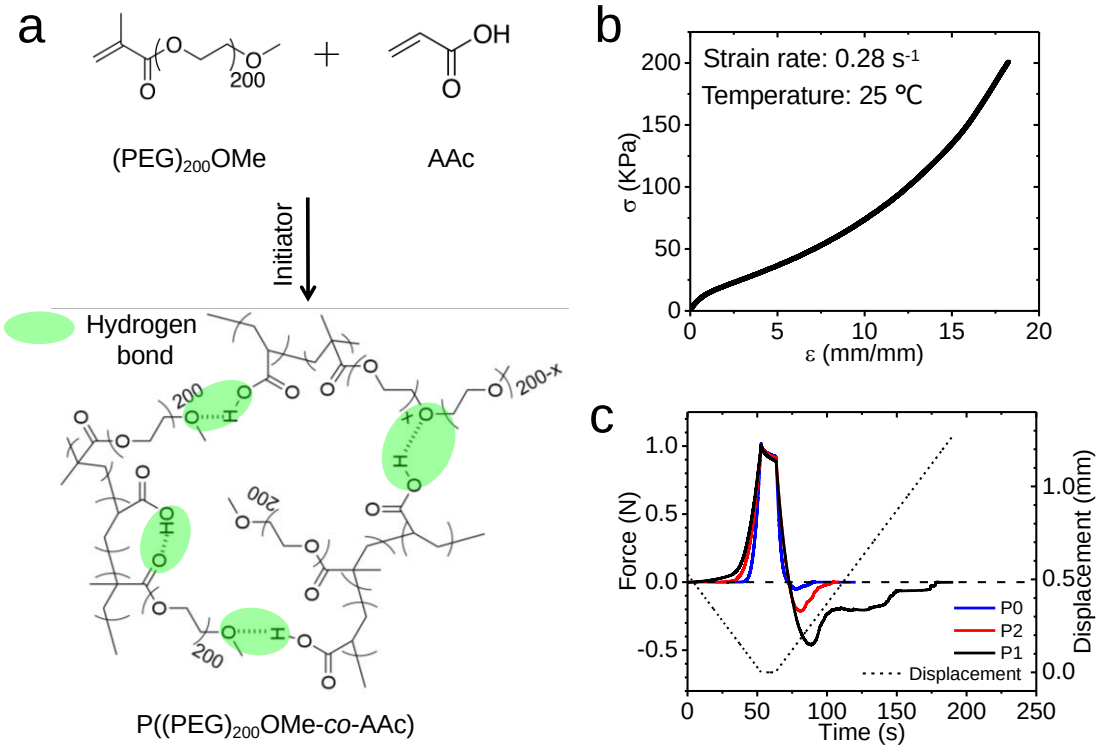

Figure S7. Underwater adhesion of the surface engineered hydrogel with hydrogen bonding. a) Chemical structures of $(PEG)_{200}OMe$, AAc, and their copolymer P($(PEG)_{200}$OMe-co-AAc), denoted as POA, formed by radical initiated polymerization. The POA forms hydrogels by hydrogen bonding. b) Tensile behavior of the hydrogen bonded hydrogels. c) Displacement-time and force-time profiles of the underwater tack test of the hydrogen bonded hydrogels with different surface patterns on glass. The sample code and dimensions of the pattern are shown in Table S2. The a, h, w, and t parameters correspond to those shown in Figure. 1f.

Supplementary Tables

Table S1. Structure parameters of surface engineered PA hydrogels. The PA hydrogels deswelled to 87.5% of their as-prepared size in each direction in water.

Sample code	Length of hexagonal facet a (mm)	Height of hexagonal facet h (mm)	Groove width w (mm)	Total thickness h+t (mm)	Relative area of hexagonal facets
P1	0.875	0.438	0.656	2.19	53%
P2	1.75				71%
P0 (flat)	-	-	-	2.19	100%

Table S2. Structure parameters of the surface engineered POA hydrogels.

Sample code	Length of hexagonal facet a (mm)	Height of hexagonal facet h (mm)	Groove width w (mm)	Total thickness h+t (mm)	Relative area of hexagonal facets
P1	0.81	0.41	0.61	2.03	53%
P2	1.62				71%
P0 (flat)	-	-	-	2.03	100%

Legends for Supplementary Movies

Movie S1 Underwater contact evolution of PA hydrogels on glass.

We recorded the contact area evolution of the flat P0, patterned P1, and P2 hydrogels on a glass prism surface in time. The display speed is 8 times faster than real time at the beginning and 128 times faster for the long drainage time for each sample.

Movie S2 Underwater adhesion of patterned PA hydrogels on hard glass.

A strip of patterned PA hydrogel was immersed in Milli-Q water. Subsequently we pressed a piece of slide glass on one end of the patterned gel strip with one finger, and another piece of glass plate on the other end of patterned gel. The two pieces of slide glass plate adhered to the patterned gel very well. We finally stretched the adhesion joints, and observed that the tough hydrogel was significantly stretched and presented considerable deformation. However, for the flat PA hydrogel, while the glass plate can adhere underwater, the adhered joint was very weak and failed quickly.

Movie S3 Underwater self-adhesion of patterned PA hydrogels.

A strip of P1 patterned PA hydrogel was cut into two pieces in Milli-Q water. Furthermore, we placed the flat surface ends of the two strips in contact underwater, and stretched the joint. While the flat surfaces could adhere to each other, they showed weak adhesion. Subsequently, we placed the patterned surface ends of the two strips in contact underwater, and stretched the joint. The gels could adhere to each other, but also showed weak adhesion. Lastly, when the end of a patterned surface strip was attached to the end

of a flat surface strip we noticed that the joint could be substantially stretched and bear large deformation.

Movie S4 Underwater adhesion of patterned PA hydrogels to bio-tissue.

A piece of beef heart was placed underwater and a strip of P1 patterned PA hydrogel was pressed to the tissue using tweezers and very little pressure. While we immediately dragged the tissue underwater and even flipped it upside down, the patterned hydrogel still strongly adhered to the tissue. Afterward, we took the tissue out of the water holding the corner of the patterned hydrogels with the tweezers. This movie clearly showed the fast and strong underwater adhesion of the patterned hydrogels to the beef heart tissue.

Movie S5 Underwater debonding of PA hydrogels on glass.

We recorded the debonding process of PA hydrogels in the underwater probe tack test for a flat P0 and a patterned P1 hydrogel on glass plates with a display speed 32 times faster than real time. For the flat hydrogel, only a small part of the surface was in contact with the glass plate due to water trapping acting as flaws, therefore the crack easily propagated during the debonding process. For the P1 hydrogel, all the hexagonal facets quickly made contact with the glass, and each hexagonal pillar significantly deformed before debonding. Each pillar debonding required re-initiation of the crack, resulting in a delayed debonding. The large deformation caused the PA hydrogel to dissipate a large amount of energy before the failure of the bonding joint, contributing to the debonding energy.

Movie S6

Underwater debonding of PA hydrogels on flat PA hydrogel.

We recorded the debonding process of PA hydrogels in the underwater probe tack test for flat P0 and patterned P1 hydrogels on the flat PA hydrogel. The speed was 32 times faster than real time. For the flat hydrogels, similar to their debonding on glass, only a small part of the surface was in contact with the hydrogel due to water trapping acting as flaws. Therefore, the crack easily propagated during the debonding process. For the P1 hydrogel, most of the pillars could be significantly stretched. Compared with the rigid glass substrate, the flat and soft PA substrates could be stretched, which also contributed to the debonding energy. The PA hydrogel was so tough that, even the substrate was stretched a lot, the bonding joint detached from the interface.

Chapter 4: In situ underwater adhesion behaviors between polyampholyte (PA) hydrogels

4.1 Introduction

Significant progress has been made in the design and fabrication of adhesives with potential applications in many fields, especially for the gecko and mussel bio-inspired adhesives [1-4]. Inspired by the fibrillar attachment mechanisms employed by geckos, researchers have focused on understanding dry adhesion and using this knowledge to design synthetic fibrillar adhesives. Inspired by the catechol-based (3, 4-dihydroxyphenylalanine (DOPA) and derivatives) adhesion mechanisms employed by mussels, various synthetic underwater adhesives with outstanding performance are developed [5-7]. The vast majority of work done in this area has focused on adhesion to rigid substrates [8, 9]. However, adhesion on soft substrates or easily deformable surfaces, especially for underwater adhesion, has not been heavily investigated, despite there are many applications that require adhesion to soft substrates, most notably in the biomedical field where the environment is usually wet or surrounded by water. Great demands for understanding the adhesion behaviors on deformable surface in wet or underwater conditions are needed. For instance, many mobile medical robots need to work well on or inside the human body which need to adhere to a soft tissues surface. Wound dressings need reliable adhesion on the soft and flexible skin [10]. Geckos work well on various solid hard substrates are expected to adhere to soft substrates as well. Unexpectedly, Stark et al. found that the geckos could not stick to the smooth PDMS under dry adhesion. Another case that researchers who evaluate the ability of micro-patterned substrates to

adhere to tissue, found that the maximum adhesion force was measure at a lower fibril density. This result is not compatible with dominating gecko-like adhesion mechanism [3]. This state suffers from several challenges. Firstly, the stickiness and the softness of the materials make it much is easier to trap water at the interface, and the trapped water will act as initial defects to weaken the bonding joints. Secondly, the deformation of the substrate as the fibers pull off couples the adhesion of neighboring fibers, resulting in a decrease in adhesion [8]. Moreover, soft substrates are expected to be easily conformed to the patterned adhesives and therefore, the mechanical interlocking effects are also expected to play a role in the adhesion performances. On the other hand, the energy dissipating matrix of the adhesive has been proved to play an important role in improving the debonding energy in many irreversible bonding joints [11], while a reversible underwater adhesives with an energy dissipating matrix is still in its infancy. In this study, we investigated the in situ underwater adhesion behaviors between polyampholyte (PA) hydrogels with reversible ionic bonds, by varying the softness of the adhesives and substrates, contact keeping time, contact/debonding velocity, and studying the effect of contact element size and surface hydrophobicity on the underwater contact adhesion behaviors. Investigations on these adhesion behaviors will help to get a better understanding the contact formation and debonding mechanism on deformable substrates underwater, and then using this knowledge to design synthetic adhesives on soft substrates such as tissue, skin.

4.2 Experiments

4.2.1 Materials

1) Preparation of polyampholyte hydrogels. A series of tough polyampholyte (PA) hydrogels used in this study were prepared by the random copolymerization of monomers with opposite charges, at a anionic : cationic monomer ratio of 0.52 : 0.48, as described in previous studies [1]. At this ratio, the composition of negative and positive charges in PA hydrogels are expected to be balanced at equilibrium state. An aqueous solution containing mixed monomers was poured into a reaction cell consisting of two pieces of templates separated by a silicone spacer with thickness of 2 mm. Then the reaction cell was irradiated with 365 nm UV light for 10 h. To remove the oxygen, the reaction cells were placed in an Ar atmosphere before use for more than 36 h. After polymerization, the gel was immersed in excess amount of water for 1 week to dialyze the mobile counter-ions, and allow the oppositely charged polyions on the copolymers to form stable ionic complexes through intra- or inter-chain interactions.

As shown in Figure 4.1, the PA hydrogels show lower modulus (call D gel for short) is prepared by the method mentioned above with an aqueous solution containing 2.3 M total monomer (NaSS and DMAEA-Q) concentration, 2.3 mM, 2-oxoglutaric acid as UV initiator; PA hydrogels with a higher modulus prepared with 2.3 M total monomer (NaSS and MPTC) concentration (call M gel for short), 2.3 mM, 2-oxoglutaric acid as UV initiator; PA hydrogels with single surface hexagonal facet were prepared with 2.5 M total monomer (NaSS and DMAEA-Q), 2.5 mM, 2-oxoglutaric acid as UV initiator, and 2.5 mM N,N-methylenebisacrylamide crosslinker.

2) Preparation of the silicone template mold. Plastic molds (10×10 cm) with a single concave hexagonal pattern with a side length of 1.5, 2 and 4 mm, a depth of 0.5 mm, specifically, were prepared using a 3D Keyence printer. The mixed two-part polymers with 0.5 wt.% silicone solution curing agent for silicone rubbers was cased into the plastic

mold, and the sample was placed in a vacuum chamber for 30 min to remove the bubbles. Subsequently, the sample was exposed to the moisture in the air at 25 ℃ for 24 h for curing the silicone rubber. After removing the plastic mold, a 5 mm thick silicone mold was obtained.

4.2.2 Measurements

1) Measurements of underwater adhesion by probe tack test.

The probe tack tests, for measuring the adhesion strength and energy dissipation of the hydrogels, were performed on a Shimadzu Autograph AG-X 20KN tensile machine in water at 25 ℃. The set-up consisted of mainly two parts: the bottom part, a cell with a rigid stage providing the deionized water environment for the tack test, and the upper one, a copper shaft connected with the load cell. The gel was cut into disc shapes of prescribed diameter, and bonded to the copper shaft using a very thin super glue (Konishi Co., Ltd.). We used a piece of flat PA gels glued to the glass plate which was fixed with screws as counter soft substrates. The thickness of the PA gel at as-prepared state is 2 mm, which will shrink to 1.7 mm, specifically.

For the test, the upper gel was first compressed to the lower substrate at a constant compressing rate until it reached the set force (F). Afterward, the sample was held in this position for the described contact time (t). Subsequently, the probe was retracted at a constant rate until the debonding finished. The force, displacement, and time were recorded during the process.

2) *Underwater tensile test.* The tensile test was performed using a tensile-compressive tester (TENSILON ORIENTEC RTC-1150A) underwater at 25 ℃. The sample was cut into a Dumbbell-shape with the JIS-K6251-7 standard size: $6\times2\times2$ mm^3. The tensile

velocity was 100 mm/min, corresponding to a 0.28 s^{-1} strain rate. The nominal stress was obtained by dividing the tensile force by the initial cross-sectional area of the sample. The Young's Modulus *E* of gels were calculated from the slope of tensile stress-strain curves.

4.3 Results and Discussion

4.3.1 Matrix energy dissipation effect on the underwater adhesion between the PA hydrogels.

Viscoelastic effects may contribute greatly to the adhesion but have not been considered for fibrillar surfaces up to now. If the material is very viscoelastic in the bulk during the time scales of the test, then the strain energy release rate becomes dependent on loading history and the adhesion energy is no longer easily separable from the energy dissipated in the bulk. In extreme cases, the elastic energy released by the deformed material may not be sufficient to propagate a crack and external work must be continuously applied. Suo and Zhao *et al* have showed the bulk energy dissipation contribute to the debonding energy of the irreversible adhesives greatly. However, hydrogels adhesives with reversible energy dissipation matrix have not been investigated heavily.

Herein, to investigate the reversible matrix energy dissipation effect on the underwater adhesion, we choose PA hydrogels with dynamic bonds for their high capacity of energy dissipation that favors toughness and strong adhesion. Most importantly, they are intrinsically adhesive in water. Since dynamic bonds are reversible in swollen hydrogels and contribute to the toughness and self-recovery of the hydrogels, they also have the potential to form reversible bridges with other surfaces in wet environments when properly choosing the surface chemistry of the substrates.

We firstly investigated the effect of debonding velocity and contact time on the bulk energy dissipation by using the underwater probe tack test. In brief, the hard M gel (PNaSS-co-MPTC) with a cylinder shape (10 mm diameter) was compressed onto the soft D gels (PNaSS-co-DMAEAQ) substrate underwater at a steady contact rate of 10 μm/s until the contact force increased to 1 N, corresponding to a 12.8 kPa nominal pressure. Then, the gel was held in that position for a designed waiting time (default 100 s), and finally, it was retracted from the substrate at a steady designed debonding rate (default 10 μm/s). The displacement-time and force-time profiles were recorded.

From the results showed in Figure 4.2a and b, with the increasing of debonding velocity, both of the adhesion peak force and debonding energy were substantially increased. As discussed in previous studies about PA hydrogels, the strength of a dynamic ionic bond strongly depends on the observed time or strain rate. At a high strain rate, more inter-chain bonds serve as strong bonds to increase the strength of gels as well as energy needed to overcome these bonds. These results indicates that for PA hydrogels adhesives with ionic bonds, the higher the debonding rate is, the higher force and more energy needed to destroy the bonding joints. However, given the reversible nature of the ionic bonds, the recovering time for the strong ionic bonds is also much longer than the weak bonds which has been proved in the hysteresis test in Chapter 3.

As shown in Figure 4.2 c and d, the longer contact time is, the higher adhesion strength and debonding energy is. These results may due to a synergistic effect of water drainage and strong ionic bonds formation. With a longer contact time, more water at the interface can be drained out which has been explored in Chapter 3, resulting in the increase of the real contact area. On the other hand, more strong ionic bonds will be formed which may also lead to the increase of the adhesion peak force and bulk energy dissipation. As shown

in Figure 4.3, when we increased the contact speeds and keep other conditions the same, both of the adhesion strength and energy dissipation firstly decreased due to the decrease of real contact area, then come to a plateau at a real contact time in several seconds. When the real contact time is very short, the difference in real contact area can be ignored. The plateau could be due to the weak ionic bonds formation which can be formed immediately in an intimate contact. However, it is still very hard to quantitatively distinguish surface ionic bonds effect from the real contact area effect with current data due to the viscoelastic effect in the approaching process. Further investigation on this point is needed in future. Moreover, we also compare the underwater tensile test results between soft gels and hard gels as showed in Figure 4.1. The hard M gels with a modulus of ~10 times higher than soft D gels, is less compliant to form a good a contact under the same pressure, compared with soft D gels. Meanwhile, according the scale theory of adhesion, the peak adhesion force is proportional to the stiffness. The M gel has a higher stiffness, resulting the in the increase in adhesion force. Finally, these two couple effects lead to the slight difference in adhesion strength. On the other hand, the soft D gels can be much more easily deformed than M gels under the same load, resulting in more energy being dissipated in the bulk.

In sum, the underwater adhesion behaviors between PA hydrogels with reversible ionic bonds are quite dependent on the debonding rates, real contact time and the stiffness of the bulk materials.

4.3.2 Underwater adhesion behaviors of PA hydrogels with different contact size.

In Chapter 3, the results showed that patterned hydrogels with smaller facets were more efficient to drain water. Here, in order to get a more clear understanding about the size effect. We prepared PA hydrogels with a single hexagonal facet on the surfaces, whose geometry parameters except the side length, were kept the same as that in Chapter 3. The

side length of the single facet varied by 1.5 mm, 2 mm, and 4 mm. For the underwater tack test, the PA gel with a single hexagonal facet was compressed onto the flat PA gels substrate underwater at a steady contact rate of 10 μm/s until the corresponding nominal pressure of 15.5 kPa. Then, the gel was held in that position for a designed waiting time, and finally, it was retracted from the substrate at a steady debonding rate of 10 μm/s. The displacement-time and force-time profiles were recorded.

Firstly, let's review the derivation of the analytical solution to the relationship between water drainage efficiency and contact element sizes. As shown in Figure 4.4, a rigid plate with a cylinder shape whose diameter is denoted as R, is pushed to drain the liquid film at the interface by a force F. The thickness of the water film is denoted as $h(t)$, and the h_0 denotes the initial thickness. We consider a cylinder shape block of water, then we have,

$$2\pi\rho h\bar{v} = -\pi\rho^2 \dot{h},\ \bar{v} = -\rho\dot{h}/2h\,,$$

While, from the Navier-Stokes equations,

$$\vec{v} = \hat{\rho}v(\rho, z, t),$$
$$\frac{\partial P}{\partial z} = 0, \frac{\partial P}{\partial \rho} = \mu\frac{\partial^2 v}{\partial z^2}$$
$$v = \frac{z(z-h)}{2\mu}\frac{\partial P}{\partial \rho}$$

Then we obtain,

$$\bar{v} = \frac{1}{h}\int_0^h v = -\frac{h^2}{12\mu}\frac{\partial P}{\partial \rho}$$

Combine the results, we can get,

$$-\frac{h^2}{12\mu}\frac{\partial P}{\partial \rho}=\frac{\rho \dot{h}}{2h}$$

Finally, we have

$$P = P_{ext} - (3\mu \dot{h}/h^3)(R^2-\rho^2), \quad \rho = R, \; P = P_{ext}$$

$$F = \int_0^R d\rho 2\pi\rho(P-P_{ext}) = -\frac{3\pi \dot{h}}{2h^3}\mu R^4$$

For water drainage efficiency, we can infer that,

$$\dot{h} = \frac{F \bullet 2h_0^3}{-3\pi\mu}\frac{1}{R^4}$$

The analytical solution for the rigid materials, indicates that the draining speed is very much depend on the diameter size.

In our experimental results, the data also agree with this trend. Figure 4.5 showed that both of the adhesion strength and debonding energy underwater increased with the decrease of the size of the facets in a short contact time of 10 s. This indicates that in a short contact time, the bigger facet need more time to drain water out to make a good contact. The water drop which cannot be drained out will be caught at the interface due to the adhesion and softness of the gels. The trapped water drop acts as defects initiating the bonding joint. The synchronous debonding details were also recorded from a side viewpoint as showed in Figure. It can be seen that, crack is more easily initiated in the bigger facet bonding joint. For 4 mm facet, macroscopical no contact area was observed, the crack propagated mainly along the surface direction quickly, resulting in the quick failure of the bonding joint. For 2 mm facet, no contact area is much smaller, and it can be seen the soft substrate is stretched up by the facet indication the weak contact, and the

crack blunting also occurred, which delayed the failure of the bonding joint. Finally, for the 1.5 mm facet, there is no obvious crack initiated at the beginning. The facet can be highly stretched, a cavitation occurred and developed mainly along the vertical direction, resulting in the final failure. In Chapter 3, the results have shown that no obvious macroscopical water drop is trapped by a patterned adhesives with a hexagonal side length of 1 mm, while it existed in ones with a hexagonal side length of 2 mm. The curves and the snapshots of the debonding joint shed light that hexagonal facets with side length less than 1.5 mm can achieve a good contact at this underwater condition. The good contact with less trapped water allow the bulk to dissipate a large amount of energy before detachment.

Moreover, probe tack of different single facets were also investigated by varying the waiting time, while the other conditions were kept as the same including the contact velocity, applied force, debonding velocity. From the adhesion strength and energy dissipation showed in Figure 4.c a and d, it can be inferred that in a short contact time, there was a big difference in adhesion strength and energy dissipated caused by real contact area effect. However, with increasing of the waiting time, more water at the interface of the bigger facet was drained out, leading to the increase of real contact. The gap between them became smaller. Although in Chapter 3, it has been shown that the macroscopical water can be drained out in tens of seconds, there is still a quite big difference in adhesion strength and energy dissipated. This state may suffered from two reasons, firstly, even though the macroscopical water are drained out, water film in a micro-or nanoscale still needs much more longer to be drained out due to the hydration of the polymer chains. Another possible effect could be that the ionic bonds formed at the interface depend on the contact time. In a short contact time, the weak bonds were mainly

formed, while strong bonds formed in a longer contact time. However, based on the current studies, it is quite hard to distinguish the two effects from each other quantitatively and further strategy is needed in future studies.

4.3.3 Underwater adhesion behaviors of PA hydrogels polymerized on different templates.

Compared to hydrophilic surfaces, hydration layers are easier to remove from the hydrophobic surfaces because the layers are less strongly attached to this type of surface. Hydrophobic interactions are an important driving force in marine adhesives. For instance, hydrophobicity is believed to promote complex coacervation of sandcastle glue, while the hydrophobic groups found in mussels protect DOPA against oxidation and reinforce the plaque by a combination of hydrophobic interactions and inter-residual H-bonding. Moreover, hydrophobic interactions become a more critical bonding strategy in case of less polar substrates. However, the underwater adhesion behaviors between hydrophilic and hydrophobic soft surfaces in hydrogels adhesives have not been heavily explored. Herein, we explore the underwater adhesion behaviors between PA hydrogels with hydrophilic and hydropjobic surfaces, polymerized on different templates. The PA hydrogels with the same composition, were synthesized on glass template and silicone rubber template, respectively. After the as-prepared hydrogels being dialysized at the equilibrium state in water. The contact angles of the surfaces are measured as shown in Figure 4.6 a, and the results showed that, PA hydrogels polymerized on the glass plate is hydrophilic (contact angle $52° \pm 4°$), while hydrogels polymerized on the silicone substrate is hydrophobic (contact angle $52° \pm 7.5°$). Here we called the gels polymerized on glass plates as G gels and gels polymerized on silicone plates denoted as S gels.

Underwater tensile test of S gels and G gels showed no significant difference of the bulk mechanical behaviors (Figure 4.6 b). On the other hand, the surface chemical composition was also checked by FTIR, and no obvious change occurred as shown in Figure 4.6 c. Then we conducted the underwater tack test with different contact pairs including G gels on G gels and G gels on S gels. The conditions of the tack test include 10 μm/s contact speed, 1 N loading force, 10 μm/s and debonding speed. The waiting time varied from 10 s to 1000 s, respectively. The results showed in Figure 4.6 d and e illustrate that, in 10 s, the adhesion PA hydrogels show a stronger adhesion on hydrophobic surfaces. While the contact time increased to 1000 s, the adhesion on the hydrophilic substrates also increased since more water are drained out and difference in adhesion strength become much smaller compared with that at a contact time of 10 s. These results implies that water layers are easier to be removed from hydrophobic substrates than hydrophilic substrates.

Hydrophobic interactions therefore have to be considered equally important for design of a proper underwater adhesive, despite being relatively weak compared to the electrostatic interactions and H-bonding.

4.4 Conclusions

In summary, studying underwater adhesion on soft substrates are meaningful to the applications such as tissue engineering, climbing soft robotics on easily deformable surfaces underwater. The PA hydrogels with ionic bonds show impressive underwater adhesion behaviors on soft hydrogels. Given the reversible nature of the ionic bonds, the PA hydrogels showed a significant effect of bulk energy dissipation on the adhesion. A

reliable surface bonding is the precondition of the bulk energy dissipation. The investigation on contact size effect clearly shows, smaller facets have a faster water drainage resulting in less defects at the interface. The smaller facet bonding joint also shows the ability to be much more insensitive to the crack initiation and propagating. In addition to the size effect, the surface hydrophobic nature may also improve the water draining efficiency. However, how to distinguish the real contact area effect from the ionic bonds formation effect quantitatively still needs further exploration.

References

[1] Autumn, K. et al. Evidence for van der Waals adhesion in gecko setae. 99, 12252-12256 (2002).

[2] Bartlett, M. D. et al. Looking beyond fibrillar features to scale gecko‐like adhesion. 24, 1078-1083 (2012).

[3] Boesel, L. F., Greiner, C., Arzt, E. & Del Campo, A. J. A. M. Gecko‐inspired surfaces: a path to strong and reversible dry adhesives. 22, 2125-2137 (2010).

[4] Del Campo, A., Greiner, C. & Arzt, E. J. L. Contact shape controls adhesion of bioinspired fibrillar surfaces. 23, 10235-10243 (2007).

[5] Faure, E. et al. Catechols as versatile platforms in polymer chemistry. 38, 236-270 (2013).

[6] Hofman, A. H., van Hees, I. A., Yang, J. & Kamperman, M. J. A. M. Bioinspired Underwater Adhesives by Using the Supramolecular Toolbox. 30, 1704640 (2018).

[7] Lee, B. P., Messersmith, P. B., Israelachvili, J. N. & Waite, J. H. J. A. r. o. m. r. Mussel-inspired adhesives and coatings. 41, 99-132 (2011).

[8] Schnarrenberger, A. A Comparison of Gecko Adhesion on Soft Substrates. (2018).

[9] Cheung, E. & Sitti, M. J. L. Adhesion of biologically inspired polymer microfibers on soft surfaces. 25, 6613-6616 (2009).

[10] Rippon, M., White, R. & Davies, P. J. W. U. Skin adhesives and their role in wound dressings. 3, 76 (2007).

[11] Li, J. et al. Tough adhesives for diverse wet surfaces. 357, 378-381 (2017)

Figures

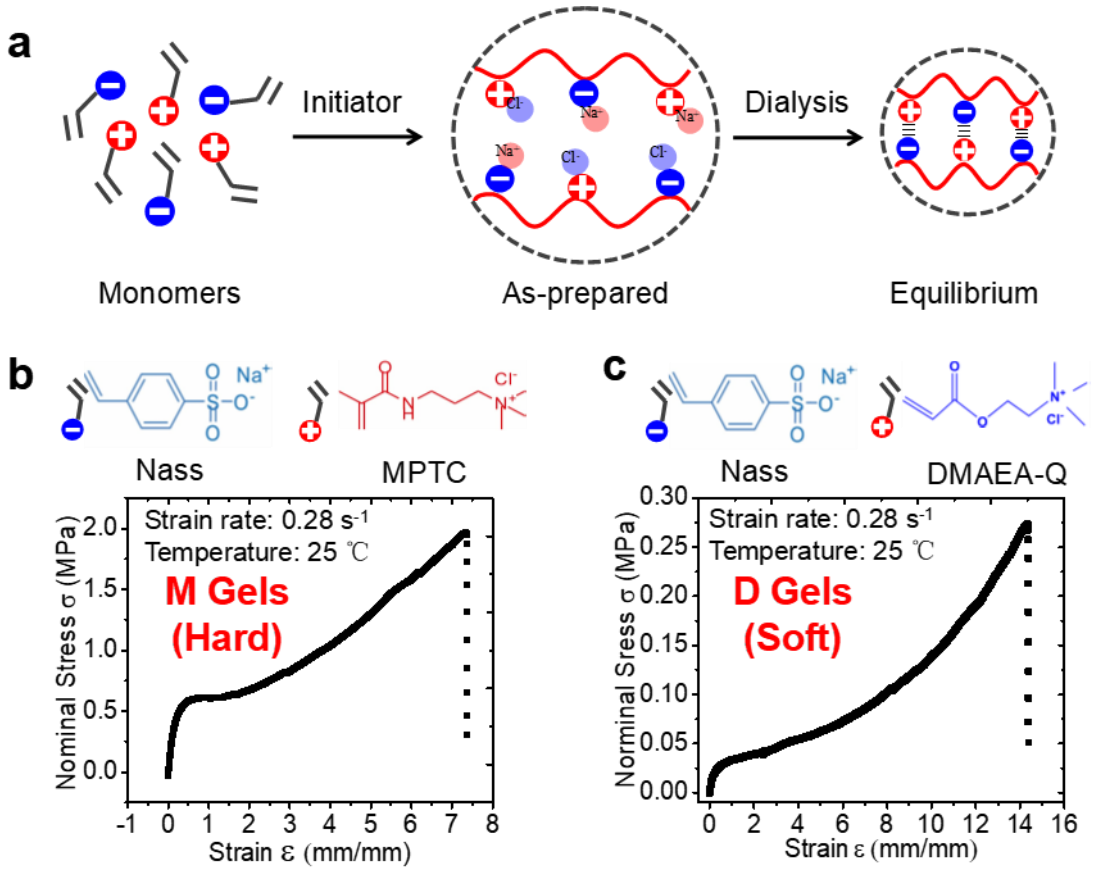

Figure 4.1 Schematic illustration of the polyampholyte (PA) hydrogels synthesis and tensile strain behavior of hard gels (M gel) and soft gel (D gel). The mechanical properties of the hydrogels are characterized using the underwater tensile at a steady 0.28 s^{-1} loading rate at 25 °C.

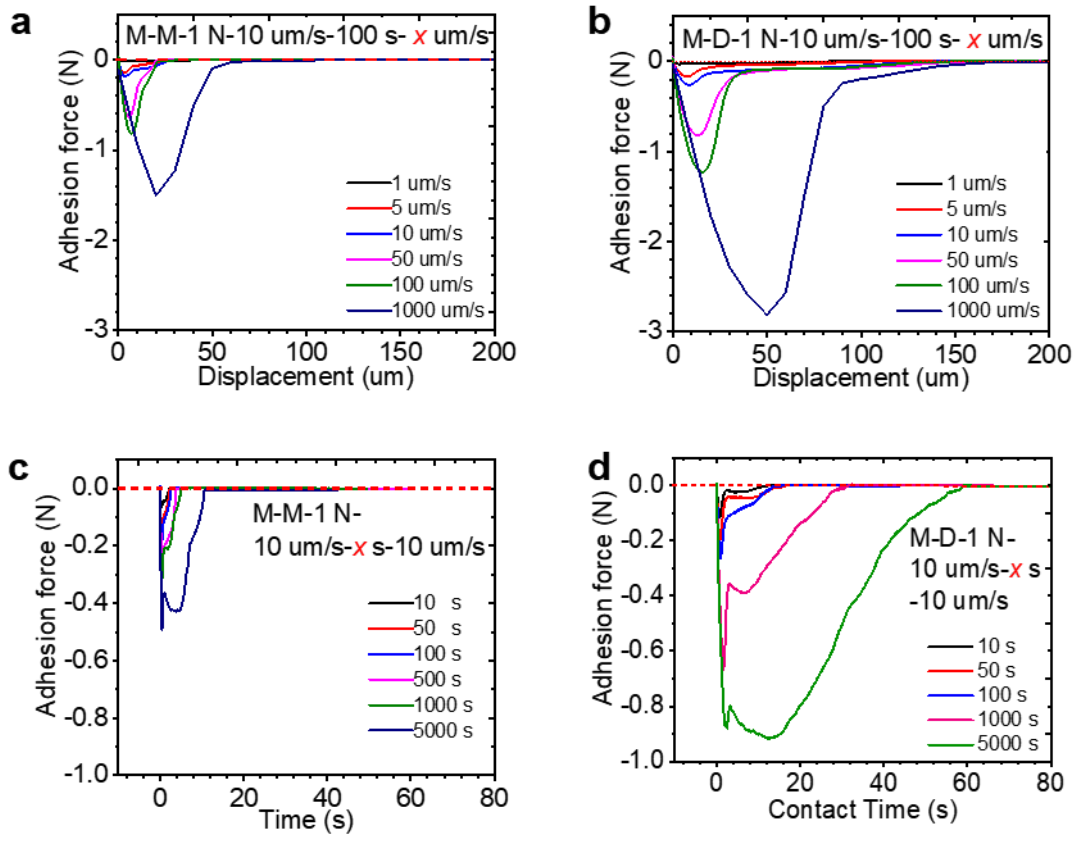

Figure 4.2 Softness effect on the underwater adhesion. Underwater adhesion between hard M gels and M gels (a), M gels and D gels (b) by changing the debonding speed. (c) Underwater adhesion between hard M gels and M gels by changing contact time, (d) Underwater adhesion between hard M gels and D gels by changing contact time. The force of 1 N was applied at a steady rate of 10 μm/s.

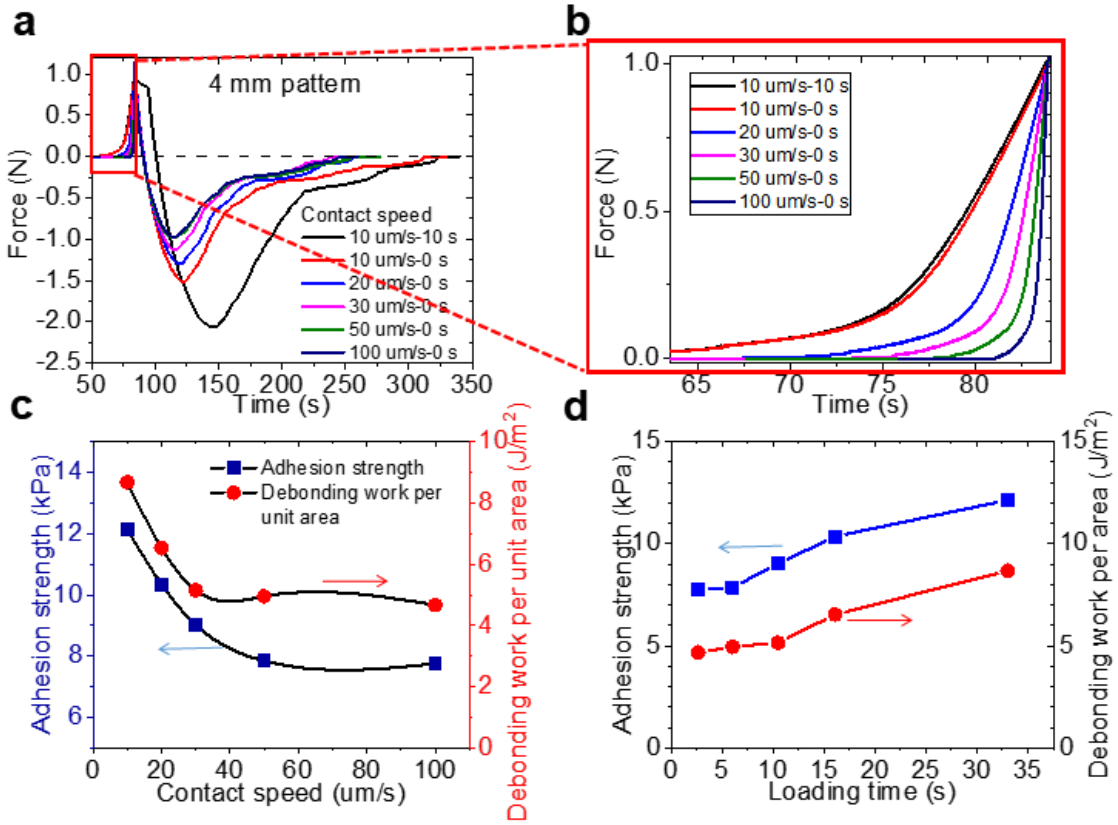

Figure 4.3 The approaching speed effect on the underwater adhesion between soft PA hydrogels. (a) Hydrogels with 4 mm surface hexagonal facets (geometry details in Chapter 3) were approached to the substrate with a various speeds. After 1 N was reached, the pattered hydrogels were retracted without waiting time. The real contact time was calculated from (b), the adhesion force vs. contact speed and debonding energy vs. real contact time (or loading time) profiles were displayed in (c) and (d), respectively.

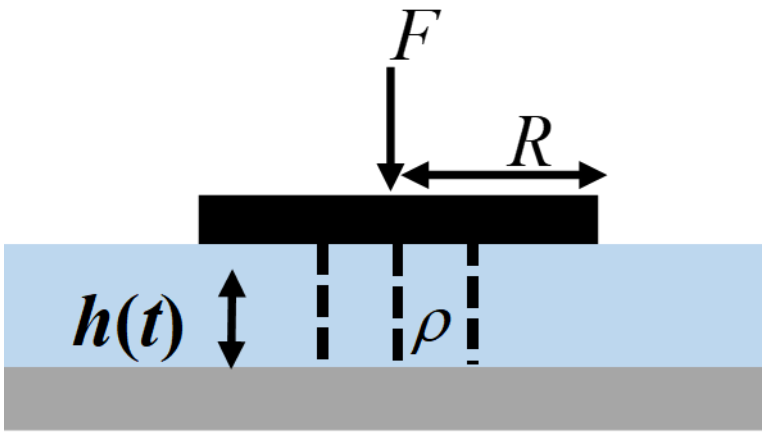

Figure 4.4 Schematic illustration of water drainage between the rigid plate and the substrate.

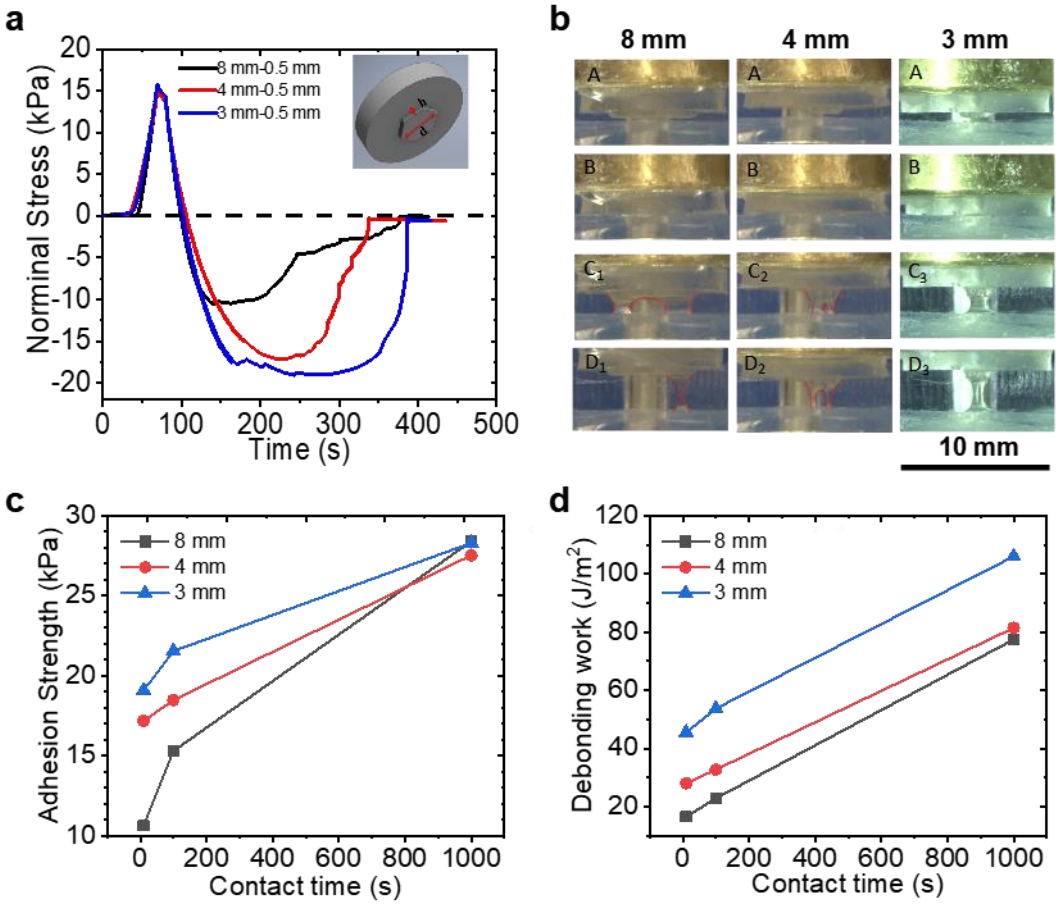

Figure 4.5 Contact elements effect on the underwater adhesion between soft PA hydrogels. (a) Underwater probe tack test between hydrogels with single facet whose diameter varied among 8 mm, 4 mm and 3 mm and a flat PA hydrogels. (b) Snapshots of the the underwater probe tack test. (c) Adhesion strength and (d) debonding energy vs. contact time profiles.

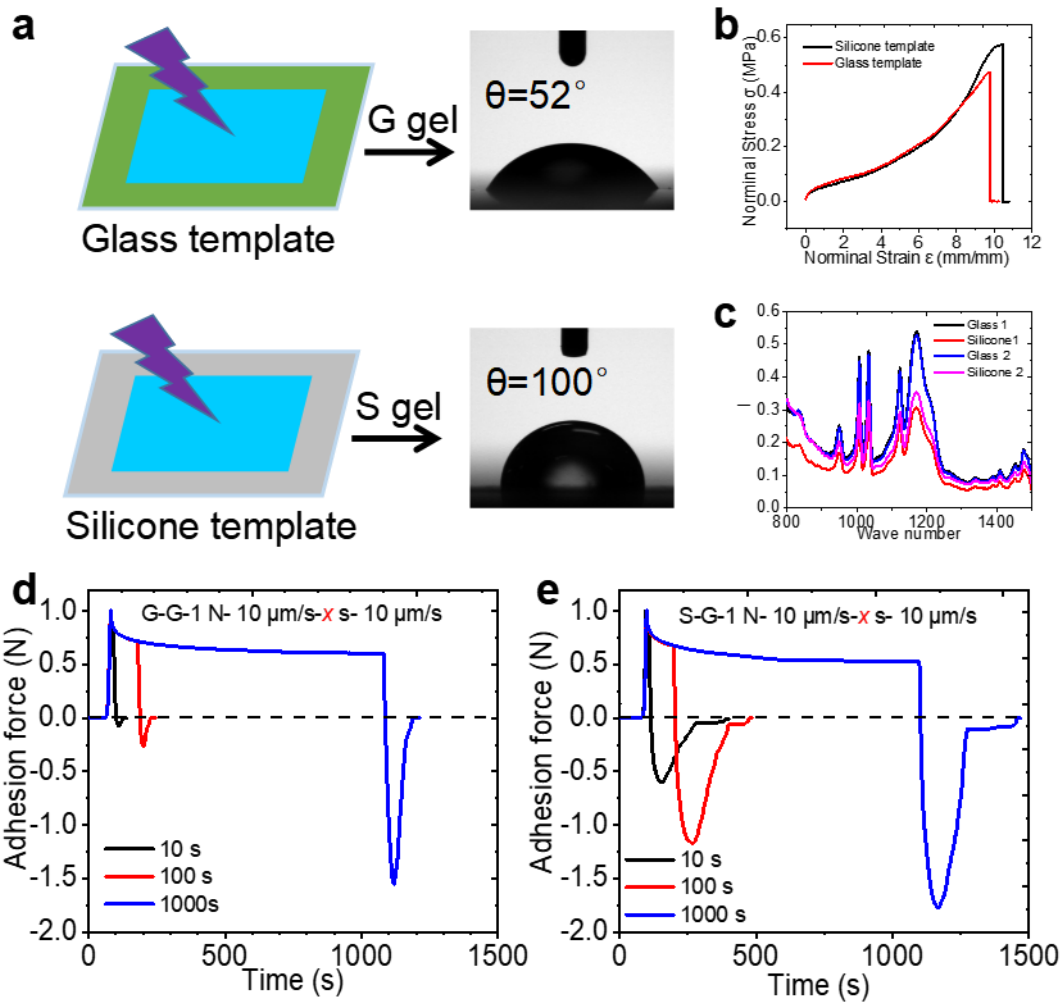

Figure 4.6 Underwater adhesion behaviors of PA hydrogels polymerized on different templates. (a) PA hydrogels polymerized on a flat glass (silicone template) and the measured contact angle is 52 °± 4 °(100 °± 7.5 °). (b) Tensile test of the PA hydrogels polymerized on different surfaces (c) FTIR measurement of the surface of the gels polymerized on glass plates. (d) Underwater probe tack adhesion test between gels polymerized on glass plates, and adhesion of gels polymerized on silicone plates on gels polymerized on glass plate with various contact time.

Chapter 5: Porous hydrogels with instant in situ underwater contact adhesion on diverse nonporous substrates

5.1 Introduction

In situ fast underwater contact adhesion is still challenging and in great demand for many applications in wet or underwater environment such as effective underwater adhesives-attaching sensors, beacons under the waterline, stopping watery leaks, in medicine, repairing wet tissues and climbing soft robotics. Hydrogels with a large amount of water are usually considered to show poor underwater adhesion performance while they have potential applications in diverse area with wet environment including tissue engineering, bio-medical device, and even soft robotics [1-4]. Existing hydrogels showing poor in situ underwater adhesion performances suffer from challenges of poor surface contact and poor efficiency to achieve a tough bonding underwater. Thin water film creating an obstacle for intimate contact at the interface may need a very long time to be drained out and water drop can be easily trapped at the interface [5] because of the hydrogels' softness, resulting in the decreasing of the real contact area and increasing of contact defects. In the previous study on PA hydrogels with surface architecture inspired from Cling fishes, it has been demonstrated that the smaller size of the contact element underwater is vital to accelerate the water drainage and prevent water entrapment at the interfaces. However, limitations exist for miniaturization of the contact elements because of mechanical factors [6]. As features get thinner, the pull-off force may exceed the fracture strength of the materials. As a consequence, very thin features will fracture before detachments occurs. In addition, features can condense or bunch together in wet environment if the work of

adhesion between them exceed the work carried out by bending them. This may stuck the water drainage channels and reduces the contact splitting effect. Another limitation is that decreasing the size while keeping the channels will reduce the total nominal contact areas. Moreover, microfibrillar surfaces were mainly produced by soft-lithography currently which are not easily extrapolated to macroscopic surfaces.

Achieving high adhesion energy not only requires surface efficient bonding, but also needs the materials inside or the substrates which can dissipate energy by hysteresis [7]. Super Glue has a high surface bonding strength but solidifies immediately and become very rigid once exposed to water. The rigid and brittle bonding joint can not survive from large deformation, resulting in a low energy dissipation. While, many kinds of soft materials with tough matrix such as double network hydrogels [8] show a very weak in situ underwater contact adhesion strength due to the hydration layers weakening physical interaction of Van der Waals's force at the interfaces, leading to no chance to dissipate energy before detachment of the surface bonding joint. Previous studies have shown that sacrificed covalent or reversible physical bonds of the bulk materials or the substrates will greatly improve the energy dissipation under large deformation [9]. Remarkable adhesion performance with an adhesion energy over 1000 J m^2 to various substrates including skin, tissue, glass, and metals have been achieved by combining a polymer interpenetrating or covalent bonding at the interface and a tough energy dissipated matrix [7]. However, they also have several shortcomings such as requirements for specific functional groups, long contact-forming time, and irreversible adhesion.

Therefore, highly efficient surface bonding as well as substantial bulk energy dissipation is the key strategy to designing a good underwater adhesives. Herein, we propose a simple but effective method to drain water out and make an instant contact adhesion with diverse

nonporous substrates including metal, silicone rubber, glass plates and beef tissue heart by using hydrogels with connective pores, and during the debonding process, the water suction effect creatively plays as a role of bulk energy dissipation. The porous hydrogels are composed of two oppositely charged polymers. The connective porous structure of the hydrogels results from the phase separation of polyelectrolyte complexation (PEC) triggered by salts exchange. Given the nature of reversible ionic bonds associations of the matrix, the porous hydrogel is tough and stretchable, enabling the bulk to accommodate the large deformation for energy dissipation. The connective pore structures greatly improve the access to drain water at the interface compared with nonporous soft materials, resulting in high water draining efficiency and less water entrapment. After water drainage, the good surface contact can be sealed by the closed pores due to the viscoelastic mechanical properties of the matrix. Detachment of the bonding joint will evolve a suction effect of the matrix, resulting in the increasing of the debonding energy. These combined characteristics of the porous hydrogels synergistically enable them can instantly and strongly adhere to diverse substrates including metal plate, glass plate, silicone rubber, aluminum film and beef heart under water.

5.2 Experiments

5.2.1 Materials

5.2.1.1 Chemicals

The porous hydrogels are prepared from two oppositely charged polymers, the ionic polymer poly(sodium 4-styrenesulfonate) (PNaSS) and cationic polymer poly(diallyldimethylammonium chloride) (PDADMAC). The PNaSS polymer solution

with 30 wt.% in water and PDADMAC polymer solution with 20 wt.% in water bought from SIGMA-ALDRICH were used as received, Sodium chloride (NaCl, Wako Pure Chemical Industries, Ltd.) were used as received, and Polyethylene Glycol (PEG, Wako Pure Chemical Industries, Ltd., Japan) were used as received.

5.2.1.2 Preparation of the porous hydrogels

The porous hydrogels were prepared from the phase separation of polyelectrolyte complexation (PEC) composed of PNaSS and PDADMAC triggered by salts exchange at a polymer PNaSS : PDADMAC ratio of 0.4 : 0.6. Firstly, an aqueous solution containing 1 M total polymers and 3.7 M NaCl concentration was prepared by heating in water bath to accelerate dissolving at a temperature of 70 ℃. Then bubbles in the viscous polymer solution were removed by vacuum centrifuge. Following, the mixing solution was poured into a cell clamped with porous aluminium oxide plates covered with semipermeable membrane on the surface (Figure 5.1). Next, the cell clamped around edges was placed into deionized water to exchange the salts with water for 24 hours. Finally, the plates were removed and the obtained sheet-shape gels were immersed in a large amount of water for sufficiently long time to reach equilibrium and to wash away the residual chemicals. The sample thickness was 4.35 mm.

5.2.2 Measurement

5.2.2.1 In situ observation of the underwater contact formation evolution

Underwater contact formation evolution was observed using a homemade system. The observation was based on the critical refraction principle [2-4]. Since the porous hydrogel has a different refractive index than glass and water, the light from the gel side reflects at angles between the critical angles of glass and water. A light image is observed when the

gel is in contact with the substrate, and a black image when water drops exist at the interface. A 35 mm diameter disc shaped gel (PA or PEC) was placed on a substrate in the stage box filled with water. An isosceles trapezoidal prism (angle 70 °, length 66 mm, height 22.08 mm, and width 50 mm), attached to the load cell using a rigid holder, approached the gel from the top at a steady 10 μm/s rate until the force reached the designed 15 N value. At the same time, the contact image of the gel on the prism surface was observed from an angle between the critical angles of water and gel using a zoom camera. The evolution of the contact image in time was subsequently recorded at the fixed displacement for different samples (see Movie S1, Supplementary Information). The contact areas for these snapshots at different times were calculated using the Image-J software, and the contact area ratios were calculated respective to the nominal area of the gels.

5.2.2.2 Underwater probe tack test

The probe tack tests, for measuring the adhesion strength and energy dissipation of the hydrogels, were performed on a Shimadzu Autograph AG-X 20KN tensile machine in water at 25 ℃. The set-up consisted of mainly two parts: the bottom part, a cell with a rigid stage providing the deionized water environment for the tack test, and the upper one, a copper shaft connected with the load cell. The gel was cut into disc shapes of prescribed diameter, and bonded to the copper shaft using a very thin super glue (Konishi Co., Ltd.). We used copper plate, aluminium plate/film, glass plate, silicone rubber, and pork heart tissue as counter substrates. The metal and glass plate we used were first washed by acetone and then washed by deionized water. The glass used was micro slide glass made by the MATSUNAMI Company of Japan (product number S2112). The glass carried negative surface charges, and the Zeta potential measured in 10 mM sodium chloride

(NaCl) aqueous solution was -32.44 mV, measured by the Zeta potential and Particle size analyzer (ELSZ-2000, Otsuka Electronics Co., Ltd (Osaka, Japan)). The contact angle to water was 19.6±2.2° at 25 ℃. Polystyrene used for Petri dish is made by the IWAKI Company of Japan. Fresh pork heart, beef heart were purchased from Nippon Food Packer Inc. (Japan) and used as received without any surface pre-treatment. Then the substrate was directly secured to the stage using a hard cover with screws. Before starting to measure, both parts were immersed in water and we waited for 30 min for the equilibrium state to be reached.

For the test, the upper gel was first compressed to the lower substrate at a constant compressing rate until it reached the set force (F). Afterward, the sample was held in this position for the described contact time (t). Subsequently, the probe was retracted at a constant rate until the debonding finished. The force, displacement, and time were recorded during the process.

5.2.2.3 Underwater compressive hysteresis test.

The underwater hysteresis tests, for illustrating the bulk suction effect of the hydrogels, were performed on a Shimadzu Autograph AG-X 20KN tensile machine in water at 25 ℃. The hysteresis test was performed using the same set-up and sample size as the underwater probe tack test. For the test, the upper gel was first compressed to the lower substrate at a constant compressing rate until it reached the designed displacement. Afterward, the sample was held in this position for the described contact time (t). Subsequently, the probe was retracted at a constant rate until the debonding finished. The force, displacement, and time were recorded during the process. Subsequent tensile cycles

were performed for various waiting times between two adjacent cycles. Hysteresis or energy dissipation was calculated from the area enclosed by the loading-unloading curve. The hysteresis ratio is calculated by hysteresis after the first loop divided by the hysteresis of the virgin samples.

5.2.2.4 Rheological test.

The rheological test was performed using an advanced rheometric expansion system (ARES) (Rheometric Science Inc.). A disc sample with a 15 mm diameter and a 4.35 mm thickness, was glued between the metal plates and surrounded by water. A rheological frequency sweep from 0.01 to 100 rad/s was performed at a constant strain of 0.1% and at temperature of 25 ℃.

5.3 Results and Discussions

We observed that the instant contact of the surface engineered gels induced quick and strong adhesion to the glass plate, alumium film, silicone rubber (Supplementary Movie S1) and beef heart tissue surfaces (Supplementary Movie S2) using only light compression. Even we heavily swayed the bonding joints underwater, the attached samples still strongly kept attached on the surface. These results illustrates that the hydrogels can realize an instant and high underwater contact adhesion capacity while only very light compressive force is applied.

Firstly, we examined the surface contact efficiency by observing the evolution of the contact formation underwater for polyampholyte (PA) hydrogels and porous hydrogels using critical refraction, as showed in Figure 5.2. Briefly, a gel disc with diameter of 35

mm and total thickness of 2.19 mm (PA gel) or 4.35 mm (Porous gel), was placed on the substrate. A trapezoidal prism, attached to the load cell, approached the gel in water from above, at a steady rate of 10 μm/s until the normal force reached the 15 N designed value, and then was held in that position. The corresponding nominal pressure estimated from the projected area of the sample surface was 15.6 kPa. During this process, the contact image of the gel to the prism surface was observed from an angle between the critical refraction angles of water θ_w and the gel θ_g (Figure 5.2).

Figure 5.2 shows snapshots of the contact images, where the bright region is in contact with the glass and the dark region is trapped with water. For the flat PA gel (P0), the contact started from the periphery then gradually and irregularly developed into the whole region as time elapsed. The normal force rapidly reached the pre-set value after 22 s (Figure 5.2), although the gel was hardly in contact with the substrate yet, indicating that the interface is intermediated by water. Even after more than 1000 s, some regions still remained dark, with lots of dark points distributed heterogeneously, indicating the permanent entrapment of water. It should be mentioned that the compressive strain rate applied to the sample, estimated from the contact rate and sample thickness, was about 4 $\times 10^{-3}$ s^{-1} (~2.5×10^{-2} rad/s). At this strain rate, the PA sample was very soft (storage shear modulus of ~30 kPa), and the 15.6 kPa nominal pressure gave a compressive deformation of ~50% average to the flat gel, which is large enough to cause full contact if there is no water entrapment. On the other hand, the contacting process finished within 60 s for porous hydrogels, much faster than the flat PA gels that took more than 1000 s. The surface instantly became brighter, indicating that the fast water drainage. Moreover, compared with the images of PA hydrogels after 1000s, no obvious trapped water drop was observed at the contact interfaces. These results imply that the porous hydrogels with

a connective channels are much more efficient to form a instant underwater contact than the flat PA non porous hydrogels.

To measure the adhesion strength, we used the standard probe tack test with a set-up as illustrated in Chapter 3. In brief, the porous gel (10 mm diameter) was compressed onto the substrate underwater at a steady contact rate of 10 μm/s until the contact force increased to 1 N, corresponding to a 12.7 kPa nominal pressure. Then, the gel was held in that position for 10 s, and finally, it was retracted from the substrate at a steady debonding rate of 10 μm/s. The glass plate we used was first washed by acetone and then washed by deionized water. It carried negative surface charges, and the Zeta potential measured in 10 mM sodium chloride (NaCl) aqueous solution was -32.44 mV and the contact angle to water was 19.6±2.2 °at the temperature of 25 ℃.

As shown in Figure 5.3, the displacement-time and force-time profiles of porous hydrogels on glass illustrates that when varying the keeping contact time, there is a slight improvement in the adhesion strength and energy dissipation. Compared with the 100 times of time consumed, the slight improvement is less important. This again implied that the porous hydrogels can achieve an instant underwater contact.

Compared with the typical debonding curves of nonporous adhesives such as PA hydrogels (Figure 5.3), the porous hydrogels demonstrate a quite different debonding behaviors as shown in Figure 5.3. Firstly, during the contact process, the applied force squeezed out the water inside the matrix. While, a large residual deformation remained once the applied force was removed. This is quite different from that of elastic DN gels or viscoelastic PA hydrogels as showed in Figure 5.3. Three kinds of samples were bonded between shaft and substrate, the same compressive strain deformation was applied underwater for three cycles without interval waiting time. It can be seen that, for

elastic DN hydrogels, there is no residual deformation; while the PA hydrogels showed some residual strain due to the viscoelastic properties which is much smaller than the PEC porous hydrogels. This indicates the residual strain mainly comes from that the pores were closed and cannot recover to the original state in time, resulting in a negative pressure inside the matrix.

Secondly, with the increasing of the debonding displacement, water will been sucked inside, and walls of the pores will recover from the bending state. Abrupt increasing of the stiffness of the total system occurred around the zero deformation point. To figure out the mechanism, we carefully analyzed the synchronous volume evolution from the recorded video, and the value of the volume was calculated from the snapshots (Figure 5.3) and demonstrated as a volume vs. time profile as shown in Figure 5.3. With the increasing of applied force, the volume of the materials decreased due to the water being squeezed out. When the displacement retracted back to the zero position, the volume were still smaller than that of the virgin samples. Following the debonding, the volume finally almost increased to 1.5 V_0. The high increasing of the volume implied water was sucked inside.

To understand the suction effect of the bulk materials, we further conducted a series of underwater compressive hysteresis test including varying the debonding speeds, changing the diameter of the samples, altering the interval time of cycles, tests in air and PEG solutions with different viscosity.

In the hysteresis test, the porous gel (10 mm diameter and 4.35 mm height) was compressed to the substrate with a thin glue until the gap were 4.30 mm (0.05 mm pre-displacement for bonding), then the water or surrounding solution was poured inside. The force and displacement are cleared to zero. After these preparation steps, the shaft was

approached at a steady velocity of 10 μm/s until the displacement reached to 2 mm. Then the porous gel was held for 10 seconds, and finally, it was retracted to the zero position from the substrate at a steady debonding rate. Subsequent tensile cycles were performed for various waiting times between two adjacent cycles.

The force-displacement profiles of samples by varying the debonding speeds with zero interval waiting time between two adjacent cycles, are shown in Figure 5.4. With the increasing of the debonding speed, the peak force and energy dissipation until the end point of each cycle is become stronger. The hysteresis effect is also become more obvious. Moreover, even changing the debonding speeds, the third cycle is almost overlapped with the second cycle, indication water squeezing and sucking dominated in this energy dissipation process. We further investigate the interval waiting time while fixing other conditions the same. The results showed in Figure 5.4 illustrates that, when the interval time is increasing, the hysteresis of the second cycle also increased, indicates the more water going inside when waiting at the zero position.

However, the explanation of viscoelastic mechanical properties and self-healing nature may also go well with these results. Therefore, further and more careful investigation are needed. Herein, to exclude the coupling effect of the materials, we conducted more tests by changing the size of the sample and the surrounding medium. Results shown in Figure 5.4, coming from the same test by varying the sample's size of 5 mm, 10 mm, and 15 mm, clearly demonstrated the trend that the bigger size samples have a higher peak force when returning to the zero position. Since changing size will not affect the viscoelastic properties of the bulk materials, we can conclude from the results that, the bigger size sample demonstrated a more obvious suction effect than smaller ones. This is because the water outside of the matrix going inside is much harder compared with the smaller ones.

Owing the instant contact formation at the interface and suction effect of the bulk materials, the porous hydrogels also show a good performance on many other nonporous substrates, including metal plate (steel, copper and aluminum plate), polymer surfaces (silicone rubber) and biology tissue (pork heart), which is summarized in Figure 5.5.

5.4 Conclusions

In summary, the above success in developing hydrogels show instant underwater contact as well as strong energy dissipation is due to the synergetic effect brought by connective porous structure and viscoelastic properties of the matrix with dynamic bonds. The connective pores not only accelerate the water drainage at the interfaces but also dissipate a large amount of energy by suction. The dynamic bonds induced the matrix a strong viscoelastic properties enabling the large residual deformation after removing the applied force, which results in the sealing of the porous hydrogels adhesives on the substrate. The porous hydrogels with high surface bonding efficiency and suction of the bulk make them available for many potential applications, such as effective underwater adhesives-attaching sensors, beacons under the waterline, stopping watery leaks, in medicine, repairing wet tissues, wound dressing.

References

1 Bačáková, L., Filova, E., Rypáček, F., Švorčík, V. & Starý, V. J. P. r. Cell adhesion on artificial materials for tissue engineering. 53, S35-S45 (2004).

2 Lu, N. & Kim, D.-H. J. S. R. Flexible and stretchable electronics paving the way for soft robotics. 1, 53-62 (2014).

3 Drury, J. L. & Mooney, D. J. J. B. Hydrogels for tissue engineering: scaffold design variables and applications. 24, 4337-4351 (2003).

4 Mi, F.-L. *et al*. Fabrication and characterization of a sponge-like asymmetric chitosan membrane as a wound dressing. 22, 165-173 (2001).

5 Rao, P. et al. Tough Hydrogels with Fast, Strong, and Reversible Underwater Adhesion Based on a Multiscale Design. 30, 1801884 (2018).

6 Boesel, L. F., Greiner, C., Arzt, E. & Del Campo, A. J. A. M. Gecko‐inspired surfaces: a path to strong and reversible dry adhesives. 22, 2125-2137 (2010).

7 Li, J. et al. Tough adhesives for diverse wet surfaces. 357, 378-381 (2017).

8 Gong, J. P., Katsuyama, Y., Kurokawa, T. & Osada, Y. J. A. m. Double‐network hydrogels with extremely high mechanical strength. 15, 1155-1158 (2003).

9 Yuk, H., Zhang, T., Lin, S., Parada, G. A. & Zhao, X. J. N. m. Tough bonding of hydrogels to diverse non-porous surfaces. 15, 190 (2016).

Figures

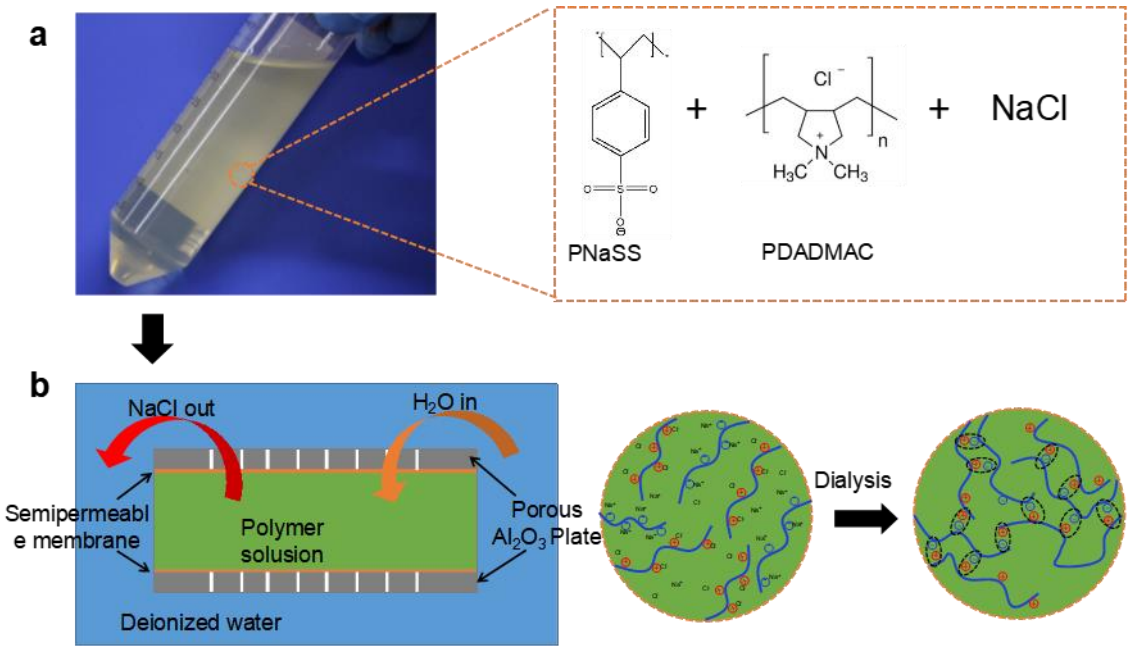

Figure 5.1. Schematic illustration of synthesizing the porous (PEC) hydrogels. (a) Positive PDAMAC and negative PNaSS polymers are dissolved in a saturated salty water. (b) The dialysis process to form PEC hydrogels with porous structure.

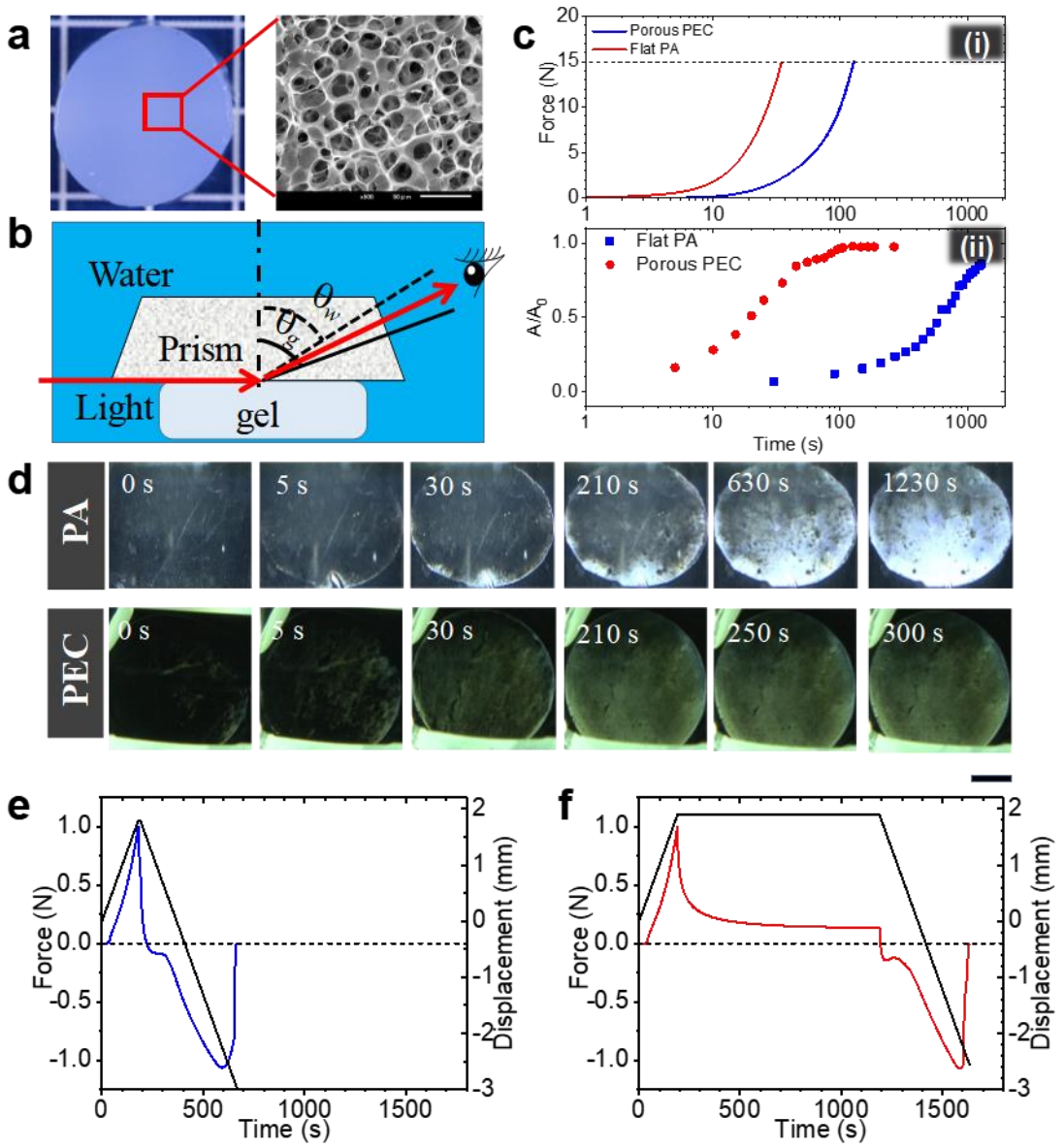

Figure 5.2. In situ instant underwater contact formation of porous hydrogels. (a) Optical and SEM image of the PEC hydrogels with porous structure. (b) Schematic illustration of in situ observation of the contact area evolution underwater. (c) (i) The loading profile of the prism to get contact with hydrogels at a steady speed of 10 μm/s. (ii) The profiles of contact area ratio developed with contact time. (d) The underwater tack test of PEC hydrogels with a short contact time (10 s) and a long contact time. (1000 s)

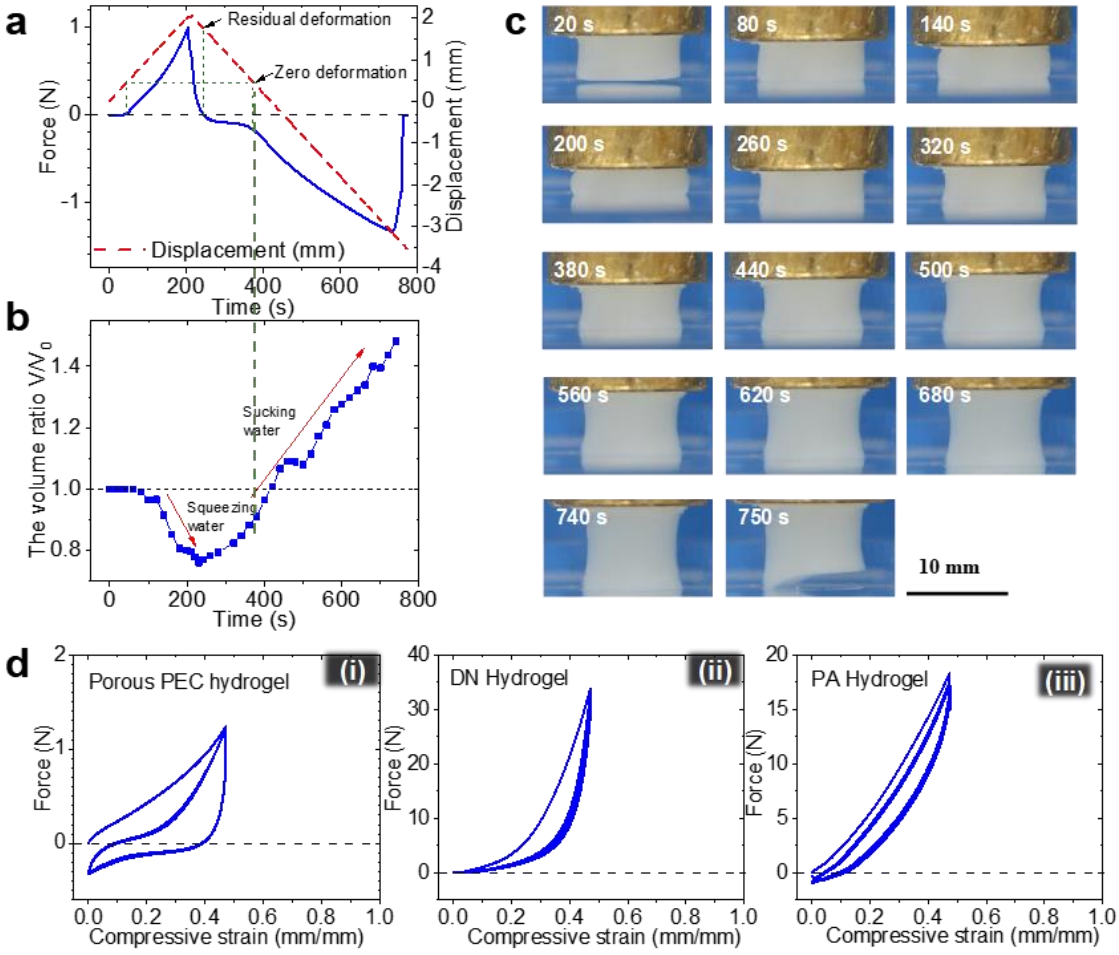

Figure 5.3. Large residual strain and notable suction effect on the underwater adhesion of the porous hydrogels. (a) The force vs. time profile of probe tack test of porous hydrogel. (b) The volume evolution of the porous hydrogel with the time during the probe tack test. (c) Snapshots of the porous PEC hydrogels in the tack test underwater. (d) The underwater cyclic tests of DN hydrogel, PA hydrogel and porous PEC hydrogel. Approaching and retracing velocities are 10 μm/s.

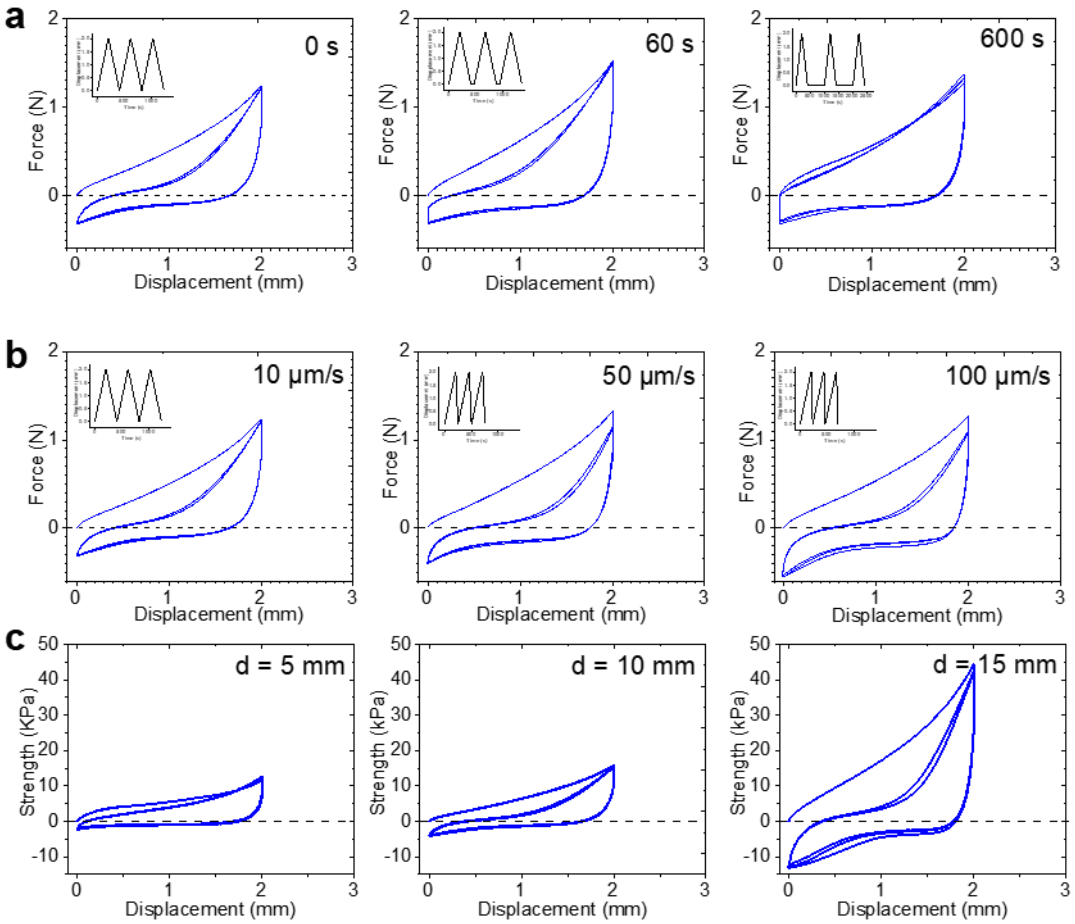

Figure 5.4. The waiting time (a), debonding speed (b) and contact size effect (c) on the suction of the bulk porous hydrogels.

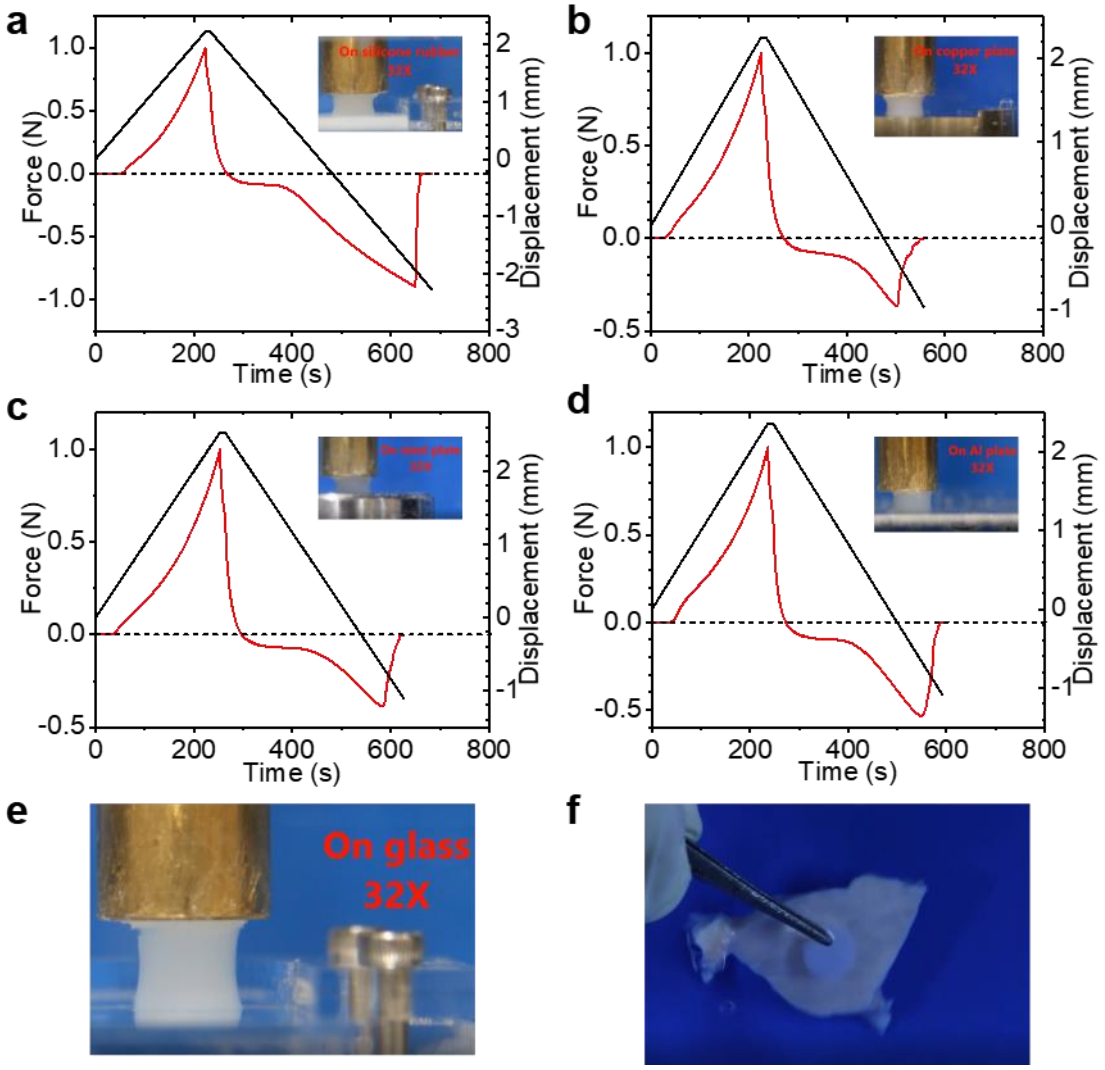

Figure 5.5. The instant underwater contact adhesion on diverse non porous substrates include metal plates, polymer substrate (silicone rubber), and tissue (beef heart).

Chapter 6: Conclusions

The dissertation proposed a design principle and developed the hydrogels showing fast and strong underwater contact adhesion based on multi-scale design. The following conclusions were given:

In **Chapter 3**, we have developed hydrogels showing fast, strong, and reversible underwater adhesion based on a multi-scale design. The success is due to the synergetic effect brought about by integrating macroscopic surface engineering and the tough hydrogels with dynamic bonds. The surface grooves not only accelerate water drainage and prevent water trapping, but also delay crack propagation during detachment. Specifically, the discontinuous contact pattern leads to independent detachment of contacts, which requires re-initiation of the crack for each contact. The splitting of contact also leads to an increase in the compliance of the contact point, which significantly enhances the bulk deformation of the gel. The dynamic bonds of the gel not only form reversible bridges at the interface to show reversible adhesion, but also dissipate a significant amount of energy in bulk during deformation. Smaller feature sizes lead to stronger underwater adhesion but poorer reversibility as the self-recovery time increases with the deformation at debonding. Such trade-off relations, determined by the adhesion strength, the modulus, and the self-recovery kinetics of the hydrogels, should be considered when designing the size of the surface features. This research could be used in some hydrogels applications requiring fast and reversible adhesion in wet environments or underwater, such as re-usable sheets for wound dressing, temporary adhesives for tissue healing, and anti-slippery gloves for wall-climbing robotics. The proposed method is simple but effective, and suitable for large-scale manufacturing with feature size dimensions of several millimeters.

In **Chapter 4**, the underwater contact adhesion behaviors between soft hydrogels were investigated. It was found that softness of the materials would affect the bonding formation and debonding energy. Rigid hydrogels got a poor contact due to the poor conforming ability to the substrate, while soft hydrogels might easily get water trapped at the interface, resulting in the reduce of the real contact area and increase of initial flaws. A well softness balance between the contact surfaces become quite important in underwater contact formation. Further study on the contact element's size showed that the smaller contact element demonstrated the ability to form a faster and better contact underwater as well as the ability to be much more insensitive to the crack initiation and competent to delay crack propagating. Moreover, the surface hydrophobic nature of the hydrogels may also improve the water draining efficiency to form a better underwater contact adhesion than hydrophilic ones. Investigations on these adhesion behaviors will help to get a better understanding the contact formation and debonding mechanism underwater, and then using this knowledge to design synthetic adhesives on soft substrates such as tissue, skin.

In **Chapter 5**, we have developed a porous hydrogels which showed instant underwater contact on diverse non porous plates as well as a high debonding energy dissipated by suction. The success is due to the synergetic effect brought by connective porous structure and viscoelastic properties of the matrix with dynamic bonds. The connective pores not only accelerate the water drainage at the interfaces but also dissipate a large amount of energy by suction. The dynamic bonds induced the matrix a strong viscoelastic properties enabling the large residual deformation after removing the applied force, which results in the sealing of the porous hydrogels adhesives on the substrate. The porous hydrogels with high surface bonding efficiency and suction of the bulk make them available for many

potential applications, such as effective underwater adhesives-attaching sensors, beacons under the waterline, stopping watery leaks, in medicine, repairing wet tissues, wound dressing. The obtained results might provide a better perception to understand the frictional properties of soft and wet materials like biological tissues, which is informative for designing low-friction biomaterials.

Accomplishments

Original papers

(1) P. Rao, T. L. Sun, L. Chen, R. Takahashi, G. Shinohara, H. Guo, D. R., King, T. Kurokawa, J. P. Gong, "Tough hydrogels with fast, strong and reversible underwater adhesion based on a multi-scale design", *Advanced Materials*, 2018, 30, 1801884.

Conferences and Presentations

(1) P. Rao, T. L. Sun, L. Chen, R. Takahashi, G. Shinohara, H. Guo, D. R. King, T. Kurokawa, J. P. Gong, "Tough hydrogels with fast, strong and reversible underwater adhesion based on a multi-scale design"; T*he 41st Annual Meeting of the Adhesion Society & the 6th World Congress on Adhesion and Related Phenomena*, in San Diego, California, March 2018. (Distinguish Poster Presentation Award)

(2) P. Rao, T. L. Sun, D. R. King, T. Kurokawa, J. P. Gong, "Tough hydrogels with fast, strong and reversible underwater adhesion", *Hokkaido University-Impact Joint Symposium*, Sapporo, Japan, August 2017.

(3) P. Rao, T. L. Sun, D. R. King, T. Kurokawa, J. P. Gong, "Tough hydrogels with fast, strong and reversible underwater adhesion", *International Soft Matter Summer School*, Sapporo, Japan, August 2017. (Distinguish Student Poster Presentation Award).

(4) P. Rao, T. L. Sun, D. R. King, T. Kurokawa, J. P. Gong, "Tough hydrogels with fast, strong and reversible underwater adhesion", *Gordon Research Conferences*, at Mount Holyoke College, MA, USA, July 2017. (Poster presentation).

(5) P. Rao, T. L. Sun, D. R. King, T. Kurokawa, J. P. Gong, "Tough hydrogels with fast, strong and reversible underwater adhesion", *SPSJ 66th Annual Meeting*, The Society of Polymer Science, Japan, May 2017. (Oral presentation)

Acknowledgments

The works in this thesis have been carried out under the supervision of Prof. Jian Ping Gong, in the Laboratory of Soft & Wet Matter (LSW), Graduate School of Life Science, Hokkaido University, Sapporo, Japan from October 2015 to March 2019.

I would like to express my deep gratitude to Professor **Jian Ping Gong**, my research supervisors, for her patient guidance, enthusiastic encouragement and useful critiques of this research work. She always provided me inspiring suggestions and deep thoughts on scientific problems, and her strict attitude on science and kindly patience to people will remain a great influence on my whole life as a good researcher. I am really thankful and appreciative for her encouragement and careful help both on my studies and life in Japan. I am sincerely grateful to her for giving me the opportunity to study in LSW.

I would like to offer my special thanks to Professor **Takayuki Kurokawa**, my sub-advisor for his instantaneous advices, solution to my experimental problems and thoughtful suggestions time to time, without which it will be tough way to finish the project in time. Advice given by the Assistant Professor Dr. **Daniel R. King** has also been a great help in my study on adhesion. Dr. Dan is an expert at gecko adhesion principle who has graduated from the famous professor Crosby's group. He is very active and I really enjoy the brainstorm group meeting with him and the reference recommended from him. I am particular grateful for the help given by Dr. **Tao Lin Sun**, who was ever an assistant professor of LSW. His kindness and encouragement had helped me to be faithful on the way to be a good researcher. Specially, I would like to thank **Liang Chen** (POA hydrogels) and **Kohei Murakawa** (PEC hydrogels) for their offering materials to study

the underwater adhesion behaviors. Without their generous help, my research will be a more zigzagging.

I would like to express my sincerely thanks to Assistant Professor **Tasuku Nakajima** and Assistant Professor **Takayuki Nonoyama**, for their helpful comments and suggestions on improving my presentations. My special thanks are extended to the technical staff Dr. **Yoshinori Katsuyama** and **Yukiko Hane** for the aid in experimental set-up design and instruction. I really appreciate all other members in LSW, the Japanese and International students' help as well as administrative secretary Ms. **Eiko Hasegawa**'s kind reminding in time for many trivial but important administrative affairs related to research, conference and daily life.

I would like to sincerely thank the IGP-RPLS (International Graduate Program for Research Pioneers in Life Sciences) and Monbukagakusho: MEXT for providing me all kinds of financial support.

Finally, I wish to express my deep thanks to my wife and my families who always stand behind to support me, for their love, tolerance, dedication and spiritual encouragement.

Ping Rao

Laboratory of Soft & Life Science

Graduate School of Life Science

Hokkaido University

Sapporo, Japan,

December 2018